NATURAL RESOURCES

GEOLOGIC MAP OF THE LAKE ROESIGER 7.5-MINUTE QUADRANGLE, SNOHOMISH COUNTY, WASHINGTON

by Joe D. Dragovich, Shannon A. Mahan, Megan L. Anderson, James H. MacDonald, Jr., Joseph F. Schilter, Christina L. Frattali, Curtis J. Koger, Daniel T. Smith, Bruce A. Stoker, S. Andrew DuFrane, Michael P. Eddy, Recep Cakir, and Kirsten B. Sauer

WASHINGTON
DIVISION OF GEOLOGY
AND EARTH RESOURCES
Map Series 2015-01
October 2015

WASHINGTON STATE DEPARTMENT OF
Natural Resources
Peter Goldmark - Commissioner of Public Lands

GEOLOGIC MAP OF THE LAKE ROESIGER 7.5-MINUTE QUADRANGLE, SNOHOMISH COUNTY, WASHINGTON

by Joe D. Dragovich, Shannon A. Mahan, Megan L. Anderson, James H. MacDonald, Jr., Joseph F. Schilter, Christina L. Frattali, Curtis J. Koger, Daniel T. Smith, Bruce A. Stoker, S. Andrew DuFrane, Michael P. Eddy, Recep Cakir, and Kirsten B. Sauer

WASHINGTON
DIVISION OF GEOLOGY
AND EARTH RESOURCES
Map Series 2015-01
October 2015

This geologic map was funded in part by the USGS National Cooperative Geologic Mapping Program, award no. G14AC00212

WASHINGTON STATE DEPARTMENT OF
Natural Resources
Peter Goldmark - Commissioner of Public Lands

DISCLAIMER

Neither the State of Washington, nor any agency thereof, nor any of their employees, makes any warranty, express or implied, or assumes any legal liability or responsibility for the accuracy, completeness, or usefulness of any information, apparatus, product, or process disclosed, or represents that its use would not infringe privately owned rights. Reference herein to any specific commercial product, process, or service by trade name, trademark, manufacturer, or otherwise, does not necessarily constitute or imply its endorsement, recommendation, or favoring by the State of Washington or any agency thereof. The views and opinions of authors expressed herein do not necessarily state or reflect those of the State of Washington or any agency thereof.

This map product has been subjected to an iterative internal review process by agency geologists, cartographers, and editors and meets Map Series standards as defined by Washington Division of Geology and Earth Resources.

INDEMNIFICATION

Research supported by the U.S. Geological Survey, National Cooperative Geologic Mapping Program, under USGS award number G14AC00212. The views and conclusions contained in this document are those of the authors and should not be interpreted as necessarily representing the official policies, either expressed or implied, of the U.S. Government.

WASHINGTON STATE DEPARTMENT OF NATURAL RESOURCES

Peter Goldmark—*Commissioner of Public Lands*

DIVISION OF GEOLOGY AND EARTH RESOURCES

David K. Norman—*State Geologist*
John P. Bromley—*Assistant State Geologist*

Washington State Department of Natural Resources
Division of Geology and Earth Resources

Mailing Address:
MS 47007
Olympia, WA 98504-7007

Street Address:
Natural Resources Bldg, Rm 148
1111 Washington St SE
Olympia, WA 98501

Phone: 360-902-1450
Fax: 360-902-1785
Email: geology@dnr.wa.gov
Website: http://www.dnr.wa.gov/geology

Publications and Maps:
www.dnr.wa.gov/programs-and-services/geology/publications-and-data/publications-and-maps

Washington Geology Library Searchable Catalog:
www.dnr.wa.gov/programs-and-services/geology/washington-geology-library

Suggested Citation: Dragovich, J. D.; Mahan, S. A.; Anderson, M. L.; MacDonald, J. H., Jr; Schilter, J. F.; Frattali, C. L.; Koger, C. J.; Smith, D. T.; Stoker, B. A.; DuFrane, Andrew; Eddy, M. P.; Cakir, Recep; Sauer, K. B., 2015, Geologic map of the Lake Roesiger 7.5-minute quadrangle, Snohomish County, Washington: Washington Division of Geology and Earth Resources Map Series 2015-01, 1 sheet, scale 1:24,000, 47 p. text. [http://www.dnr.wa.gov/publications/ger_ms2015-01_geol_map_lake_roesiger_24k.zip]

© 2015 Washington Division of Geology and Earth Resources
Published in the United States of America

Contents

FIGURES

TABLES

MAP SHEET

Geologic Map of the Lake Roesiger 7.5-minute Quadrangle, Snohomish County, Washington

by Joe D. Dragovich[1], Shannon A. Mahan[2], Megan L. Anderson[3], James H. MacDonald, Jr.[4], Joseph F. Schilter[1], Christina L. Frattali[1], Curtis J. Koger[5], Daniel T. Smith[6], Bruce A. Stoker[7], S. Andrew DuFrane[8], Michael P. Eddy[9], Recep Cakir[1], and Kirsten B. Sauer[10]

[1] Washington Division of Geology and Earth Resources
MS 47007
Olympia, WA 98504-7007

[2] U.S. Geological Survey
Box 25046, MS 974
Denver Federal Center
Denver, CO 80225-5046

[3] Colorado College
Department of Geology
14 E Cache La Poudre St
Colorado Springs, CO 80903

[4] Florida Gulf Coast University
Department of Marine and Ecological Science
Fort Myers, FL 33965

[5] Associated Earth Sciences, Inc.
911 5th Ave, Suite 100
Kirkland, WA 98033

[6] King County Department of Natural Resources and Parks,
Water and Land Resource Division
201 S Jackson St
Seattle, WA 98104

[7] Earth Systems
19729 207th Ave SE
Monroe, WA 98272

[8] University of Alberta
Department of Earth and Atmospheric Sciences
1-26 Earth Sciences Building
Edmonton, Alberta,
Canada T6G 2E3

[9] Department of Earth, Atmospheric and Planetary Sciences,
Massachusetts Institute of Technology,
Cambridge, MA 02139, USA

[10] University of Nevada, Reno
Department of Geological Sciences and Engineering
1664 N Virginia St
Reno, NV 89503

INTRODUCTION

The Lake Roesiger 7.5-minute quadrangle is directly north of Monroe, WA, and is the ninth quadrangle in a series of geologic maps along the eastern margin of the Puget Lowland. Each map represents a year-long effort to document surficial and bedrock geology and geologic structures in the lower Snoqualmie and Skykomish River basins of King and Snohomish Counties, a densely populated region that is seismically active. The Lake Chaplain reservoir is directly east of the map area and supplies water for three-quarters of Snohomish County, including the city of Everett.

Major active or potentially active structures in and near the quadrangle include the southern Whidbey Island fault zone (SWIF), Cherry Creek fault zone (CCFZ), Carnation fault, Monroe fault, and Monroe syncline (Fig. 1). The map area is northeast of the Rattlesnake Mountain fault zone and the SWIF, fault zones that cut late Pleistocene strata in King and Snohomish Counties. The active CCFZ is conjugate to the SWIF and was responsible for the shallow 1996 Duvall earthquake (M5.4). Both of these structures are responding to north–south crustal compression across the Puget Lowland (Wells and others, 1998). The Explorer Falls basin (EFB) is a Pleistocene graben that was initially mapped in the northwest part of the adjacent Lake Chaplain quadrangle. This basin continues across the northern part of the Lake Roesiger quadrangle and is bound by the newly named Carpenter Creek and Three Lakes Hill faults.

The map sheet presents the geologic map, two cross sections, correlation diagram, geophysical maps and models of the cross sections (Figs. M1 and M2), and a sample location map (Fig. M3). Appendix A contains infrared stimulated luminescence (IRSL) age information for Quaternary deposits. Appendices B and C provide earthquake and U-Pb zircon age data, respectively. Appendix D provides geochemical data for sand and rock samples.

The Lake Roesiger quadrangle abuts three recently completed 7.5-minute quadrangles—the Sultan (Dragovich and others, 2013), Monroe (Dragovich and others, 2011a,b), and Lake Chaplain (Dragovich and others, 2014a) quadrangles and is a northward and westward continuation of the mapping in these areas. To reduce the number of references to these adjacent studies, we use the terms “Monroe quadrangle”, “Sultan quadrangle”, and “Lake Chaplain quadrangle” to refer to the corresponding references. Mapping in the Lake Roesiger quadrangle has resulted in new insights into the geology of the adjacent quadrangles. Differences between maps and figures presented here and earlier versions are intentional and based on new data.

To enhance our mapping, we compiled several types of geologic analyses, including prior geologic mapping—for example, Booth (1990) and Tabor and others (1993), geotechnical findings from Snohomish County and the city of Everett engineering studies, and surface and subsurface information from geotechnical companies. We follow the nomenclature of Booth (1990) for many glacial features. For example, ‘Glacial Lake Skykomish’ describes the proglacial lake that occupied much of the Skykomish Valley during Vashon Stade deglaciation. Our fault, fold, and geomorphic feature nomenclature, such as the Monroe syncline and the various glacial recessional complexes, are informal. We use the informal term ‘Olympia beds’ in the

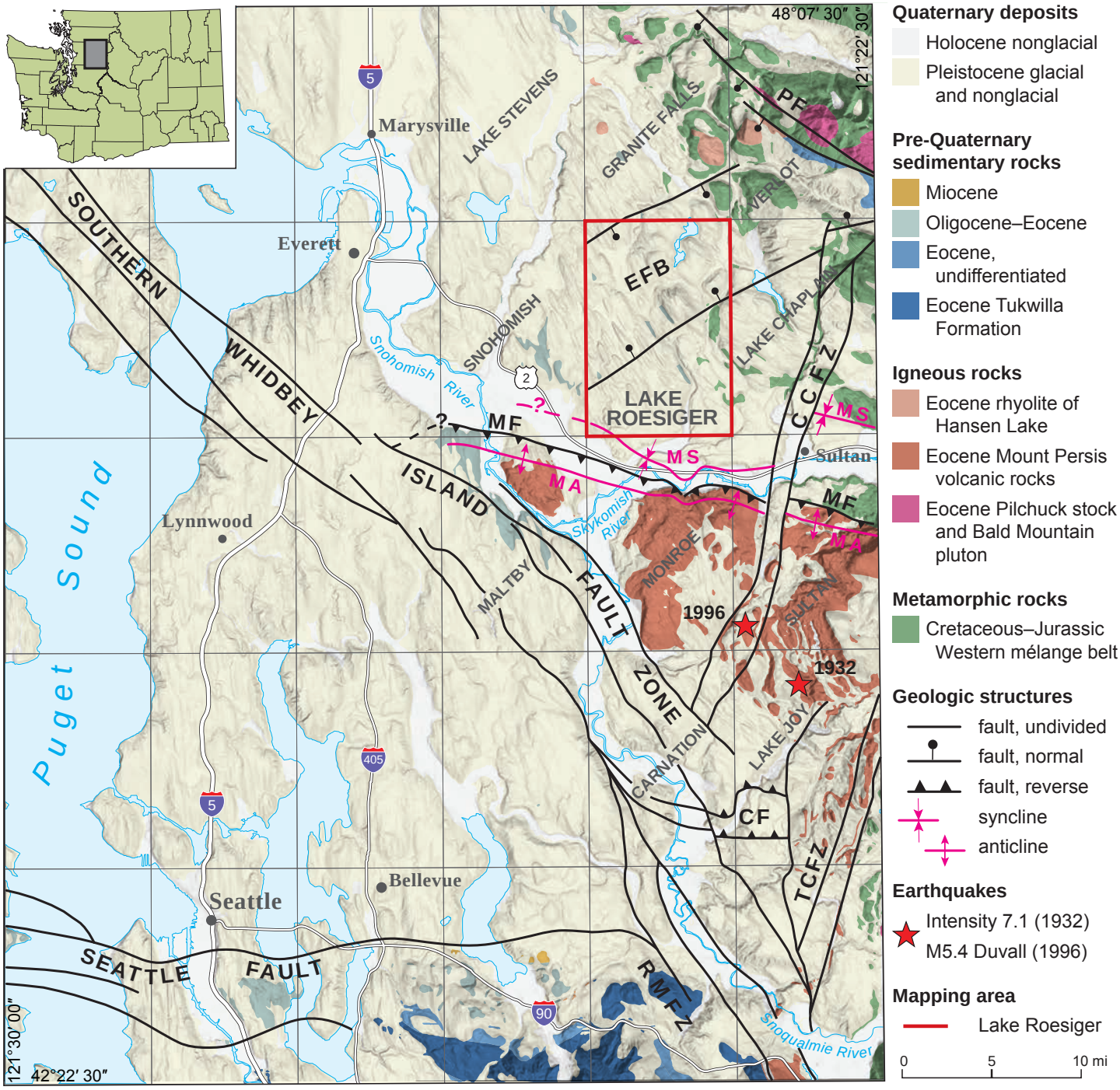

Figure 1. Simplified regional tectonic map of the central Puget Lowland and Cascade Range foothills showing the Lake Roesiger 7.5-minute quadrangle (red rectangle). New work maps the Explorer Falls basin (EFB) from the Lake Chaplain quadrangle (Dragovich and others, 2014a) into the Lake Roesiger quadrangle. The EFB is bound by the Three Lakes Hill fault on the south, and the Carpenter Creek fault on the north. We also show the Pilchuck River fault (PF) of Tabor and others (2002) north of the map area. The PF and EFB might be related extensional structures that preserve Paleogene to Pleistocene basin sediments in the Pilchuck River valley. We also map the Monroe syncline (MS) through the southwestern corner of the map area. This synclinal basin is north of the Monroe fault (MF) and the Monroe anticline (MA). The bedrock high south of the Monroe fault and north of the Carnation fault is likely uplifted between the two oppositely dipping MF and CF reverse faults. The Cherry Creek fault zone (CCFZ) is mapped northward into the Lake Chaplain quadrangle from previous mapping in the Sultan, Lake Joy, and Carnation quadrangles (Dragovich and others, 2011a,b, 2012, 2013, 2014a). The Tokul Creek fault zone (TCFZ) is similar to the CCFZ. They are likely left-lateral conjugates of the southern Whidbey Island fault zone (SWIF). The Rattlesnake Mountain fault zone (RMFZ) is likely a southern continuation of the SWIF. The Seattle fault and the SWIF are significantly simplified from Dragovich and others (2002) and Sherrod and others (2008).

same manner as Pessl and others (1989) to describe the deposits of the Olympia nonglacial interval.

METHODS

We use the Udden-Wentworth scale (Pettijohn, 1957) to classify unconsolidated sediments, Dickinson's (1970) terminology for sandstones, and Le Maitre and others' (2002) and Frost and others' (2001) terminology for igneous rocks. Clinopyroxenes are collectively described as 'augite' but may include other petrographically similar varieties. We use the time scales of the U.S. Geological Survey Geologic Names Committee (2010) and Wolfe and others (1998). Description of weathering rinds on basaltic clasts follows the methodology of Colman and Pierce (1981). We used the landslide classification system of Varnes (1978a,b). Quaternary sand deposit provenance is defined by compositional data derived from sand point-count data, petrographic observations, and sand geochemistry, as well as field data and observations (Table 1). Thin-section point-count data on sand-size fractions helped differentiate several glacial and nonglacial units. An important compositional discriminator for Quaternary strata studied for this report is the ternary system composed of monocrystalline quartz (Qm_x); quartz-mica tectonite, polycrystalline quartz, and chert (Qp_x); and potassium feldspar (PF_x). The normalized $Qm_xQp_xPF_x$ data provided below were obtained from petrographic examination of 49 sand samples from the Lake Roesiger quadrangle as well as from Dragovich (2007) and Dragovich and others (2009b, 2010a,b, 2012, 2013, 2014a). Elsewhere, percentages for individual mineral or lithic grains are not normalized and represent their abundance within the total clast population. See *Geochemistry* for a presentation and discussion of major and trace element compositions of the Western mélange belt (WMB), rhyolite of Hughes Lake, and Quaternary sand deposit samples. These data mostly agree with other compositional metrics, such as petrologic data.

DESCRIPTION OF MAP UNITS

Quaternary Sedimentary Deposits

HOLOCENE NONGLACIAL DEPOSITS

Qp **Peat**—Loose or soft peat, muck, and organic silt and clay, locally with diatomite and thin beds of Mazama ash (Rigg, 1958). Peat is found in abandoned river-channel depressions where it is interstratified with alluvial deposits (for example, in the Woods Creek valley) or deposited in upland depressions and kettles over low-permeability glacial deposits such as till or poorly sorted ice-contact deposits. Most peat was mapped using lidar, USGS topographic maps, and the previous mapping of Booth (1990). Rigg (1958) cored the Winters Lake peat deposit directly east of the map area and documented a 6 m-thick stratigraphic sequence of sphagnum, fibrous, and sedimentary peat interbedded with wood, muck, diatomite, and ash. See Rigg (1958) for a more-detailed description of peat deposits near the study area.

Qa **Alluvium**—Sand, silt, gravelly sand, and sandy pebble gravel; unit locally includes peat and organic sediments and (or) cobble gravel; clasts subrounded to rounded; some subangular to angular clasts in Woods Creek alluvium; loose; well stratified and sorted; planar-bedded sand, woody debris, and detrital wood are common; sand is typically light olive gray to light brownish gray. Skykomish River sand (70–76% SiO_2) in the southwestern corner of the map area contains monocrystalline quartz, plagioclase, K-spar (5–10%), hornblende (≤10%), and less, but significant amounts of pyroxene, granitic lithic grains, and mica, with rare garnet or metamorphic lithic grains. This combination of minerals and lithic grains (and their relative proportions) are indicative of sediment eroded from the central Cascade Range and transported by the Skykomish River (SP provenance; Table 1). Woods Creek alluvium consists mostly of sand, silt, and peat. At significant site 44D in the southeastern part of the map area, Woods Creek sand (~75% SiO_2) contains significant angular to subangular monocrystalline quartz (~25%), mica (5–15%), plagioclase (15–20%), polycrystalline quartz (~15%), K-spar (4–5%), and hornblende/pyroxene (~5%). Lithic grains (20–25%) vary and include significant amounts of metasedimentary fragments and some greenstone (LP provenance; Table 1). Woods Creek alluvium contains reworked Pleistocene sediment (unit Qc$_{ph}$) partly as a result of glacial to sub-glacial or proglacial erosion of these thick unconsolidated deposits during Vashon ice recession. Woods Creek alluvium is typically 4.5 to 7.5 m thick in the southeast part of the map area (significant sites B6 and B7), but due to map scale, we do not show alluvium along narrow portions of Woods Creek. Our field examination of the Carpenter Creek alluvium indicates that it is dominated by sand, silt, clay, and peat and is similar to the mica-rich, locally derived Woods Creek alluvium.

Qls **Landslide deposits (Holocene to latest Pleistocene)**—Diamicton or boulder gravel with minor sand or gravel beds; locally modified by stream processes; loose or soft; typically poorly sorted and unstratified; clasts are angular to subangular where derived from bedrock, but are mostly rounded where the landslide originated in Quaternary deposits. Mapped landslides include lateral spreads, slump earthflows, debris slumps, larger debris-flow deposits, and a few areas of thick colluvium and talus. This unit may include chaotic or stratified slump blocks or debris-flow aprons that originated in unstable Vashon recessional deposits perched on hillslopes. Some landslides may have initiated during late Pleistocene deglaciation. We show only the most prominent landslide complexes in the study area. In the northern part of the study area the tilted and weathered Pleistocene stratigraphy have created hydrologic conditions conducive to landsliding. Groundwater flow through highly weathered and clay-rich sediments has resulted in both deep-seated and shallow landslides. This is most evident

Table 1. Sedimentary provenances for Quaternary deposits in the Lake Roesiger, Lake Chaplain, Sultan, Lake Joy, Monroe, Carnation, North Bend, Fall City, and Snoqualmie quadrangles (Dragovich, 2007; Dragovich and others, 2009a,b,c, 2010a,b, 2011a,b, 2012, 2013, 2014a, this study). The top-most row of the table explains the organization of each provenance type. Geologic units from the Lake Roesiger quadrangle are black; adjacent quadrangles are gray. Provenance is assigned using composition from sand point-count data, petrographic observations, geochemistry, field data, and detrital zircon ages. Nonglacial Pleistocene geologic units were deposited in fluvial depositional environments similar to modern (Holocene) rivers of the same provenance. EFB, Explorer Falls basin; RMFZ, Rattlesnake Mountain fault zone; SWIF, southern Whidbey Island fault zone.

Provenance name	Dominant lithology	Other relevant information
Lithofacies type		
River type or name	Flow direction	
Geologic units		
SP provenance	Abundant monocrystalline quartz, K-spar, and plagioclase, with minor but distinct granitic lithic grains, biotite, pyroxene, and hornblende.	The major bedrock sources for SP sediments are Tertiary intrusive rocks such as the widely exposed Snoqualmie, Index, and Grotto batholiths. Ancient (Pleistocene) and modern Skykomish River alluvial facies are similar in composition to ancient and modern Snoqualmie River alluvial facies. The Monroe synclinal basin hosts a substantial thickness of these deposits. These major river valleys appear to be structurally controlled by faults such as the RMFZ–SWIF and (or) Monroe fault.
Cascade Range lithofacies		
Snoqualmie and Skykomish rivers	Regional-scale modern and ancient rivers; generally flow west from the Cascade Range.	
Qa (Snoqualmie and Skykomish Rivers), Qc_o, Qc_{ws}, Qc_h, Qc_{pf}, Qc_{ph}		
PP provenance	Monocrystalline quartz, K-spar, and plagioclase, with lesser but distinct metasedimentary lithic grains, biotite, pyroxene, and hornblende.	Ancient Pilchuck River alluvium is generally more weathered than correlative SP deposits to the south, but they are compositionally similar. In detail, these deposits have more detritus from the Western mélange belt—particularly metasedimentary detritus—as supported by detrital zircon ages (Dragovich and others, 2014a, this study). Thick deposits of ancient Pilchuck River sediment (unit Qc_{ph}) are mapped in the Pleistocene Explorer Falls basin where PP-provenance sediment fills the valley axis and LP-provenance (unit Qc_{phl}) alluvial fan deposits occur along the basin margin.
Cascade Range lithofacies		
Pilchuck River	Regional-scale modern and ancient Pilchuck River; generally flows west from the Cascade Range.	
Qc_{ph}		
LP provenance	Lithic grains are common and include volcanic, meta-argillite, and metasandstone, and are primarily derived from the volcanic rocks of Mount Persis and the Western mélange belt (WMB).	Ancient Tolt River alluvium and alluvial fan deposits are similar to modern Tolt River alluvium. Like the modern Tolt River fan at Carnation, ancient Tolt River alluvium interfingers with ancient Snoqualmie River alluvium. Ancient Youngs–Elwell Creek alluvium interfingers with ancient Skykomish River alluvium (unit Qc_o) southwest of Sultan, similar to the present. Ancient alluvium (unit Qc_{phl}) dominated by metasedimentary clasts of the WMB distinctly interfinger with PP Pleistocene alluvium (unit Qc_{ph}) in the Explorer Falls basin.
Western mélange belt and (or) Mount Persis lithofacies		
Local rivers and streams	Low-order rivers and local streams that generally flow west in the foothills of the Cascade Range. Includes the modern and ancient Tolt River, Sultan River, and Youngs–Elwell Creek.	
Qa (Tolt River, Youngs–Elwell Creek, and Sultan River), Qc_{ol}, Qc_{hmp}, Qc_{phl}		
PG provenance	Abundant lithic grains of andesite and recycled arkosic (feldspathic) sandstone and siltstone clasts from the Tukwila, Renton, and Tiger Mountain Formations.	These deposits are similar to the locally derived LP deposits, but differ because their source regions have distinctive and unique lithologies that provide paleogeographic information about ancient sediment dispersal systems. Fluvial PG sediments likely interfinger with fluvial SP sediments southwest of the map area near Carnation.
Puget Group lithofacies		
Local rivers and streams	Local rivers and streams that flow north and northwest into the lowlands.	
Qc_{wp}		
NP provenance	Polymict lithic clast types—including high-grade metamorphic clasts—and a high polycrystalline/ monocrystalline quartz ratio; less K-spar compared to Cascade Range sources. Locally mixed with Cascade Range lithofacies.	See Booth (1990) for further discussion of the provenance and depositional environments of NP glacial deposits. These sediments are locally mixed with some sediments of eastern and northeastern Cascade Range provenance (particularly for some Vashon Stade recessional deposits transported by ice-marginal meltwater).
Northern lithofacies		
Continental glaciers	Deposited by continental glaciers that advanced from the north. Flow directions vary based on local glacial conditions and topography.	
Qglr, Qgos, Qgod, Qgof, Qgic, Qgik, Qgog, Qgtv, Qga_v, Qglv, Qgt_p, Qgo_p, Qgl_p, Qgd_d, Qgtd, Qgd_{pd}		

on Three Lakes Hill where several landslide complexes and large, active alluvial fan complexes emanate from steep slopes where units Qc_{ph} and Qc_{phl} are exposed.

Qaf **Alluvial fan deposits (Holocene to latest Pleistocene)**—Diamicton, gravel, boulder gravel, and sand; loose; poorly to moderately sorted; moderately stratified to massive; locally contains locally voluminous debris flow deposits. Fan-shaped morphology results where streams emerge from confining valleys. Unit Qaf was distinguished from unit Qls by location and morphology from lidar imagery and (or) aerial photographs. We attribute some of the alluvial fan complexes in the northern part of the map area to local instability of weathered mid-to-early Pleistocene deposits of the Explorer Falls basin (for example, near Three Lakes Hill). Some fans may have begun as fan deltas that graded to local proglacial lakes, similar to the 'Monroe fan', which graded to Glacial Lake Skykomish at the close of the last glaciation Dragovich and others (2011a).

PLEISTOCENE GLACIAL AND NONGLACIAL DEPOSITS

Vashon Stade of the Fraser Glaciation

The continental ice of the Puget lobe advanced south from British Columbia across the Puget Lowland during the Vashon glaciation. The ice flowed southeast to east across the foothills of the Cascade Range, up major west-draining river valleys, covered the map area, and terminated along the Cascade Range 9 to 13 miles farther east (Booth, 1990). Deposits of the Vashon Stade of the Fraser Glaciation are widely distributed across the study area. Glacial ice and meltwater deposited glacial drift and carved the southern Puget Lowland into a complex geomorphology that provides insight into late Pleistocene glacial processes. Vashon deposits are typically fresh or slightly weathered; basalt clasts have very thin (commonly <1.0 mm) or no weathering rinds.

Vashon Recessional Deposits

Deglaciation of the Puget lobe ice sheet began ~14,000 yr BP along the Cascade foothills directly east of the map area, and the map area was ice free by ~13,500 yr BP (Porter and Swanson, 1998; Dragovich and others, 2014a). The ice front of the Puget lobe receded northwest across the map area, leaving behind Vashon-age recessional deposits. These deposits are horizontally and vertically complex due to facies changes generated by dynamic glacial depositional environments. During ice recession, a series of ice-marginal lakes and connecting glaciofluvial channels formed in the wake of the retreating ice lobe. The geometry, inset relationships, and elevation of the recessional deposits reflect successive lowering of base level as lower valleys became ice-free and spillways migrated west and north. This process resulted in younger inset or terraced recessional deposits grading to these new spillways (Knoll, 1967; Booth, 1990; Porter and Swanson, 1998; Dragovich and others, 2014a). Sand in these recessional deposits is polycrystalline quartz-rich and compositionally distinct from the Pleistocene Cascade Range provenance (Table 1), although local glacial erosion of older unconsolidated deposits in the EFB resulted in some recessional sand deposits containing reworked Cascade Range detritus.

Booth (1990) subdivided recessional outwash deposits into six stages of deglaciation and emphasized the importance of both ice-marginal and subglacial meltwater paths. For example, some of the southwest-trending valleys traversing the glacial uplands are the result of meltwater erosion and sedimentation in subglacial tunnels and open recessional valleys. The Richardson Creek ice-contact complex contains unequivocal subglacial channels that probably terminated in glacial Lake Skykomish (see unit Qgic). Areally restricted fluvial and lake kame deposits (units Qgik and Qgl_r) are either part of larger ice-contact complexes or are isolated accumulations that formed along the interface between the ice margin and deglaciated uplands. Our mapping confirms that ice-marginal meltwater followed several elevated pathways during glacial recession and deposited fluvial, deltaic, lacustrine, and ice-contact sediments. Glacial Lakes Snoqualmie and Skykomish were ice-dammed lakes that inundated the Skykomish and Snoqualmie valleys during deglaciation and merged as ice tongues receded down the Snoqualmie and Skykomish valleys to the Monroe area (Mackin, 1941; Booth, 1990; Dragovich and others, 2007, 2009a,c, 2010a,b, 2011a,b, 2012, 2013, 2014a) and later merged to form Glacial Lake Snohomish (Thorson, 1989).

The elevation of glacial lakes controlled the location of recessional outwash and smaller lakes in the region. Inset fluvial terraces and outwash channel landforms of unit Qgof are the result of fluvial incision or erosion in response to dropping glacial lake levels during deglaciation. These features are inset against slightly older ice-contact complexes in some parts of the map area. As observed in adjacent quadrangles, these terraces record Pleistocene southwest-trending recessional meltwater pathways that descended to Glacial Lake Skykomish or the later Glacial Lake Snohomish elevations.

The lowering of Glacial Lake Skykomish lake levels as the Vashon glacial ice receded west-northwesterly reflects the lowering of regional meltwater outlets (base levels) over time. For example, early Glacial Lake Skykomish had elevations of ~720–800 ft and 660–760 ft directly east in the Lake Chaplain quadrangle, whereas these lake deposits have a maximum elevation of ~480 ft in the current map area. This 480 ft elevation is similar to the maximum glacial lake elevations derived from the Sultan River fluvial-deltaic complex and the Pipeline Road kame-delta complex in the Lake Chaplain map area, as well as the maximum glacial lake elevations derived from recessional lake facies adjacent to the Lake Cochran ice-contact deposit (480–400 ft) and the Woods Creek fluvial deltaic complex (480–380 ft). This is further discussed in the description of unit Qgos. The persistence of the 480 ft level suggests a relatively stable Glacial Lake Skykomish elevation during deglaciation of the southwestern and southeastern parts of the Lake Chaplain and Lake Roesiger quadrangles, respectively. As inferred by Booth (1990), geomorphic relations imply that ice extended up the Skykomish River valley during recession. Similarly, the French Creek kame complex, located in the southwestern part of the map area, is graded to this ~480 ft Glacial Lake Skykomish lake level. This ice probably persisted until Glacial Lakes Skykomish and Snoqualmie merged (after the ice margin decayed past the Monroe area). Outwash deposits

graded to an elevation of ~480 ft likely represent the final sedimentation into Glacial Lake Skykomish before the regional lake level substantially dropped to Glacial Lake Snohomish. Deposits associated with this new lake (Glacial Lake Snohomish) are the inset fluvial recessional outwash terraces along Woods Creek that grade to and merge with the Woods Creek delta (near Monroe) at ~200 ft elevation.

Qgl_r **Recessional glaciolacustrine deposits**—Silt, clayey or sandy silt, and silty sand, typically with scattered dropstones; local lenses or beds of sand or gravel; loose or soft; massive or laminated to thinly bedded; locally displays varve-like rhythmites. Upward-fining sequences record waning lake sedimentation in small proglacial lakes.

Upward-coarsening sequences may begin as glacial-lake deposits (units Qgl_r and Qgos) and grade into overlying deltaic (unit Qgod) or fluvial (unit Qgof) deposits as a result of progradation of outwash into Glacial Lake Skykomish or smaller ice-marginal glacial lake environments. Sediments of Glacial Lake Skykomish were deposited at various elevations in the southern part of the map area and record a westward-receding glacial ice margin and an episodic lowering of lake level. Broecker and others (1956) reported a radiocarbon date of 11,900 yr BP from peat overlying soft blue clay (unit Qgl_r) in the Lake Joy quadrangle that indicates the area was ice free before that time.

Qgos **Outwash sand**—Sand and pebbly sand with some interbeds of silty sand, silt, or gravel; sand (~73% SiO_2) is typically dark blue-gray and weathers light brownish gray; loose or soft; varies from unstratified to weakly stratified; locally planar-bedded, laminated, or rarely crossbedded. Sand contains monocrystalline quartz (~20%), polycrystalline quartz (~20%), plagioclase (~15%), mica (~5%), and minor hornblende/pyroxene (~3%), locally with minor K-spar (0–3%). Lithic grains (30–35%) are comprised of metasedimentary grains and fewer volcanic, greenstone, and granitic grains.

The overall sand composition and fining trends indicate substantial subglacial to proglacial erosion of older deposits with a Cascade Range provenance during glacial recession. Unit Qgos is interbedded with recessional lake deposits (unit Qgl_r), fluvial outwash deposits (unit Qgof), and deltaic or kame-delta deposits (unit Qgod). Vertical and horizontal fining trends indicate mostly shallow-water glaciolacustrine deposition along delta fronts or as a sandy lake facies adjacent to silty glaciolacustrine deposits (unit Qgl_r). In some cases, sandy deposits may be higher-energy lake facies that represent former shorelines or sandy turbidites in finer-grained lake facies. Most of the lateral and vertical fining trends—from gravel to sand to silt across these complexes—are best explained as textural changes resulting from simple southeastward progradation of a delta into a glacial lake environment. This is best exemplified by the Woods Creek delta complex: in this area, sand (unit Qgos) coarsens upward into sand and gravel (unit Qgod or Qgof) and fines downward or laterally into silty lake deposits (unit Qgl_r). In the southwestern part of the map, however, the general transition from unit Qgl_r lake facies to unit Qgos sand may also represent higher energy marginal shore or beach facies of Glacial Lake Skykomish. Additionally, local differences in the proximity of outwash and ice-front deposits can complicate this relatively simple interpretation.

Qgod **Deltaic outwash and kame deltas**—Sandy cobble gravel, gravel, and pebbly sand; sand is typically dark blue-gray to light gray and weathers to yellowish brown or brownish gray; loose; moderately to well sorted and well stratified in thin to very thick beds. Deltas have high-amplitude planar foreset beds that graded to temporary ice-dammed lake levels. Mapping in this quadrangle, and adjacent mapping to the east, documents several deltas and delta complexes in the map area, including the Woods Creek fluvial-deltaic complex. Delta-front gravel consistently grades to more distal delta front sand (unit Qgos) and glacial-lake silt (unit Qgl_r) in most areas. The delta complexes are graded to various levels of Glacial Lake Skykomish and mostly accumulated adjacent to ice-contact complexes or have pitted outwash plains or other evidence for ice-proximal deposition. These deposits have a northern source provenance (NP provenance; Table 1).

Qgof **Fluvial outwash deposits**—Cobble and boulder gravel, gravel, pebbly sand, and interbeds of sand and (or) rare silt; sand is gray-brown and weathers olive-yellow; loose; moderately to well stratified and commonly contains medium to very thick subhorizontal beds that have local bar or ripple crossbedding, imbricated gravel, scour structures, and (or) rip-up clasts. This unit generally lacks ice-contact sedimentary structures and other geomorphic and stratigraphic evidence for nearby ice. Some outwash—such as the Woods Creek fluvial-deltaic complex near the Lake Cochran ice-contact complex—grades laterally into ice-contact complexes and suggests a near-ice origin for these deposits. In several areas we map unit Qgof as the topset beds of deltas (unit Qgod).

Erosional fluvial terraces are mapped on several Vashon outwash recessional deposits in the map area. These terraces are the result of meltwater incision into recessional outwash or older deposits as the base level of Glacial Lake Skykomish dropped during deglaciation. A falling Glacial Lake Skykomish elevation controlled subaerial incision of fluvial outwash over much of the map area and resulted in the development of local inset terraces. Prominent terrace levels above the West Fork of Woods Creek at ~210 and 270 ft elevation are generally graded to the Woods Creek delta in Monroe. The timing and elevation of controlling outlet lakes, deltas, and connecting channels in the area is further discussed by Booth (1990) and Dragovich and others (2011a, 2013, 2014a).

Qgic **Ice-contact deposits, undivided**—Cobble to boulder gravel and gravel, locally containing diamicton, silty pebble gravel, sand, pebbly sand, and silt; loose or soft; moderately stratified; medium to very thickly bedded with varied sorting; abrupt grain-size changes are common. Ice-contact primary structures include oversteepened and contorted bedding and other ice-shear features, all of which produce strata of variable dip. Diamicton was deposited in a variety of settings, including melt-out, debris flow, and dropstone-rich lacustrine environments. The upper surface of the deposit is typically hummocky and contains kettle depressions. The Lake Cochran ice-contact complex has several mappable ice-contact facies, including glaciolacustrine, glaciofluvial outwash, and hummocky dead-ice facies. Dead-ice deposits on the northwest grade southeast into recessional outwash fluvial and deltaic deposits (units Qgof and Qgod) of the Woods Creek fluvial deltaic complex and Glacial Lake Skykomish facies (units Qgl_r and Qgos). The Richardson Creek ice-contact complex in the south-central part of the map area also contains a variety of ice-contact and near-ice depositional facies. These deposits grade southward into fluvial outwash deposits (unit Qgof) that are in turn graded to Glacial Lake Skykomish.

Sub-ice recessional outwash channels (mapped as unit Qgog) are noteworthy and are found around the significant site labeled "SUBGLACIAL TUNNEL" in the southern part of the map area. Lidar, field data, and topography show that these "channels" are likely subglacial tunnels that generally flowed southeast towards the ice margin. The most compelling evidence for the subglacial tunnel origin is local uphill flow features that require elevated pore pressures to overcome topographic barriers.

Ice-contact deposits and related kames and fluvial outwash deposits form a crude north–northeast-trending belt which implies that the ice margin progressively waned or stagnated along highland areas during ice recession in the southern part of the map area. Similar events were documented in the Lake Chaplain and Sultan quadrangles, where ice-contact deposits progressively young to the west or northwest. We note that here, some of the smaller and isolated ice-contact deposits were likely deposited adjacent to local ice lobes that were stable long enough for debris to accumulate, but do not necessarily represent large-scale ice stagnation. See Booth (1990) or Knoll (1967) for a discussion of the temporal and spatial relations of deglaciation, and Booth (1984, 1986, 1990) for a subglacial depositional model. Unit Qgic is locally divided into:

Qgik **Kames**—Cobble and boulder gravel, gravel, sand, pebbly sand, and rare lenses of diamicton (mostly flow till or melt-out till from buried sediment-laden ice blocks); sand is typically dark yellowish gray to gray; loose; moderately to well stratified, medium to very thickly bedded, and commonly contains rip-up clasts of till or silt, cut-and-fill structures, and (or) localized oversteepened or slumped bedding. This unit includes both fluvial and local deltaic kame deposits. Kames were mapped where sedimentary structures, geomorphology, and (or) geologic setting imply lateral ice buttressing. The French Creek kame complex contains both ice-contact diamicton and fluvial gravels (unit Qgic) that form a distinct inset terrace at 380–400 ft elevation. Lower elevation portions of this complex, along the westernmost edge of the quadrangle, form an inset kame terrace composed of fluvial and deltaic deposits that grade southward into lake deposits. These deposits are younger and likely represent a substantial lowering of base level, with the overall distribution of the facies and the elevation of the kame topset beds suggesting a new lake level at about 280 ft (Minard, 1985; this study). In other areas, receding or wasting ice impinged upon highlands, leaving small isolated kame deposits. In some of these areas, fluvial-deltaic deposits grade laterally into or overlie kame deltas (unit Qgod) and (or) proglacial-lake deposits (units Qgos and Qgl_r), forming upward-coarsening sequences.

Qgog **Outwash gravel deposits, undivided**—Boulder–pebble gravel to pebbly sand; loose; massive to crudely bedded; mostly ice-contact deposits—including kame outwash—but may include any of the gravelly Vashon recessional facies or gravelly glacial lake beach facies. We were mostly unable to assign a depositional environment to unit Qgog because it is poorly exposed. In the southern part of the map area, however, unit Qgog in the Richardson Creek ice-contact complex west of Woods Creek formed as subglacial meltwater tunnel deposits (see description of unit Qgic and significant site "SUBGLACIAL TUNNEL").

Vashon Advance Proglacial and Subglacial Deposits

Throughout the map area, drumlins and flutes show that ice of the Puget lobe advanced from northwest to southeast. Ice advance over this part of the lowland occurred about 14,500 radiocarbon years ago and blocked Pleistocene rivers, creating extensive temporary lakes across much of the map area (Mackin, 1941; Booth, 1990). Most advance outwash consists of proglacial fluvial-deltaic deposits; the remainder are comprised of kame, other ice-contact, or subglacial ice-tunnel sediments that were deposited between advancing ice and restricting highlands. Facies relationships among river and delta deposits (unit Qga_V) and lake deposits (unit Qgl_V), as well as their thickness and widespread distribution, indicate that one or more large proglacial lakes progressively occupied significant portions of the region during ice advance (Knoll, 1967; Dragovich and others, 2007, 2009a,c, 2010b, 2011a, 2012, 2013, 2014a).

Facies, structural, and geomorphic relations indicate that several fluvial-deltaic complexes mantle the pre-Vashon Stade

topography, with delta progradation into paleovalleys, particularly along the east-southeastern portions of major hills in the map area. Similar to relations in the Sultan and Lake Chaplain quadrangles, a complex series of advance deposits formed in front of the advancing ice as it interacted with the foothills and paleovalleys. Bedding in advance outwash and lake deposits generally has a southeast dip. This dip reflects either glaciofluvial or deltaic deposition of foreset beds on the lee side of fluvial bars that slope away from the advancing ice, or steep gradient, high-energy braided streams. These subtle dips slope away from the advancing ice and probably do not indicate significant tectonic tilting in most areas. This differs from older Pleistocene ('ancient') alluvial nonglacial deposits—unit Qc$_{ph}$ for example—that were originally subhorizontal and have been subsequently tilted.

Advance outwash is polycrystalline-quartz-rich, contains a variety of lithic sedimentary, igneous, and metamorphic grain types (unnormalized ~50–70%), and has an average ternary composition of ~$Qm_{40}Qp_{54}PF_6$. This composition is distinctly different from nonglacial deposits that have a Cascade Range provenance and contain less monocrystalline quartz, plagioclase, and little or no hornblende, K-spar, or mica (0–4%; Table 1). Petrographic and geochemical analyses of polymict advance outwash sand (unit Qga$_v$)(65–71% SiO_2) indicate a complex provenance involving local and northern sources, particularly in settings where advance outwash has scoured and incorporated the pre-existing underlying strata (see sample 40D in *Geochemistry*).

Qgt$_v$ **Lodgment till**—Unstratified mixture of clay, silt, sand, and gravel (diamicton), with rare lenses of sand and gravel; grayish blue to very dark gray, locally slightly weathered to mottled yellow-brown; larger clasts are supported in a matrix of sand and silt; unsorted; dense; accreted at the base of the Vashon-age ice sheet and typically displays a subhorizontal and friable shear fabric. Clasts are both locally derived and northern-sourced and rounded to subangular. Angular clasts are present where this unit directly overlies bedrock. Till is generally 1.5 to ~30 m thick and is unconformable on advance deposits, older Quaternary deposits, and bedrock. Outcrops along Dubuque Road near significant site 23N are likely Vashon-age till and have a sub-vertical, east-west striking shear fabric that we suspect is tectonic. These fractures are locally injected by steeply dipping sand dikes (Fig. 2) related to the newly mapped Dubuque Road fault (see unit Qtz and Dubuque Road fault). Older till was rarely observed in the map area. Although not shown on the map, a till layer exists below ~64 ka Olympia beds at age site 33E and above nonglacial deposits correlated with the Whidbey Formation in the southwest corner of the map area. Because of these relationships, we correlate this older till with the Possession Glaciation. Extensive Possession-age deposits were mapped in the Monroe quadrangle to the south and also in a few locations in the Lake Chaplain quadrangle to the east.

Qga$_v$ **Advance outwash deposits**—Sand and pebble gravel, sand and cobble gravel, and local silt; dense; sandy beds are dark green-gray, weathering to yellowish brown, light-yellowish brown, or pale brown; typically well sorted; mostly thinly to very thickly bedded with local silt interbeds, rip-up clasts, deltaic and bar foresets, and cut-and fill-structures; contains detritus reworked from underlying Quaternary units—such as units Qc$_{ws}$ and Qc$_{ph}$—including up to boulder-sized rip-up clasts where the deposit overlies these older units. Advance outwash is intricately interlayered with, conformably overlies, or may locally underlie glacial-lake deposits (unit Qgl$_v$). Unit Qga$_v$ is most commonly overlain by Vashon lodgment till (unit Qgt$_v$) along a sharp contact. Composite sections of fluvial-deltaic advance outwash and glacial-lake deposits are thick where deltas prograded into restricted proglacial lakes during ice advance. Radiocarbon dates reported for unit Qga$_v$ from studies south or west of the map area are 14,450 to 14,560 yr BP (17,313–17,426 cal yr BP)(Porter and Swanson, 1998; Associated Earth Sciences, Inc., 2003; Dragovich and others, 2007, 2014a). OSL and IRSL ages of 14.1 ±0.59 ka and 16.4 ±0.64 ka and a radiocarbon age of 14,900 ±50 yr BP (17,985–18,250 cal yr BP) are from unit Qga$_v$ directly west of the Sultan River in the adjacent Lake Chaplain quadrangle. A steeply dipping northwest-striking fault

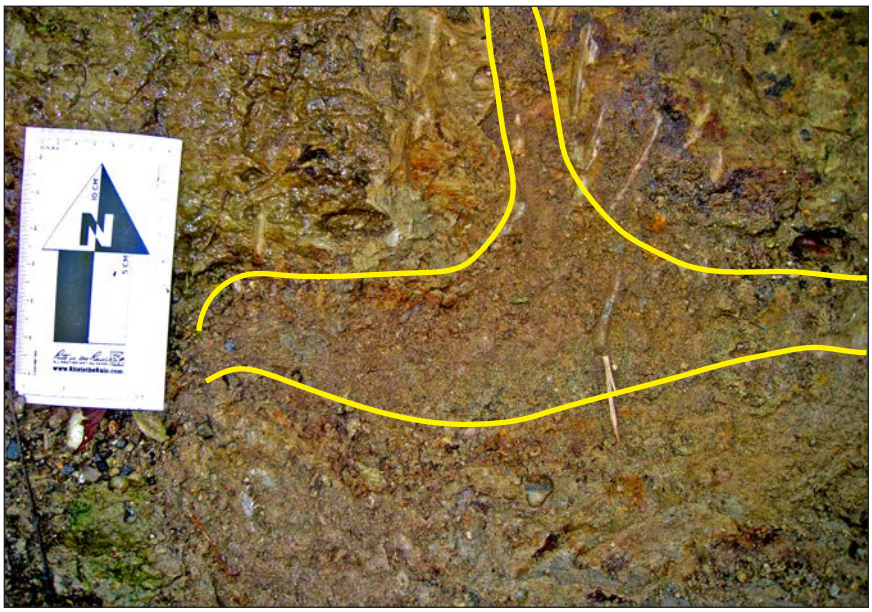

Figure 2. Deformed Vashon-age till (unit Qtz) at significant site 23N, directly south of the Dubuque Road fault. Several outcrops on Dubuque Road reveal a sub-vertical, east-west striking fracture fabric in the till. The limited weathering of the till suggests a Vashon age. The fractures are locally intruded by thin sand dikes or seams (highlighted in yellow). Although we do not conclusively know that these sand dikes are a result of activity on the Dubuque Road fault, their intrusion into fractures we correlate with the fault and the lack of sand dikes in other nearby deposits suggests that intrusion and fracturing are genetically and spatially related. If confirmed by further work, these features and the age of the deposit suggest that the Dubuque Road fault is active.

displaces advance outwash at significant site 10M along the eastern margin of the study area.

Qgl_v **Advance glaciolacustrine deposits**—Silt, clayey silt, pebbly silt, and diamicton, locally with very thin to thick beds of sand or pebbly sand; stiff to hard, or dense to very dense; stratification and sorting varies, but commonly massive or thinly bedded, laminated, or varved; typically contains scattered dropstones and beds or lenses of massive till-like diamicton that may be iceberg melt-out till or flow till. Some exposures are mostly diamicton with thin, wispy interbeds of silt or laminated silt and sand. Outcrops with contorted or folded bedding as a result of ice-shear are rare in the map area compared to the Sultan and Lake Chaplain quadrangles. At significant site 41AF, near Flowing Lake along the western part of the map area, delta-front sand and silt contain sand dikes and small injectites. Similarly, compact lake deposits with injectites are found along the southwestern edge of the map area at significant site 28M. Because these advance lake deposits likely contain ice-contact deposits, we suspect that the injectites are the result of ice-loading on saturated ice-marginal lake sediment. Unit Qga_v regionally overlies unit Qgl_v—as a result of simple progradation of fluvial and deltaic outwash over proglacial lake deposits—but there are local exceptions where this order is reversed; elsewhere, the two units are complexly interbedded or display inset relations. We suspect that some of the more complexly layered advance outwash and lake sections are the result of partial draining of proglacial lakes, and (or) changes to the outwash channels or depocenters. Unit Qgl_v includes some of the transitional beds of Booth (1990) and correlates with the Lawton Clay mapped elsewhere in the Puget Lowland. See Pessl and others (1989) and Minard (1985) for a regional description of the 'transitional beds'.

Pre-Fraser Glacial and Nonglacial Deposits

Qc_o **Deposits of the Olympia nonglacial interval (Olympia beds), ancient Skykomish River facies (Pleistocene)**—Sand, sandy silt, silty sand, and silt, with some clay, and organic silty-clay; minor peat and (or) gravel beds observed regionally; typically yellow, gray-brown, or brown-gray with distinctive dark gray-orange oxidation; dense; laminated to very thickly bedded and well stratified. Unit Qc_o locally contains charcoal, disseminated detrital organic matter, trough-and-ripple crossbedding, and (or) local graded beds. Regionally, Olympia beds preserve moderate to intense liquefaction features, such as sand dikes or folded bedding; chaotic bedding was observed in the study area. These features are likely Pleistocene in age and represent earthquake-induced liquefaction of saturated sediment prior to compaction by the Vashon-age ice sheet. Olympia beds are inferred to be only 12–24 m thick in the core of the Monroe syncline in the southwest corner of the map area. This is thinner than the Olympia beds in the core of the Monroe syncline farther southeast in the adjacent Monroe, Sultan, and Lake Chaplain quadrangles (Fig. 1; Cross Section A; *Monroe Syncline*).

Unit Qc_o represents Pleistocene alluvium of the Skykomish River (SP provenance; Table 1). Dragovich and others (2014a,b) refined the Cascade Range provenance for the Olympia beds using detrital zircon ages in concert with stratigraphy, age, and other compositional information. Upward-fining sequences of pebbly sand, sand, and silt with local organic beds comprise most of the strata and are typical of meandering river systems with overbank deposits. Although channel deposits are common in Olympia beds in nearby quadrangles, we did not observe them in the Lake Roesiger quadrangle.

South and east of the map area, 55 radiocarbon and IRSL/OSL ages indicate that the Olympia beds are between 15.5–51.5 ka (Associated Earth Sciences, 2001, 2002, 2004, 2007; Dragovich and others, 2007, 2009a,b,c, 2010a,b, 2011a,b, 2012, 2013, 2014a,b). We obtained a new 65 ±4.5 ka IRSL age from silty to fine-grained SP-provenance sand in the southeastern part of the map area (age site 33E; Appendix A). Regional and worldwide chronologies indicate that marine isotope stage 3 begins at 57–60 ka (Siddall and others, 2008). This information, combined with the 4.5 ka uncertainty for sample 33E, prompts us to assign an age of 60–61 ka for the base of the Olympia nonglacial interval in this area. This new age confirms that the core of the Monroe syncline contains Olympia beds in the southwestern corner of the Lake Roesiger quadrangle. The presence of Possession-age till directly below Olympia beds and above Whidbey Formation at this location (age site 33E) suggests that the base of the Olympia nonglacial interval must be directly below the age site. Olympia beds include some of the transitional beds of Booth (1990) and correlate with the deposits of the Olympia nonglacial interval of Pessl and others (1989).

Qc_{ws} **Whidbey Formation, Skykomish River facies (Pleistocene)**—Sand, silt, clayey silt, and silty sand with less pebbly sand, clay, gravel, and (or) organic sediment including peat; lenses of cobble gravel observed regionally; sand is a light yellowish brown and weathers to a distinctive orange-gray; dense or hard; well sorted and stratified; mostly laminated to thickly bedded sand and silt with thin beds or laminae of clay locally; commonly planar bedded; may contain charcoal, disseminated organic matter, trough-and-ripple crossbedding, graded beds; fluting, flame structures, sand dikes, and dish structures; folds and chaotic bedding are regionally common in nearby quadrangles and indicate liquefaction. Sand contains abundant monocrystalline quartz (25–40%) and plagioclase (20–25%) with minor, but significant K-spar (4–8%), hornblende (3–10%), and mica (5–20%), and accessory augite, epidote, and opaque minerals. These sand beds are generally lithic poor (~15%), with the lithic fraction dominantly composed of granitic grains, and are similar to other SP-provenance deposits (units Qa, Qc_o, and $Qc_{ph\text{-}south}$). Geochemically,

these deposits were derived from an intermediate arc source with minor sedimentary or metamorphic input (Dragovich and others, 2010a,b; 2011a,b; 2012; 2013; 2014a). Microscopically, sand is distinctly less weathered than early to mid-Pleistocene alluvium (unit Qc_{ph}) from the Explorer Falls basin and some younger—but anomalously weathered—Olympia bed deposits.

The Whidbey Formation is gently tilted to the south along the broad northern limb of the Monroe syncline in the southern part of the map area. Both the Olympia beds and the older Whidbey Formation are inferred to be folded across this structure (see *Monroe Syncline*). We obtained two new ages for unit Qc_{ws}: a 77.0 ±6.5 ka age at site 33C, and an 81.0 ±4.6 ka age at site 33F (Appendix A; Fig. M3). These ages agree with 11 IRSL and OSL ages in unit Qc_{ws} from nearby quadrangles that range from ~75 to 143 ka and several infinite radiocarbon ages (Dragovich and others, 2009a,c, 2011a,b, 2012, 2014a,b). We correlate these deposits with the Whidbey Formation (75, 000–130,000 yr BP) on the basis of age, composition, and stratigraphic position. For additional information on the Whidbey Formation southeast to southwest of the present quadrangle, see references above, Dragovich and others (2010a,b), and Capps and others (1973).

Qgt_d **Double Bluff till (Pleistocene)(cross-section only)**—Diamicton; very dense and massive; observed in wells and geotechnical borings only. We tentatively correlate a laterally extensive subsurface diamicton below the Whidbey Formation in the southern part of the map area with deposits of the Double Bluff glaciation (Cross Section A). Similar till was also encountered below the Whidbey Formation during geotechnical borings for the bridge across the East Fork of Woods Creek (sites BH6 and BH7). For additional descriptions of unit Qgt_d in nearby quadrangles, please see Dragovich and others (2009a,b, 2010a,b, 2011a) and Booth (1990).

Qc_{ph} **Pre-Hamm Creek nonglacial deposits (Pleistocene)**—Pebble gravel, gravelly sand, pebbly sand, sand, silty sand, and silt, locally with some cobble gravel and clay; sand is typically yellowish brown to pale brown and weathers to orange; oxidized, and strongly weathered; thin to very thickly bedded; well stratified; rip-up clasts, cross bedding, graded beds, leaves, twigs, charcoal, logs, or disseminated organic matter are common; liquefaction features such as flame structures are found in a few outcrops. Rarely observed lenticular lenses of diamicton are likely interbedded landslide deposits. Gravel clasts are generally WMB metasediments and vein quartz with fewer clasts of metagabbro, greenstone, granite, volcanics, and older sediments. Detailed petrographic inspection of several sand samples revealed significant angular to subangular monocrystalline quartz (20–40%), conspicuous biotite and white mica (15–25%), K-spar (2–10%), and plagioclase (20–25%), with minor but significant hornblende (5–10%) and lithic grains (10–30%) of phyllite, metasandstone, meta-argillite, metachert, and foliated quartz-mica aggregates. Most samples have minor—but distinct—amounts of granitic lithic grains, and some sand has minor pyroxene, garnet, epidote, greenstone, and greenschist. Sand (67–76% SiO_2) has a strong metamorphic to granitic provenance from local WMB basement and Tertiary plutonic rocks (Table 1). The abundant mica is likely from the Tertiary plutonic or foliated WMB rocks such as phyllite or meta-argillite. Polycrystalline quartz is a conspicuous minor constituent, and is most likely derived from metachert and (or) vein quartz that is common to the northeast to east in the eastern and Western mélange belts of Tabor and others (1993, 2002). Overall, unit Qc_{ph} sediments were derived from the Cascade Range via the Pleistocene Pilchuck valley which likely had a paleogeography broadly similar to the modern river valley. Deposits with a Pilchuck River provenance (PP; Table 1) contain more mélange belt detritus than the Holocene and Pleistocene Skykomish River deposits (SP; Table 1), but are otherwise broadly similar.

Weathering rinds on basaltic clasts are 0.2 to 5.0 mm thick (average of 2.5 mm); clay and other microcrystalline or cryptocrystalline weathering products were observed petrographically in the sand samples. The high loss on ignition (LOI)(~2.5–5.5%) and chemical index of alteration (CIA)(~62–66) of the geochemical samples in this unit and unit Qc_{phl} are likely the result of moderate to intense weathering of the sand grains (Appendix D).

Units Qc_{ph} and Qc_{phl} are restricted to the structural basin termed the Explorer Falls basin (EFB) by Dragovich and others (2014a). The EFB is bound by the Three Lakes Hill and Carpenter Creek faults. Pleistocene Pilchuck alluvium occupies the more axial parts of this now-inverted basin and intertongue with locally derived Pleistocene alluvium (unit Qc_{phl}) along the northern and southern edges of the fault-bound EFB (see Fig. 9). Interbedding of these two lithologies can be observed or confidently inferred at many sites, including significant site 39A in the northwestern part of the EFB. Unit Qc_{ph} deposits of the EFB have a Pilchuck River provenance (PP) that differs from more granitic Skykomish River provenance (SP) deposits found in the southernmost parts of the map area. These isolated southern exposures are termed $Qc_{ph\text{-}south}$, are poorly exposed, and likely restricted to the Monroe syncline.

The distribution of outcrops, internal deformation, kinematics of bounding faults, and the thickness of basin sediments (up to 215–245 m locally) all suggest that the basin has been locally inverted. Dragovich and others (2014a) suggest that the west tilt of the basin in the Lake Chaplain quadrangle is a result of uplift of the Cascade Range.

We obtained an IRSL age of >370 ka at age site 33A directly northeast of Lake Roesiger, an IRSL age of >455 ka at age site 33B directly east of Lake Roesiger, and an age of >540 ka at age site 35A from the northern top of Three Lakes Hill (Fig. M3; Appendix A).

Dragovich and others (2014a) obtained a similar >550 ka IRSL age along the central part of the EFB, just outside of the Lake Roesiger quadrangle (site 37D; Fig. M3). We obtained detrital zircon ages from 10–20 cm below this site (our site 47A) and found that the sand is dominantly derived from the WMB metasedimentary lithologies (Appendix C). Our new IRSL ages from this unit, its deep and persistent weathering, and amount and style of deformation all suggest that the unit entirely predates the Hamm Creek nonglacial interval of Troost and others (2005), which spans 243 to 188 ka and correlates with MIS 7 of Morrison (1991).

In the southernmost part of the map area, a new IRSL age of >430 ka at age site 33D indicates that mid-to-early Pleistocene nonglacial sediment underlies the Whidbey Formation in the Monroe syncline. These deposits contain monocrystalline quartz (25%), plagioclase (25%), K-spar (7%), hornblende and mica (6%), with some polycrystalline quartz (7%) and lithic fragments (30%), including granitic grains. These deposits have a distinct SP provenance (Appendix A), in contrast to the more locally derived unit Qc_{ph}, and we use the term "$Qc_{ph\text{-}south}$" to differentiate the two deposits. Dragovich and others (2013) obtained an infinite IRSL age of >300 ka from similar deposits near Sultan. Together, these data suggest that the Monroe syncline has guided the distribution of SP-provenance deposits since at least the mid to late Pleistocene.

Qc_{phl} **Pre-Hamm Creek nonglacial deposits, locally derived (Pleistocene)**—Pebbly sand, sand, sandy pebble gravel, with less gravel, cobble to boulder gravel, and rare silt; locally contains peat, logs or organic sediments; thinly to thickly bedded commonly with lenticular interbeds; low-angle foreset beds rarely observed; well sorted; angular to subrounded; distinctive dark bluish gray, weathers grayish brown. These deposits are very lithic rich and contain 70 to 95% WMB-derived metasedimentary grains—meta-argillite, phyllite, metasandstone, and metachert—with some WMB greenstone, serpentinite and metagabbro. These clasts locally form very distinctive dark-colored lithic sand deposits (Fig. 3). The deposits also contain 5 to 15% monocrystalline and polycrystalline quartz and plagioclase with very little K-spar and hornblende (0–2%). Unlike unit Qc_{ph}, these locally derived sediments mostly lack distinct Cascade Range detritus such as K-spar, mica, pyroxene and granitic lithic grains (0–2%)(Table 1). Like unit Qc_{ph}, weathering of the deposits are observed at outcrop and thin-section scale, with conspicuous 2 to 6 mm-thick weathering rinds on basalt and basaltic greenstone gravel clasts and abundant brown sand- and silt-sized cryptocrystalline weathering products observed petrographically. Weathering is also recorded geochemically by the high LOI (~5%) and CIA (~61–65)(Appendix D).

These sediments were deposited in alluvial fans along the northern and southern margins of the EFB and pass laterally into fluvial Cascade Range-provenance sediments of unit Qc_{ph} mapped along the basin axis (Cross Section B; see Fig. 9). A new IRSL age of 455 ka ±65 ka along the southern edge of Three Lakes Hill (site 35B), the weathering characteristics, and other age constraints for unit Qc_{ph} all indicate a middle to early Pleistocene age for this unit.

Qgn_{pf} **Pre-Fraser glacial and nonglacial deposits (Pleistocene to Pliocene?)(cross sections only)**—Dense to very dense gravel, boulder gravel, sand, silt, clay, and diamicton; locally contains peat or organic sediments; observed in wells and inferred in the subsurface along the Monroe syncline. Dragovich and others (2014a) infer pre-Whidbey Formation SP-provenance deposits in deep water-well logs within the Monroe synclinal basin. Additional constraints on the distribution of this unit are provided in *Isostatic Gravity and Aeromagnetic Analyses.* Knoll (1967), Booth (1990), and Dragovich and others (2007, 2009a,b,c, 2010a,b, 2012) describe outcrops of old and undivided glacial and nonglacial deposits elsewhere in the Snoqualmie and Skykomish Valleys.

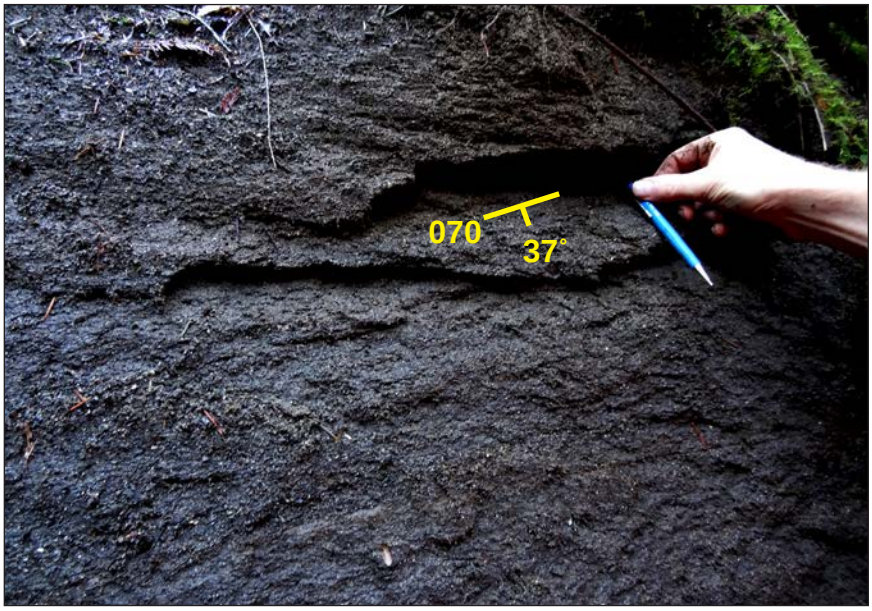

Figure 3. Outcrop of very dense, well sorted, medium sand of unit Qc_{phl}. Located in a ravine 30 m above, and directly east of the East Fork of Woods Creek and west of Lake Cochran at site 120D. Weathering has produced some clayification of this sand. Note the distinctive dark color of the sand, which contains 80–90% WMB metasedimentary lithic grains (meta-argillite, metasandstone, metachert and phyllite). Bedding strikes sub-parallel to the Three Lakes Hill fault to the north.

Tertiary Volcanic, Intrusive, and Sedimentary Rocks

Mvr **Rhyolite of Hughes Lake (Miocene)**—Poorly exposed, high-K, calc-alkaline rhyolite flow and crystal-vitric to vitric-crystal (lapilli) tuff; white to pinkish white, weathers light yellowish brown; massive with a slight flow alignment. Rhyolite is composed of a matrix of clear volcanic glass (~45%) with very fine microlites of plagioclase, stained pods of fine-grained potassium feldspar (either primary potassium silicate or secondary altered glass) and a few grains of biotite. The unit contains white pumice grains (~25%) with circular amygdales filled with opal or cristobalite. These pumice grains are flattened and wispy (up to 2 cm long), and locally have resorbed boundaries with spherulites; they also generally contain quartz and are plagioclase microphenocryst rich. Phenocrysts in pumice grains include plagioclase (~10%), quartz (~10%), and some probable sanidine (~2%). Plagioclase is mostly euhedral and lightly sericitized with good albite twinning. Quartz is clear, locally embayed, and subhedral to anhedral. Strained quartz phenocrysts with undulatory extinction are related to either intrusion and (or) deformation near faults. Geochemically, sample 31S is peraluminous and is interpreted to have assimilated continental crust prior to eruption (see *Geochemistry*). The presence of angular to subangular xenoliths of WMB arkosic metasediments (containing pumpellyite), greenstone, and mineral grains is consistent with this interpretation

The rhyolite crops out on the northwestern and southeastern slopes of the hill southeast of Hughes Lake, in the northeastern part of the map area; thus we assign the informal name "rhyolite of Hughes Lake". We suspect that this hill is an eroded rhyolite dome that intruded the Western mélange belt near the modern intersection of the Woods Creek fault zone (WCFZ) and the Three Lakes Hill fault. The role of these faults in the intrusive history of the rhyolite is uncertain at this time. We obtained a CA-IDTIMS U-Pb zircon age of 23.300 ±0.032 Ma at age site 31S (Appendix C) and we suggest that the rhyolite of Hughes Lake is the extrusive equivalent of the Grotto batholith. The 23–25 Ma Grotto batholith is north of and slightly older than the Snoqualmie batholith, which has its extrusive equivalents in the 18–25 Ma volcanic rocks of Snoqualmie Falls (Dragovich and others, 2009a,b). The rhyolite of Hughes Lake is younger, and geochemically distinct from the volcanic rocks of Snoqualmie Pass. It is noteworthy that the Miocene intrusive rocks near Snoqualmie Falls and Hughes Lake are both associated with major fault zones; the southern Whidbey Island fault zone and the Three Lakes Hill fault, respectively.

ΦEc **Rocks of Bulson Creek (Oligocene to Eocene)**—Lithic to lithofeldspathic sandstone with lesser conglomerate, pebbly sandstone, siltstone, and (or) coal with minor claystone; rare metachert pebble conglomerate; locally tuffaceous; light yellowish brown to light olive brown. Sandstone is generally moderately well sorted to well sorted with mostly subangular to subrounded grains. Siltstone grains are mostly angular to subangular. Unit is well stratified and thinly to very thickly bedded with local foresets, troughs, or scoured beds. Fossil leaves, twigs, and logs are common (Danner, 1957). Lithic sandstones have a wide distribution within the Explorer Falls basin. These sandstones contain abundant metasedimentary rock fragments (meta-argillite, metasandstone, phyllite, and metachert—locally with radiolarian fossils)(60–80%), other lithics, including greenstone, metagabbro, volcanic lithics, and a few granitic lithic grains (0–10%), with less plagioclase (3–10%), polycrystalline quartz (7–10%), and monocrystalline quartz (~5%). Minor detrital epidote and pumpellyite with rare K-spar and hornblende (0–2%); detrital mica was not observed. Conglomerate beds generally contain substantial WMB-derived clasts, predominantly metasedimentary detritus with some volcanic clasts.

Lithofeldspathic sandstone and siltstone along the axial part of the EFB—such as around significant site 37N—are compositionally more mature, and contain subangular to subrounded grains of monocrystalline quartz (~30%), plagioclase (~20%), and polycrystalline quartz (~15%), with coarse mica (~12%), lithic grains (~15%), and K-spar (~5%), with minor pyroxene and hornblende (~2%). Lithic grains include metachert with radiolarians, metasandstone, greenstone, phyllite or schist, and sedimentary lithic grains. These basin-axis sandstone beds have an overall intrusive igneous provenance. Metasedimentary lithic grains, such as phyllite, are relatively minor (<10%) compared to the basin margin lithic-rich facies described above. The predominance of locally derived detritus in sandstone near the margins of the Pleistocene EFB suggests that it may have also been an active transtensional basin during the Eocene through Oligocene.

Surface mapping and subsurface data, along with geophysical modeling, indicate that the thickness unit ΦEc is highly variable throughout the map area. Overall the unit thickens west from just a few meters along the Woods Creek fault zone to greater than 1,000 m in the southwestern part of the quadrangle near the Monroe syncline and Everett basin (Cross Section A). This exceptional thickness is documented by three moderate- to high-quality logs from oil and gas wells directly west of the quadrangle (Sh-3, Sh-4, and Sh-8 on Fig. M3) that record >940 m of sandstone, shale, carbonaceous shale, coal with rare oil and gas shows, and conglomerate (McFarland, 1981). Unit ΦEc also appears to thicken into the Explorer Falls basin along the western part of the map area (Cross Section B; Fig. 4) and only exists in the EFB in the northeastern part of the map area.

The depositional environment of unit ΦEc is fluvial, possibly with local alluvial fans along the margins of the EFB. However, similar to the rocks of Bulson Creek to the north (Marcus, 1991), unit ΦEc likely grades westward into a nearshore and deeper marine depositional

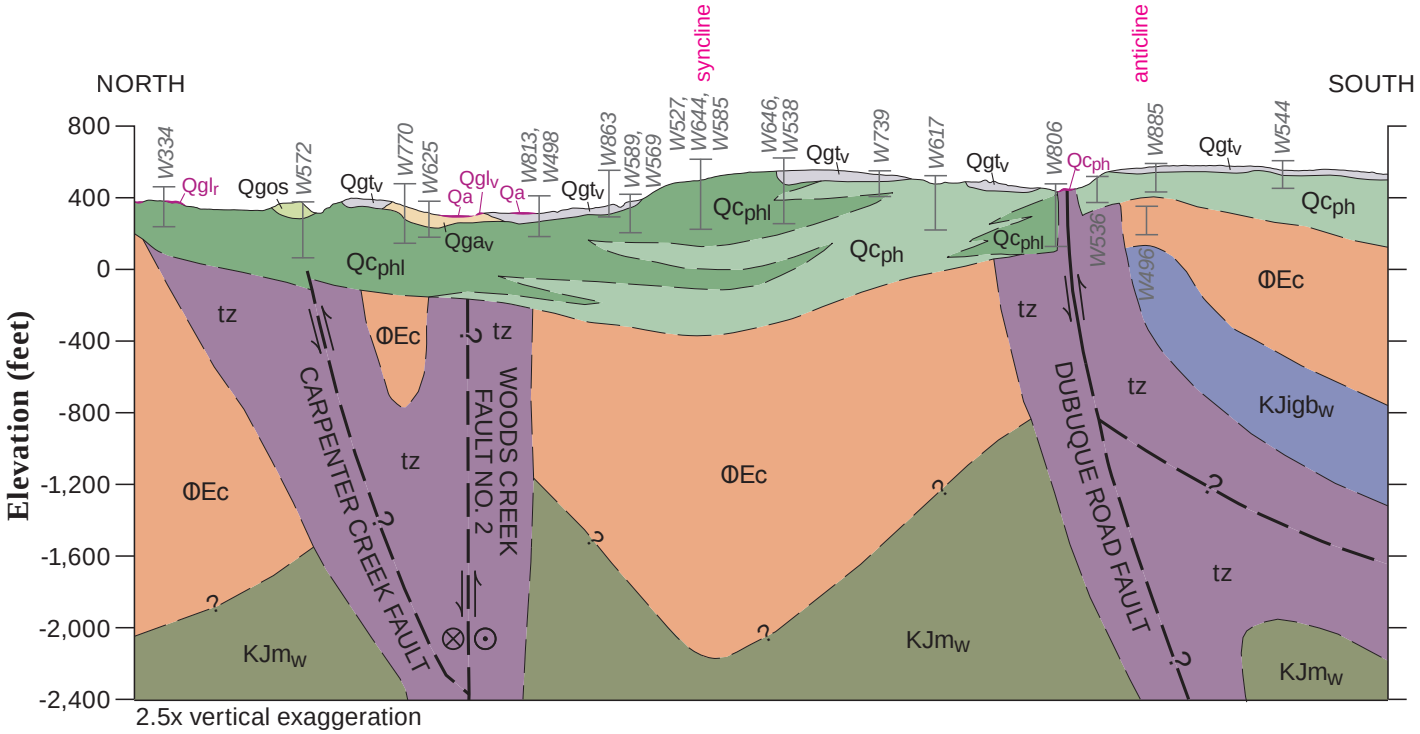

Figure 4. Schematic cross-section across the Dubuque Road fault in the northwest part of the Lake Roesiger quadrangle (see Map Sheet for location, legend, and the location of 51 well logs used in the interpretation). The Dubuque Road fault is an intrabasinal fault in the Explorer Falls basin (EFB) that we interpret as a south-dipping reverse fault. The high magnetic susceptibility directly south of the fault (Fig. M2) is interpreted to be uplifted metagabbro (unit KJigb$_w$).This uplift is consistent with the occurrence of deformed unit ΦEc directly south of the fault trace. A hanging wall anticline is suggested by the geophysics, and is supported by limited bedding orientations. Offest till (unit Qgt$_v$) in an outcrop along Dubuque Road suggests that, at least locally, the fault may be active. Subsurface well logs and gravity anomalies indicate that the EFB significantly thickens north of the fault, perhaps as a result of Pleistocene synclinal basin development.

environments. As a result, unit ΦEc likely interfingers with units ΦEn or ΦEm of Dragovich and others (2002) at depth along the western margin of the quadrangle as a result of fluvial-deltaic progradation into a Tertiary nearshore marine environment. On the basis of composition, stratigraphy, and structure we correlate these rocks with the Bulson Creek unit of Marcus (1991) and Lovseth (1975). See Danner (1957), Minard (1981), Tabor and others (1993), and Whetten and others (1988) for further information about other potential correlatives for unit ΦEc.

Mesozoic Low- to Medium-Grade Metamorphic Rocks of the Western Mélange Belt

The metamorphic basement in the map area is the Western mélange belt, a low- to medium-grade sequence of highly disrupted oceanic and arc rocks mapped widely in the region (Frizzel and others, 1987; Tabor and others, 1993, 2002). Tabor and others (1993, 2000) indicate that meta-argillite forms the mélange matrix and encloses tectonic bodies—such as metagabbro knockers—and this finding is confirmed by our mapping in many areas. However, very thick sequences of less-deformed strata are locally and regionally well exposed. In these locations, meta-argillite forms thin to thick interbeds within metasandstone or well-stratified metasediments are interbedded with metavolcanics (Dragovich and others, 2013, 2014a). The stratigraphic style, including partial Bouma sequences, indicates that the WMB metasedimentary rocks were deposited as turbidites along an accretionary wedge near volcanic centers (Jett, 1986; Frizzel and others, 1987; Jett and Heller, 1988). Locally, distinct volcanic arc flows are interbedded with volcanic-provenance metasediments and may be shallow-water forearc deposits. Although the WMB is regionally a structural amalgamation of various tectonic environments, most of the nearby WMB originated as Cretaceous to Jurassic arc volcanics and near-arc turbidites (Dragovich and others, 2014a; MacDonald and others, 2014). Feldspathic metasedimentary rocks in unit KJms$_w$ originated as turbidites eroded from a two-mica granitic source, perhaps due to exhumation and erosion of the arc's plutonic root or from other extra-regional late Cretaceous-age sources (Sauer and others, 2014; Dragovich and others, 2014a,b).

A moderate to strong syn-metamorphic foliation is subparallel to bedding and likely resulted from the shearing of turbidites in an accretionary prism. The disruption of beds, crude foliation, and (or) pervasive cataclasis is apparent in many outcrops (Frizzell and others, 1987). This primary foliation generally dips steeply to the northeast and suggests that the foliation was broadly synchronous with progressive deformation during the first accretionary shear deformation across the belt (Dragovich and others, 2014a). Variation in foliation orientation is related to post-metamorphism folding and fault-block rotation. Although internal deformation and tectonic mixing of lithologies

is minimal in some areas, large overturned folds locally record significant shortening (for example, near the Sultan River east of the map area). Whereas rocks of the WMB in the map area are predominantly metamorphosed to prehnite-pumpellyite facies, the metamorphic grade generally increases northeastward to greenschist facies (Dragovich and others, 2014a; Tabor and others, 1993, 2002). Rocks of the Lake Chaplain nappe are found in the study area and grade up to amphibolite facies.

Tabor and others (1993) assigned earliest Cretaceous and Late Jurassic ages from sheared and deformed "Buchia concentria" and "Aucella sp. (Buchia sp.)" along the Sultan River in the adjacent Lake Chaplain quadrangle. The age of these bivalves is restricted to the Tithonian (Late Jurassic)(Danner, 1957). Danner (1957) reports that a collection of Aucellus, possible Terebellina tubes, and radiolarian fossils suggests an Early Cretaceous to Late Jurassic depositional age for the phyllitic metasediments in the same area. Tabor and others (1993, 2000) and Frizzell and others (1987) reported Kimmeridgian to Valanginian (157–134 Ma) radiolarian ages from metachert beds south of the map area. Tabor and others (1993, p. 14) summarized WMB fossil age information as follows:

> "A Buchia from matrix argillite (table 1, no. 1F-3F) appears to be restricted to the Tithonian (Danner, 1957, p. 410), and more definitive radiolarian samples indicate ages from Kimmeridgian to Valanginian (Frizzell and others, 1987) that in numerical age range from 156 to 131 Ma based on the time scale of Harland and others (1982)."

Work in nearby quadrangles indicates that the WMB metasediments contain a number of Late Jurassic to Early Cretaceous fossils that are most consistent with an age range of ~134–157 Ma (Danner, 1957; Tabor and others, 1993, 2000). However, limiting depositional ages from detrital zircon studies in the WMB arkosic metasedimentary rocks indicate that these deposits are younger than previously accepted and at least locally Late Cretaceous (~74 Ma) in age (Dragovich and others, 2009a,b, 2014a; Brown, 2012; Sauer and others, 2014). The young age for this facies is consistent with exhumation of the volcanic arc and a transition to younger intrusive igneous provenances in the sediments of the accretionary prism.

KJm_W **Western mélange belt of Tabor and others (1993), undivided (Cretaceous to Jurassic)(cross sections only)**—Meta-argillite, metasandstone, greenstone, metachert, with less metadiabase, metatonalite (metatrondhjemite), slate, (banded) amphibolite and hornblendite, and phyllite, minor marble with metaquartz-diorite, and rare ultramafic rocks observed regionally (Fuller, 1925; Danner, 1957; Tabor and others, 1993, 2002; Dragovich and others, 2007, 2009a,b,c, 2010a,b, 2011a,b, 2012, 2013, 2014a). Although meta-argillite is easily eroded and does not form prominent outcrops in many areas, its voluminous presence as detritus in unit Qc_{phl} suggests that erodible metasedimentary rocks—including meta-argillite—are likely common beneath Quaternary cover.

$KJmv_W$ **Metavolcanic rocks**—Greenstone derived from metamorphosed basaltic to andesitic tuff, basaltic andesite to dacitic volcanic flows (55–70% SiO_2), with regionally common basalt flows and rare volcanic breccia; greenish gray to dark greenish black. Tabor and others (2000) described boudins of metamorphosed quartz-porphyry dikes in faintly foliated greenstone south of the study area. Regionally metamorphosed flows are mostly massive to moderately foliated metabasaltic andesite, locally with amygdaloids, pillow textures, and eutaxitic flow structures (Dragovich and others, 2009a,b,c, 2013, 2014a). Amygdaloidal metadacitic greenstone flows, characteristic of island arcs (MacDonald and others, 2014), are relatively abundant in the Lake Chaplain quadrangle and contain microlitic and eutaxitic plagioclase microphenocrysts, with a few large plagioclase phenocrysts in a homogeneous clear matrix containing interstitial quartz. Higher-grade actinolite-bearing greenschist is also found in the Lake Chaplain quadrangle.

We observed very thin to thick metatuffs interbedded within metasedimentary rocks in the present study area. These tuffs contain abundant augite with interstitial plagioclase, chlorite, opaque minerals, and a few euhedral plagioclase phenocrysts. The tuffs are similar to dacitic to rhyolitic crystal-vitric 'apple green' metatuffs (~77% SiO_2) in adjacent quadrangles. Metamorphosed basaltic to andesitic flows typically contain plagioclase microlites in a light green chloritized or saussuritzed matrix.

The only mappable greenstone body is directly southwest of the Sultan River thrust, in the southeastern part of the map area. This metabasalt contains euhedral plagioclase (~40%) interlaced with augite blades (~40%) in a chloritized glass matrix (~15%) with accessory sphene (~5%). Metamorphic minerals in the greenstone include chlorite, epidote, prehnite, calcite, and occasionally pumpellyite. This composition is similar to that of the metatuffs (Dragovich and others, 2009a,b,c, 2014a; this study). Southeast of the map area, a very thick mafic mugearitic (basaltic trachyandesite) flow interbedded with metachert has an alkali oceanic-island basalt (OIB) provenance (Dragovich and others, 2013).

$KJms_W$ **Metasedimentary rocks**—Marine feldspathic to feldspatholithic subquartzose metasandstone, silty metasandstone, meta-argillite, metatuff, and chert pebble metaconglomerate; minor metachert and rare marble; typically greenish gray, dark or bluish gray, or gray-green; weathers brown; meta-argillite is typically black or greenish blue-black to dark gray. Relict sand grains in metasandstone and meta-argillite are subrounded to angular with locally preserved graded bedding and load casts. Unit $KJms_W$ is moderately foliated and partially recrystallized to a prehnite-pumpellyite facies. A synkinematic metamorphic fabric is defined by subparallel white mica and relict clasts. Metamorphic minerals are white mica, epidote or clinozoisite, chlorite ± pumpellyite, and prehnite. We divided metasandstone in the

Lake Roesiger quadrangle into two distinct groups: feldspathic metasandstone, similar to the arkosic facies of Tabor and others (1993) and Jett and Heller (1988), and feldspatholithic to lithofeldspathic metasandstone, generally similar to the lithic petrofacies of Jett and Heller (1988). Our new geochemical, petrographic, stratigraphic, and detrital-zircon data support this general subdivision.

The feldspathic metasandstone (63–73% SiO_2) contains angular to subangular relict grains of monocrystalline quartz (30–50%), plagioclase (25–30%), and K-spar (3–20%), with minor polycrystalline quartz (0–10%), significant detrital biotite and muscovite, and few opaque minerals. These rocks locally contain some volcanic or granitic lithic grains, but are generally lithic poor and are likely derived from felsic two-mica granites. Rip-up clasts of argillite are locally abundant. The general angularity of the grains suggests 'first cycle' sediments or sediments that generally lack substantial reworking and were derived from a homogeneous, perhaps proximal, intrusive source. The arkosic facies are observed at significant sites 5Q, 36N, and 302C near the center of the quadrangle, and near the northeastern and southeastern corners of the map area.

The feldspatholithic to lithofeldspathic metasandstone in the quadrangle generally contain monocrystalline quartz (~30%), plagioclase (~25%), less polycrystalline quartz (~15%), and very little or no relict K-spar. Volcanic lithic grains (up to 20%) commonly have a felty or microlitic texture, indicative of andesitic to dacitic volcanism in the adjacent arc (Jett and Heller, 1988). This metasandstone is typically a wacke that is both compositionally and texturally immature, consistent with a near-arc volcanic provenance. Tuffaceous feldspatholithic metasandstone contains significant relict quartz and plagioclase, and likely originated as reworked crystal-vitric tuffs. Interbeds of vitric and crystal-vitric metatuff are visually distinctive in the sections with much volcaniclastic metasediments and contain relict plagioclase and quartz phenocrysts, locally with pyroxene, in a light green, semi-transparent chloritic matrix. These widespread metatuffs record a major pyroclastic contribution to the WMB, which also contains arc gabbro, volcaniclastics, and volcanic flows (see unit $KJmv_W$).

Relative to the WMB as a whole, metachert in the map area is relatively rare and was found only at significant site 26T in the southeastern part of the map area. This erosionally resistant metachert cores an elongate ridge bound by steep slopes of deformed and erodable meta-argillite and metasandstone (unit tz; significant site 302C) formed within the Woods Creek fault zone (WCFZ). The metachert along the ridge is dominantly composed of recrystallized polygonal quartz with relict recrystallized radiolarian fossils and locally banded with very thin interbeds of meta-argillite. The chert bands vary from undeformed to strongly deformed, and some bands are traversed by sub-vertical, en echelon quartz veins that trend northeast and may be related to deformation along the WCFZ. The geometry of these veins and structures indicates a shallowly plunging and northwest-trending elongation direction, consistent with strike-slip deformation.

Detrital zircon ages can be an effective means of determining the maximum depositional age of sediments. For the forearc clastic components of the WMB where there was presumably a relatively steady supply of volcanic zircons, the youngest detrital zircon age peak can approximate the age of the sedimentary deposit. Previous work in nearby quadrangles has resulted in maximum depositional ages in arkosic metasandstones of ~74 Ma (Dragovich and others, 2014a), ~87 Ma (Brown, 2012), and ~96 Ma (Dragovich and others, 2009a,b). The ~74 Ma age is significantly younger than previous estimates for the WMB, indicating that the arkosic petrofacies is locally as young as latest Cretaceous and, thus, accretionary mélange belt formation and sedimentation continued to at least the latest Cretaceous. The composition and age of the arkosic facies suggests a two-mica granitic source such as the Idaho Batholith. The youngest age population (72–87 Ma) is also consistent with unroofing of the volcanic arc and exhumation of younger intrusive igneous rocks. We obtained new detrital-zircon ages from an interbedded meta-argillite and metasandstone in the central part of the map area at age site 39S (Appendix C). This sample mostly contains subangular to subrounded grains of monocrystalline quartz (~30%), plagioclase (~25%), polycrystalline quartz (~15%), and felsic to intermediate microlitic volcanic grains (~20%). The limiting maximum depositional age for this arc-related meta-argillite is ~110 Ma. This peak, as well as the distinct peak at ~160 Ma, are similar to the published ages for the metagabbro and metatonalite intrusive rocks underlying the arc.

$KJigb_W$ **Metagabbro**—Metagabbro, quartz metagabbro, feldspathic hornblendite and gneissic amphibolite; regionally, less metatrondhjemite/metatonalite and metadiabase, and rare metaquartz-diorite are reported; greenish gray; medium to coarse grained; hypidiomorphic granular massive to slightly foliated; locally schistose or gneissose with occasional flaser gneissic fabric. In the Lake Chaplain quadrangle, metadiabase dikes locally intrude metagabbro, and there are large outcrops of metatrondhjemite. Metagabbro (44–59% SiO_2; possibly enriched by metamorphism) generally contains actinolized hornblende (40–70%) and plagioclase (35–45%) with opaque minerals including magnetite. Metamorphosed quartz gabbro has a similar composition, but with up to 10–12% quartz. Amphibolites contain hornblende (40–45%), plagioclase (40–45%), and opaque minerals (~5%) and display a strong syn-metamorphic schistose fabric with aligned hornblende. Some amphibolites contain up to 10% quartz. Tabor and others (1993) reported that metagabbro near Woods Creek contains

hypersthene and clinopyroxene relicts. Although mostly poorly exposed, we interpret amphibolite layers to be either thick metagabbroic melanosomes or metamorphosed mafic dikes within the metagabbro. However, we cannot completely exclude the possibility that the protolith was mafic country rock that was subsequently metamorphosed, similar to other gneissic amphibolites (Dragovich and others, 2009c). Metamorphic minerals include hornblende, actinolite, prehnite, pumpellyite, chlorite, epidote, sphene, and calcite.

Metagabbroic rocks are faulted against metasedimentary and metavolcanic rocks, and are tectonic fragments within the mélange belt (Tabor and others, 1993; Dragovich and others, 2013). Deformed quartz metagabbro in the large rock pit at significant site 2A has steeply plunging slickenlines related to faulting along the Three Lakes Hill fault (Fig. 5). Metagabbro and metatrondhjemite in the Lake Chaplain area are confined to a thrust sheet termed the Lake Chaplain nappe (Fig. 6) by Dragovich and others (2014a). Metagabbro west of the Sultan River and directly east of the quadrangle has a hornblende K-Ar age of 118 ±7.7 Ma (Tabor and others, 1993). They also reported regional U-Th-Pb zircon ages of 150 to 170 Ma for metagabbro and metatonalite, indicating that the plutonic rocks are minimally the same age as, or older, than the enclosing Jurassic and Lower Cretaceous metasedimentary rocks.

Figure 5. Slickensided face of metagabbro (unit $KJigb_W$) at significant site 2A, located in a rock quarry directly south of Three Lakes Hill. The deeply excavated and active rock pit exposes a fault zone (unit tz) that is subsidiary to the Three Lakes Hill fault. The faults and fractures form tectonic zones that thicken north of the pit. These faults strike east-west, are sub-vertical to vertical, and locally have slickenlines that plunge moderately to steeply southeast (slickenline rake highlighted in yellow). The slickenlines are consistent with vertical components of slip inferred on the nearby Three Lakes Hill fault.

Holocene to Tertiary Tectonic Zones

tz, Qtz **Tectonic zone**—Cataclasite, fault breccia, clay-rich fault gouge, protomylonite, and moderately to strongly slickenlined, fractured, and veined rocks in fault zones; green and yellow to orange to variously colored, mottled, and altered. Broadly, unit tz is mapped in distinct areas of brittle or brittle–ductile deformation along two types of faults: high-angle faults with Tertiary and younger deformation, such as the Woods Creek fault zone (WCFZ), and Cretaceous–Jurassic-age WMB thrust faults—such as the Sultan River thrust—where thick zones of unit tz are well-exposed in the eastern part of the map area around significant site 25H. See the mapping of tectonic zones associated with the WCFZ and the Sultan thrust in the adjacent Lake Chaplain quadrangle.

Deformed metagabbro in the Sultan River thrust is fractured and contains a retrograde mineral assemblage; primary minerals are replaced by pumpellyite, quartz, with less epidote. The rock is traversed by a retrogressive sub-planar shear fabric of fractures or protomylonite zones which are partially defined by secondary chlorite.

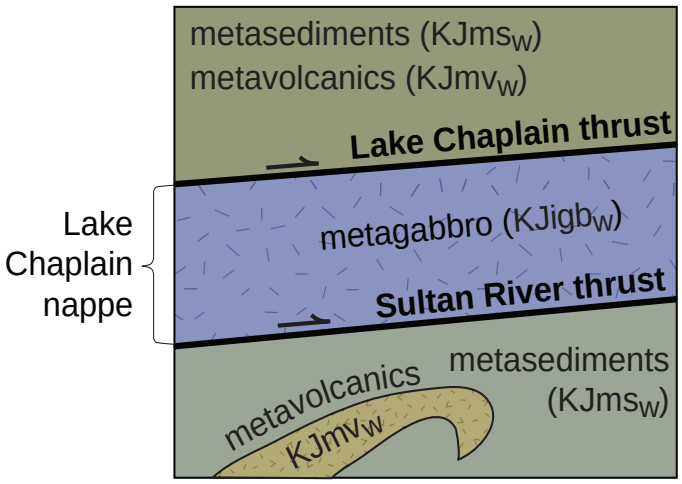

Figure 6. Structural block diagram showing the Lake Chaplain nappe (LCN) and the Sultan River and Lake Chaplain thrusts of Dragovich and others (2014a). West of the map area, low-grade metasedimentary and metavolcanic rocks (for example, units $KJms_W$ and $KJmv_W$) underlie and overlie the LCN in the Sultan River area. The LCN contains disrupted arc metagabbroic rocks (unit $KJigb_W$) in the map area. Geophysical modelling suggests that the metagabbro and LCN are not laterally continuous across the map area. Although the LCN and Sultan River thrust appear uninterrupted within a wide zone northeast of the Woods Creek fault zone, these fault strands dissect metagabbro of the LCN locally. This deformation has resulted in northwest displacement of the metagabbro, producing tabular cigar- or watermelon-seed-shaped bodies. Overall, the deformation has created sub-horizontal long axes that trend northwest, sub-parallel to the WCFZ shear direction.

Figure 7. Deformed metagabbro (unit tz) at significant site 25H, located directly above the Sultan River thrust fault. Nearly continuous cut-slopes in a logging road have exposed thrust fabrics that intensify towards the Sultan thrust fault. These well-defined, brittle-ductile fabrics are semi-penetrative to penetrative, with well-developed cataclasite or mylonite at millimeter to centimeter scale. Shear-induced retrogression (metamorphic retrogression that accompanies semi-penetrative shear) of the metagabbro has resulted in local replacement of hornblende and plagioclase by pumpellyite and chlorite ± epidote. This process has produced a sub-planar protomylonitic fabric and secondary quartz veins. Petrography and field observations indicate the thrust fabric formed between brittle and ductile P-T conditions. The fabric forms S-C mylonite intersections, from which we infer a general easterly vergence during thrusting.

Secondary quartz is also found in veins. Hornblende is retrogressed but plagioclase is locally preserved (Fig. 7). Unit tz mylonitic rocks have a retrogressive chloritic low-temperature shear foliation, sutured quartz, and plagioclase—indicative of semi-ductile shear. The relationship between regional metamorphism and shear fabrics indicate a late-to-post metamorphic thrusting in the WMB. Widespread calcite and quartz veins are prominent within most mapped tectonic zones, particularly along thrust and reverse faults (Dragovich and others, 2014a).

Shear fabric along high-angle faults varies from brittle gouge to chloritized protomylonite. Zones of hydrothermal alteration were noted along some faults within the WCFZ, but unlike nearby mapping, we did not depict these as separate map units. Common alteration minerals include chlorite and calcite. The alteration locally includes some opal or secondary quartz, zeolite, white mica, biotite, and (or) clay. K-spar with sulfide mineralization is also locally conspicuous in the WCFZ. Alteration mineral assemblages are principally propylitic but may include phyllitic and potassic assemblages.

Quaternary tectonic deformation (unit Qtz) was mapped in one area along the Dubuque Road fault in the western part of the quadrangle at significant site 23N. At this location, Vashon-age till contains a sub-vertical shear fabric intruded by sand dikes (Fig. 2). Quaternary deformation is also inferred in the subsurface on Cross Section B, adjacent to potentially active faults—such as the Three Lakes Hill fault—where early- to mid-Pleistocene sediments of the EFB are deformed. For further information, see *Dubuque Road fault.*

GEOCHEMISTRY

We obtained major and trace element geochemistry for 13 Quaternary sand and 9 rock samples to study the composition, provenance, original tectonic setting, and depositional environment in and around the Lake Roesiger quadrangle. Appendix D contains analytical methods and geochemical data.

Western Mélange Belt

We analyzed 8 new WMB samples (1 metagabbro, 1 amphibolite, 4 metasandstone, and 2 meta-argillite) for this study and the results are reported in Appendix D. This work has increased the WMB dataset to 26 samples (Dragovich and others, 2009a,b, 2013, 2014a, this study). The WMB has undergone prehnite-pumpellyite to amphibolite-facies metamorphism, and many important geochemical elements are mobile under these conditions (for example, K and Ca; Cann, 1970; Pearce, 1996, 2014). Because of this mobility, we only utilize elements that are immobile up to and including amphibolite-facies metamorphism (Pearce, 1996, 2014).

The metagabbro sample from this study (2A; Appendix D) is plotted on Figure 8A because the element ratios for this diagram are not greatly affected by mineral fractionation or accumulation (Pearce, 1996). The metagabbro and amphibolite from this study have the same low Nb/Yb ratios as a majority of the previously studied WMB samples (Fig. 8A)(Dragovich and others, 2013, 2014a; MacDonald and others, 2014) and these two samples plot in the volcanic arc field due to their high Th/Yb ratios (Fig. 8A). Their position on this plot suggests that these new samples originated from a volcanic arc with a depleted mantle source (Fig. 8A) (Pearce, 1996, 2008, 2014; McDonough and Sun, 1995). These new data are consistent with previous interpretations in nearby areas (Dragovich and others, 2009a,b, 2013, 2014a; MacDonald and others, 2014). Few meta-igneous samples from the WMB have non-arc geochemical affinities (Fig. 8A). Vance and others (1980) and Tabor (1994) also identified volcanic arc as the primary geochemical affinity for WMB meta-igneous samples.

Metasandstone from this study and Dragovich and others (2009a,b, 2014a) has high V and Sc and plots in the oceanic arc-derived sediment field on Figure 8B. These samples also plot in the mafic and intermediate igneous provenance field on the discriminant function diagram of Roser and Korsch (1988), and in or around the fields defined by modern back-arc basin volcaniclastic sediments (Fig. 8C). Additionally, these sample also have low Hf, Th, and Zr (Appendix D). Together, these data suggest that the provenance for the metasedimentary samples was a volcanic island arc, with the mafic detritus mostly derived from the

arc (Bhatia and Crook, 1986; Roser and Korsch, 1988; McLennan and others, 1990). The low Hf, Th, and Zr suggest that recycled or cratonic detritus was not a major component (Bhatia and Crook, 1986; McLennan and others, 1990).

Two arkosic samples (5Q and 302C; Appendix D) have lower Sc and V, and higher Th and Zr than other WMB metasedimentary samples (Fig. 8B). These samples, along with another arkosic (sample 36N), plot in the intermediate igneous provenance field (Fig. 8C) and suggest a continental arc provenance (Bhatia and Crook, 1986; Roser and Korsch, 1988; McLennan and others, 1990). This interpretation is supported by data from Dragovich and others (2014a) and Sauer and others (2014) that tentatively suggest the Idaho batholith may have been the source of ~74 Ma zircons, enriched Nd isotopes, and two-mica granitic detritus in sample 13–35J. The single meta-argillite sample from Dragovich and others (2014a) has very high V and Sc, and very low Th and Zr has a very mafic arc source (Fig. 8C)(Bhatia and Crook, 1986; Roser and Korsch, 1988; McLennan and others, 1990).

The geochemistry of WMB metasedimentary rocks is consistent with deposition in a back-arc basin or forearc setting within an accretionary prism. Detrital zircon age distributions, fossil ages, petrography, and geochemistry all suggest that multiple arcs of different ages may have contributed detritus to the WMB metasedimentary rocks. The inference that the meta-intrusives were originally arc plutons is consistent with the petrologic variation (from gabbro and amphibolite to quartz diorite, quartz amphibolite, tonalite, and trondhjemite) and the igneous provenance of most metasedimentary rocks (MacDonald and others, 2014). Evidence from field relations, petrology, the youngest detrital zircon age population, and geochemical information confirm that, although the belt is dominated by structurally disseminated arc material, the WMB also contains volcanic island arc, oceanic island (hotspot), and local oceanic ridge deposits all juxtaposed along an active tectonic margin (Vance and others, 1980; Tabor, 1994; Brown, 2012; Dragovich and others, 2014a; MacDonald and others, 2014; Sauer and others, 2014). This predominantly arc setting is consistent with previous WMB studies and is likely correlative with the De Roux unit and Russell Ranch complex in the central Washington Cascade Range (Miller, 1985; Frizzell and others, 1987; Jett and Heller, 1988; Miller, 1989; MacDonald and others, 2009).

Rhyolite of Hughes Lake

We analyzed the geochemistry of one sample from unit Mvr (site 31S) near Hughes Lake and the results are reported in Appendix D. This is the same sample that was dated at ~23.3 Ma (Appendix C). This high-K and calc-alkaline sample plots in the rhyolite field on the total alkali silica diagram of Le Maitre and others (2002)(SiO_2 = 75.71 wt %). It has an aluminum saturation index of 1.24 (molecular Al/[Ca-1.67P+Na+K]) and molecular Al/(Na+K) = 1.29 which classifies the sample as peraluminous (Frost and others, 2001). Some trace elements (U, Ba, and Pb, for example) are 100-times greater than primitive mantle sources (McDonough and Sun, 1995). The high Th/Yb ratio of this sample is typical of arc settings and the Nb/Tb ratio of this sample suggests an enriched mantle source (Fig. 8A)(McDonough and Sun, 1995; Pearce, 1996, 2008, 2014). The peraluminous geochemistry and very high trace element values suggest that this sample assimilated continental crust and formed from the fractionation of enriched magma in a continental arc setting. This interpretation is consistent with the abundant xenoliths of WMB metasediments found in this sample that suggest significant incorporation and melting of surrounding mélange belt country rock.

Quaternary Sand Deposits

We have compiled a large geochemical dataset from our previously published mapping studies (n = 136) and add 13 new samples; these data now cover 8 quadrangles (Dragovich and others, 2007, 2009, 2010a,b, 2011a,b, 2012, 2013, 2014a,b, this study). These samples include Pleistocene ('ancient') and modern nonglacial alluvium, as well as various glacial deposits. We have been able to discriminate between locally derived deposits and deposits that have a fluvial Skykomish or Snoqualmie provenance (SP) based on their Sc and V concentrations (Fig. 8B)(Dragovich and others, 2010a,b, 2011a,b). We are also able to generally discriminate between glacial and nonglacial sediments using trace element ratios (Fig. 8D)(Dragovich and others, 2010a,b, 2011a,b, 2014a).

The Holocene and Pleistocene alluvium of the Skykomish River and Pleistocene alluvium of the Pilchuck River both have a Cascade Range provenance (SP and PP; Table 1). These deposits, in addition to the Holocene alluvium of Woods Creek (units Qa, Qcws, and Qcph), have Sc and V values that suggest an intermediate igneous source (Fig. 8B)(Bhatia and Crook, 1986). These three units also plot transitionally between intermediate and mafic igneous provenances on Figure 8C. The high Pb/Yb ratios of the ancient Pilchuck and Skykomish alluvium samples (Fig. 8D) suggest a granitic source (McLennan and others, 1990; McDonough and Sun, 1995). Tabor and others (1993) report that the mafic to felsic Tertiary intrusive rocks, such as Grotto and Index batholiths east of the study area, are intermediate in composition. Together, the geochemistry and petrography of units Qcws and Qcph (Figs. 8B and 8C) suggests they were most likely derived from these intermediate plutons.

A strong WMB provenance is observed petrographically and geochemically in the modern alluvium of Woods Creek and Pleistocene alluvium of the Pilchuck River (Appendix A; Table 1). On Figure 8B, Pleistocene Pilchuck alluvium (unit Qcph) is transitional between locally derived alluvium (LP; Table 1) and other provenances. The modern alluvium (unit Qa) of Woods Creek plots near unit Qcph on Figure 8B, and also near locally derived sand deposits of unit Qcphl on Figure 8C and, in particular, on Figure 8D. These relations are consistent with the petrography of the alluvium of Woods Creek which is recycled mica-bearing sediment, similar to PP deposits, but with significant locally derived WMB metasedimentary detritus (25%). In general, the modern alluvium of Woods Creek and Pleistocene alluvium of the Pilchuck River had a mixed geochemical provenance, consisting of a plutonic source and the WMB. In contrast, the geochemistry of Pleistocene alluvium of the Skykomish River suggests that it was derived mostly from plutonic sources. These interpretations agree with petrography and are consistent with previous interpretations in adjacent quadrangles.

Pleistocene alluvial fans along the boundaries of the Explorer Falls basin (unit Qcphl) have abundant WMB metasedimentary detritus and are classified as LP provenance (Table 1).

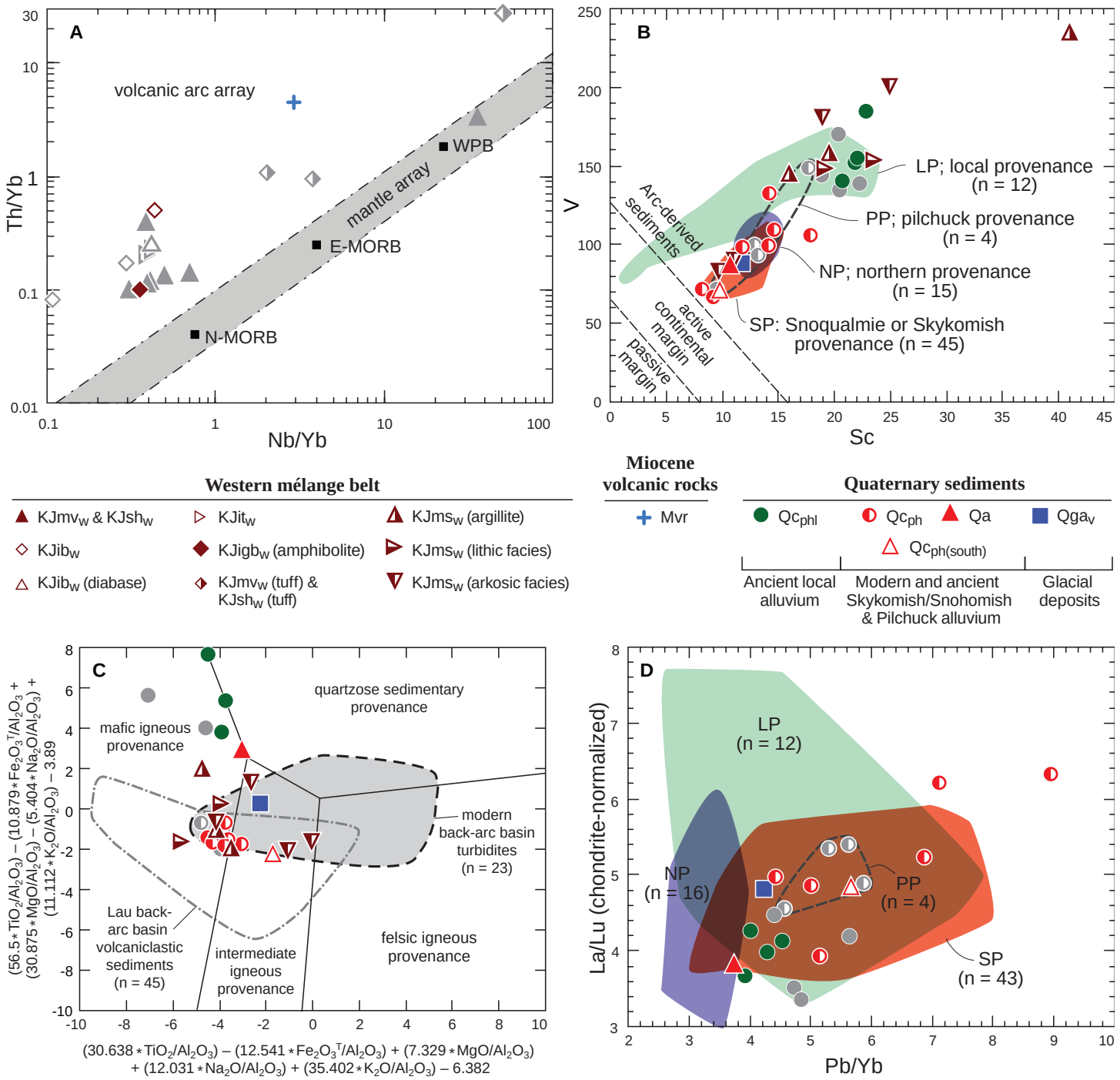

Figure 8A. Thorium/Ytterbium (Th/Yb) vs. Niobium/ Ytterbium (Nb/Yb) diagram of Pearce (1982, 2008) adapted for WMB meta-igneous samples and rhyolite of Hughes Lake. Note the primarily arc composition of these meta-igneous samples. Data from Dragovich and others (2009a,b, 2013, 2014a)(gray symbols) and this study. E-MORB, enriched mid-ocean ridge basalt; N-MORB, normal mid-ocean ridge basalt; WPB, within-plate basalt.

Figure 8B. Vanadium (V) vs. Scandium (Sc) provenance diagram of Bhatia and Crook (1986) for Quaternary sand samples and metasediments of the WMB. LP, local provenance from Tolt River and Youngs–Elwell Creek; NP, northern provenance deposited during continental glaciations; PP, ancient Pilchuck River provenance; SP, Skykomish and Snoqualmie Rivers provenance. Colored fields for NP, SP, and LP are from Dragovich and others (2007, 2009a,b, 2010a,b, 2011a,b, 2013, 2014a)(gray symbols). See Table 1 for more provenance information. n, number of samples.

Figure 8C. Roser and Korsch discriminant function diagram for Quaternary samples and metasediments of the WMB (Roser and Korsch, 1988). Data from Dragovich and others (2014a)(gray symbols) and this study. Note that the ancient local, modern Skykomish, and ancient Pilchuck River samples plot primarily in the mafic igneous provenance field, consistent with their petrography (Table 1).

Figure 8D. Chondrite-normalized Lanthanum/Lutetium (La/Lu) vs. Lead/ Ytterbium (Pb/Yb) diagram for Quaternary sand samples. Chondrite normalization values are from McDonough and Sun (1995). Provenance field names (LP, NP, PP, and SP) are the same as Figure 8B and in Table 1. Colored fields for NP, SP, and LP are from Dragovich and others (2007, 2010a,b, 2011a,b, 2013, 2014a)(gray symbols). n, number of samples; Gray symbols are LP and PP data from the Lake Chaplain area (Dragovich and others, 2014a). See Table 1 for more provenance information. n, number of samples.

These deposits have high Sc and V (Fig. 8B) and plot in the mafic igneous provenance field (Fig. 8C). The geochemistry of the Pleistocene deposits is similar to that of the meta-igneous and metasedimentary WMB bedrock (Vance and others, 1980; Tabor, 1994; Dragovich and others, 2014a; MacDonald and others, 2014), with LP provenance samples plotting near WMB metasediments on Figures 8A and 8B. The geochemistry supports the petrographic observation that the WMB provided the majority of the detritus for unit Qc_{phl}. These petrographically distinct sands can be distinguished from SP- and PP-provenance deposits in the study area by their higher Sc and V, more mafic sources, and lower amount of SiO_2 (Figs. 8B and 8C; Appendix D).

Advance glacial outwash (sample 40D, unit Qga_v) directly overlies unit Qc_{ph} and contains significant amounts of this older unit as detritus within the outwash. This sample plots in the intermediate field on the Roser and Korsch diagram and has a high Pb/Yb ratio (Figs. 8C and 8D). This sample has Sc and V values that are similar to other glacially derived sediments with a northern provenance (Fig. 8B), but plots near sediments with a Pilchuck River provenance (PP) on Figures 8B and 8C as expected from its stratigraphic position and erosive basal contact.

ISOSTATIC GRAVITY AND AEROMAGNETIC ANALYSES

High-quality aeromagnetic data define the geomagnetic anomalies in the quadrangle (Fig. M1; Blakely and others, 1999), and a combination of published and unpublished regional gravity data (see Anderson and others, 2006, for an overview of published data) constrain the isostatic gravity anomalies. We use both of these data sets to constrain our structural interpretations. Additional gravity data collected in 2013 and 2014 supplement the existing data and define more detailed anomalies in the quadrangle. Extensive sampling and measurement of density and magnetic susceptibility for units in this and five neighboring quadrangles (Dragovich and others, 2010a,b, 2011a,b, 2012, 2013, 2014a) provide strong support for predicting geophysical anomalies in terms of subsurface geologic units (Fig. M2), as well as a means for interpreting map-view anomalies in terms of subsurface geologic units and faults.

Negative gravity anomalies predominantly arise from Eocene–Oligocene to Quaternary basins. These lows include the Explorer Falls basin (EFB), and the larger and older Everett basin. The geophysical signals of the EFB and Monroe syncline merge with those from the Everett basin along the western part of the map area. Gravity modeling indicates that Eocene–Oligocene basin fill in the western half of the quadrangle continues west into the deep Everett basin. Consistent with our approach for other models in the region (for example, Dragovich and others, 2013, 2014a), we find that we must use low densities for modeling tectonic zones (unit tz) in the cross sections in order to achieve good fits between the model and geophysical observations.

Geophysical anomalies arising from basement rocks vary depending on their lithology. In particular, metagabbro (unit $KJigb_w$) creates large positive magnetic anomalies and metasediments (unit $KJms_w$) create relatively low gravity anomalies (Dragovich and others, 2014a). The association of metagabbro with strong aeromagnetic highs is supported by outcrops collocated with the strongest magnetic highs (GB1–4 on Fig. M1)—a relationship also observed in Lake Chaplin quadrangle—and high magnetic susceptibilities from hand-sample and outcrop measurements (Dragovich and others, 2014a).

The general distribution of metagabbro on the cross-sections (Fig. M2) is required to match the aeromagnetic data, but the exact shape and thickness are uncertain, and several geometries are plausible. This uncertainty is compounded by large variation in hand-sample magnetic susceptibility, and the observation that weathering and deformation lead to hand sample magnetic susceptibility that is lower than that required in the deep subsurface for geologically reasonable structural models (Dragovich and others, 2014a). Despite these uncertainties, a few aspects of the distribution of metagabbro are more certain. Most metagabbro is thick (~450 m or more) and bound by near-vertical faults, as shown by extremely steep gradients along most aeromagnetic anomaly edges (Fig. M2). A major exception to this is the northeast edge of anomaly GB1 (Fig. M2). Though an abrupt change in aeromagnetic anomaly values suggests an abrupt change in thickness across Woods Creek fault no. 5, the remainder of this gradient northeast of the fault is wide and gradual, suggesting that the metagabbro gradually tapers in the subsurface to the northeast in a wedge shape. This interpretation is supported by exploratory modeling across this feature. The location and orientation of sharp aeromagnetic gradients indicate that faults which bound metagabbro strike northwest. This observation helped constrain the location and orientation of the various strands of the Woods Creek fault zone. The sub-horizontal fault below the metagabbro on both geophysical models (Figs. M1 and M2)—and the underlying wedge-shaped body northeast of Woods Creek fault no. 5—is interpreted as the Sultan River thrust of Dragovich and others (2014a), which is mapped at the surface in the southeastern part of the quadrangle.

Although various geophysical solutions are possible, available information suggests that the metagabbro in the Woods Creek fault zone is tabular and (or) cigar shaped and that the long GB1 anomaly is dissected by faults. We further interpret these anomalies to potentially indicate that metagabbro is offset by reverse faults, including the Three Lakes Hill and Carpenter Creek faults, as well as a transfer fault in the Woods Creek fault zone. However, given the complex tectonic history of the WMB, the distribution of geophysical anomalies could also result from other fault geometries.

Based on geologic mapping, metasedimentary rocks (unit $KJms_w$) comprise a larger percentage of Western mélange belt rocks compared to past studies in nearby areas (for example, the Sultan and Lake Chaplain quadrangles). Areas with predominantly metasediments in the subsurface appear to coincide with subtle gravity lows, in accordance with its slightly lower density in hand sample (Dragovich and others, 2014a). However, given the large effect of thick Oligocene and Quaternary sediments on the gravity anomalies, the more subtle effects of unit $KJms_w$ in the subsurface only manifest through the modeling process. For example, a large region of metasediment is required in model A–A' (Fig. M2) to fit the gravity anomaly on the east side of the cross section.

A general disassociation of gravity anomalies with strong magnetic anomalies suggests that the gravity is predominantly affected by Eocene–Oligocene basins. It is interesting to note that

while the EFB is generally associated with an area of lower gravity, in many places the lowest gravity anomalies do not appear to coincide with the areas of thickest Quaternary sediment, as constrained by geologic mapping and well data. We conclude that these areas are largely underlain by thicker Eocene–Oligocene-age sediment (unit ΦEc), an interpretation that is supported by the presence of unit ΦEc below a blanket of Quaternary sediment in many wells. An abrupt change in the thickness of unit ΦEc (for example, A–A' in Fig. M2) may account for strong gravity gradients on the edges of these zones of lower gravity (OL on Fig. M1). In many of these areas, we do not interpret faults continuing to the surface because there is no evidence for either Quaternary-age deformation nor abrupt thickness changes in Quaternary sediments. Additionally, while many of these gradients trend north or northwest, a few trend northeast (NE1 and NE2 on Fig. M1), similar to the inferred strike of faults associated with the EFB. NE1 is likely uplifted basement due to EFB inversion along the Three Lakes Hill fault whereby rocks of the WMB were exhumed during reverse faulting (Fig. M2, B–B').

Gravity lows within or bordering the Monroe syncline (label MS1 on Fig. M1) are clearly associated with zones of both thicker unit ΦEc and Quaternary sediment. We interpret this as an indication that the Monroe syncline is a long-lived structural feature. Steep gravity gradients bordering these lows indicate steeply dipping faults along the edge of the Monroe synclinal basin (Fig. M1). These high-angle faults are continued from the adjacent Monroe quadrangle and include the Johnsons Swamp fault zone. M2 is a poorly understood northeast-trending basin that might be bound by northeast-striking faults. We speculate that this is a transtensional fault zone, similar to the Cherry Creek fault zone of Dragovich and others (2013, 2014a) that may accommodate strain between the Johnsons Swamp and Woods Creek fault zones.

There is an important correlation of weak aeromagnetic highs with thick accumulations of Quaternary sediment (SP1–4 on Fig. M1) that broadly correspond to the tilted SP-provenance deposits on the northern limb of the Monroe synclinal basin, similar to observations in the Lake Chaplain quadrangle. We account for this correlation by increasing the magnetic susceptibility of units containing substantial Pleistocene SP-provenance deposits, such as units Qgn_{pf}, Qc_{o}, and Qc_{ws}. This approach helped us fit the aeromagnetic data more closely. Edges of thick Quaternary sediment are clearly defined by the gravity data along the Woods Creek fault and the Johnsons Swamp fault zone and may indicate higher rates of neotectonic activity. Similar to the mapping of the Cherry Creek fault zone in the Lake Chaplain and Sultan quadrangles, lower density fault damage zones (unit tz) along the Woods Creek fault zone appear to be required by geophysical modeling and may suggest more pervasive shallow crustal cataclasis compared to other faults in the map area. If confirmed by other methods, it suggests that the WCFZ is a major zone of deformation.

MESOZOIC TECTONICS AND THE WESTERN MÉLANGE BELT—SELECTED NOTES

In the study area, metasedimentary and metavolcanic rocks are predominantly in the prehnite-pumpellyite facies, with greenschist to amphibolite facies metasedimentary and metavolcanic rocks found in the highest grade part of the WMB outside of the map area. This is a regional grade change whereby, "the eastern part of the Western [mélange] belt is more thoroughly metamorphosed than the rest of the belt; in the general area of the lower Sultan Basin the disrupted rocks grade to slate, phyllite, and semischist and contain minor greenschist and chert" (Tabor and others, 1993, p. 12). The WMB contains outcrop- to mountain-sized phacoids of metagabbro, metadiabase, amphibolite and metatonalite that are metamorphosed to the greenschist or amphibolite facies. Dragovich and others (2014a) suggested that some or all of the meta-intrusive rocks lie within the Lake Chaplain nappe, a structural unit bound by the Sultan River and Lake Chaplain thrusts and composed mostly of Jurassic (150–170 Ma) metagabbro and metatonalite (Fig. 6). The intensity of deformation in the mélange is greatest in the Lake Chaplain nappe where the meta-intrusive rocks appear to be deformed at most scales. These higher grade meta-igneous rocks are structurally confined to the Lake Chaplain nappe, locally resulting in "jumps" in metamorphic grade. One of several problems related to deciphering the WMB structural and metamorphic history is whether the schistose to gneissic fabric in the meta-intrusive rocks of the nappe is tectonic in origin or partly to wholly an igneous fabric. Because the higher-grade meta-igneous rocks of the Lake Chaplain nappe are thrust over low-grade metasediments and metavolcanics, we suspect that the fabric for meta-igneous rocks is metamorphic and not igneous. Therefore, the juxtaposition of low-grade rocks above and below is most likely a result of late- to post-metamorphism movement.

Tabor (1994) and others suggested that the Eastern and Western mélange belts were thrust over the Northwest Cascades System—a set of nappe-bounding thrusts and associated structures containing Mesozoic and older rocks, likened to a regional mélange by Brown (2012). Tabor and others (2002) indicate that the eastern mélange belt is thrust over the Western mélange belt. These relationships indicate that both regionally, and locally or intraformationally, thrusting appears to be the primary structural model for obduction of accretionary rocks.

Within the WMB, the Sultan River thrust is the fault that bounds the lower part of the Lake Chaplain nappe and is mapped in the southwestern part of the Lake Roesiger quadrangle. This nappe was defined by Dragovich and others (2014a) and is an informal structural unit within the WMB. In this area (significant site 25H), metagabbro is thrust over metasediments along a thick zone of sheared metagabbro (unit tz) containing thrust fabrics (Fig. 7). The orientation of Cretaceous faults, shear fabrics, and folds—including isoclinal folds in the Lake Chaplain quadrangle—all suggest a general southwest or northeast-directed thrust direction during progressive formation of the accretionary prism. Sub-horizontal and west-southwest-trending mineral stretching lineations in a mylonitized metatonalite along the Sultan River thrust in the Lake Chaplain quadrangle also support this interpretation. We suspect that the relationships seen in this area—of older Jurassic–Cretaceous arc components being thrust over younger metasediments with a granitic source—may be representative of the WMB as a whole, but further work is needed.

Substantial post-Cretaceous vertical offset can be inferred from the vertical distribution of meta-intrusive rocks if these

rocks are indeed confined to the Lake Chaplain nappe. In the current map area, the WCFZ has displaced meta-intrusive rocks of the Lake Chaplain nappe down-to-the-west towards the Everett basin (Cross Sections A and B). This relationship is best demonstrated along the Dubuque Road fault, where reverse motion has likely resulted in the emergence of metagabbro in the hanging wall (Fig. 4). In the Lake Chaplain quadrangle to the east, the Blue Mountain klippe exposes the nappe at high elevation. Stratigraphic relations and geophysical anomalies are all consistent with down-to-the-west oblique slip on the Cherry Creek (CCFZ) and Woods Creek fault zones (WCFZ). The west tilt of the Pleistocene EFB in the northwest Lake Chaplain quadrangle may also result from vertical offset along the CCFZ and (or) uplift of the Cascade Range. In this way, oblique movement within these broad strike-slip fault zones has tilted, uplifted, and deformed the Lake Chaplain nappe, resulting in overall east-side uplift of the Cascade Range. These interpretations, combined with our geophysical modelling, suggest that the Lake Chaplain nappe resides at depth—but probably not as a continuous structural unit—within the eastern part of the Everett basin.

Our interpretation of east-directed under-thrusting during progressive accretion is opposite to the expected regional vergence. It is possible that the Lake Chaplain nappe was obducted onto the accretionary prism, or backthrusting in the accretionary prism exhumed the higher-grade Lake Chaplain nappe late in the evolution of the mélange belt. Further work is required to clearly define the tectonic emplacement of the WMB, including the relationships between metamorphism and structural fabrics. Further work is also needed to determine if meta-intrusive rocks outside of the Lake Chaplain and Lake Roesiger area are also confined to a nappe, and to determine the kinematics and vergence history of the high-grade rocks within the nappe.

EOCENE TECTONICS AND THE PROTO-EXPLORER FALLS BASIN

Structural and stratigraphic data, facies trends, and provenance relationships indicate that several east-west trending fluvial and basins within western Washington were probably bounded by normal or oblique-normal faults in the early Eocene. Regionally, this is important for basins such as the Chuckanut Basin in Whatcom County, where the basin-bounding Boulder Creek fault was a normal fault during deposition of the early Eocene Bellingham Bay member. Fluvial arkose of this member contains distinct exotic detritus from the Omineca Belt of north-central Washington and little locally derived sediment. Later Eocene units had a more locally derived lithic-dominated provenance as a result of basin instability (Johnson, 1982; Evans and Ristow, 1994). The Boulder Creek fault is now an active reverse fault in response to north–south compression (Kelsey and others, 2012; Siedlecki, 2008, Barnett and others, 2006). Directly south of the Lake Roesiger quadrangle, the Monroe fault was demonstrably a basin-bounding normal fault during deposition of the Eocene-age volcanic rocks of Mount Persis. Similar to the Boulder Creek fault, the Monroe fault was later rejuvenated by regional north-south compression as a reverse structure, and is potentially active (Dragovich and others, 2011a,b, 2013, 2014b). The lower Skykomish River valley parallels this major reverse fault which juxtaposes Eocene volcanic rocks against Jurassic–Cretaceous rocks of the WMB.

Although not shown in the cross sections, we suspect that early Eocene arkosic sandstone—correlatives of the Chuckanut or Swauk Formation—locally underlie unit ΦEc in the Explorer Falls basin (EFB). Early Eocene feldspathic fluvial sandstone deposits are mapped in the nearby Lake Chaplain quadrangle and contain little or no detritus from the WMB. This lack of WMB detritus suggests that the deposits predate the development of the EFB. These feldspathic sandstones contain monocrystalline quartz (~40%), K-spar (~25%), plagioclase (~20%), and some polycrystalline quartz, muscovite, and biotite and were exposed as a result of westward tilting and erosion of the easternmost part of the EFB. The sandstone deposits are compositionally mature and similar to the unnamed feldspathic sandstone of Pilchuck valley that Tabor and others (2002) correlated with the oldest part of the early and middle Eocene Swauk Formation (about 50 Ma), or with the lowest part of the Chuckanut Formation of Evans and Ristoe (1994). Alternatively, they may correlate with fluvial sandstone of the Puget Group that is mapped in the Monroe syncline by Dragovich and others (2011a). These deposits also seem slightly more compositionally mature than micaceous sandstone of unit ΦEc near the axis of the EFB (significant site 37N), which contain less monocrystalline quartz (~30%) and K-spar (~5%), but more polycrystalline quartz (~15%) and lithic grains (~15%).

Although much work remains, we speculate that these early Eocene sedimentary rocks are restricted to the oldest part of a wide transtensional basin between the Pilchuck River fault of Tabor and others (2002) and the Three Lakes Hill fault (Fig. 1). The compositional maturity and lack of significant amounts of locally derived detritus within these early Eocene deposits suggests relatively uninterrupted basin growth, and that local uplift and basin instability did not occur until later.

Sandstone provenance in younger unit ΦEc deposits suggests a significant change to this regional trend. Eocene feldspathic sandstone of unit ΦEc is mapped near the axis of the Pleistocene-age EFB. These Eocene deposits are overlain by or interfinger with later Eocene or Oligocene lithic sandstone that has a strong local WMB provenance and lies adjacent to the Three Lakes Hill fault (significant site 11P). The amount of WMB-derived metasedimentary rock fragments (60–80%) is similar to the amount in unit Qc_{phl} (70–95%) and this population of grains is conspicuously absent from the Eocene feldspathic sandstone deposits. These relationships are best explained by normal faulting along the Three Lakes Hill fault which shed abundant WMB detritus to the basin (Fig. 9) and probably reflects the transtensional basin development in the early Eocene that is inferred regionally.

Lithic-rich sandstone deposits near the Three Lake Hill fault in the Eocene–Oligocene and Pleistocene suggest that this basin is a structurally recurring phenomena. Regional information suggests that the basin was probably inverted after the Eocene. Our data show that the basin was renewed in the early- to mid-Pleistocene or Pliocene, and filled with a thick accumulation of sediment. Since the mid to late Pleistocene, the basin has been inverted yet again, and we suspect that this cycle of basin development followed by inversion is a persistent theme in western Washington.

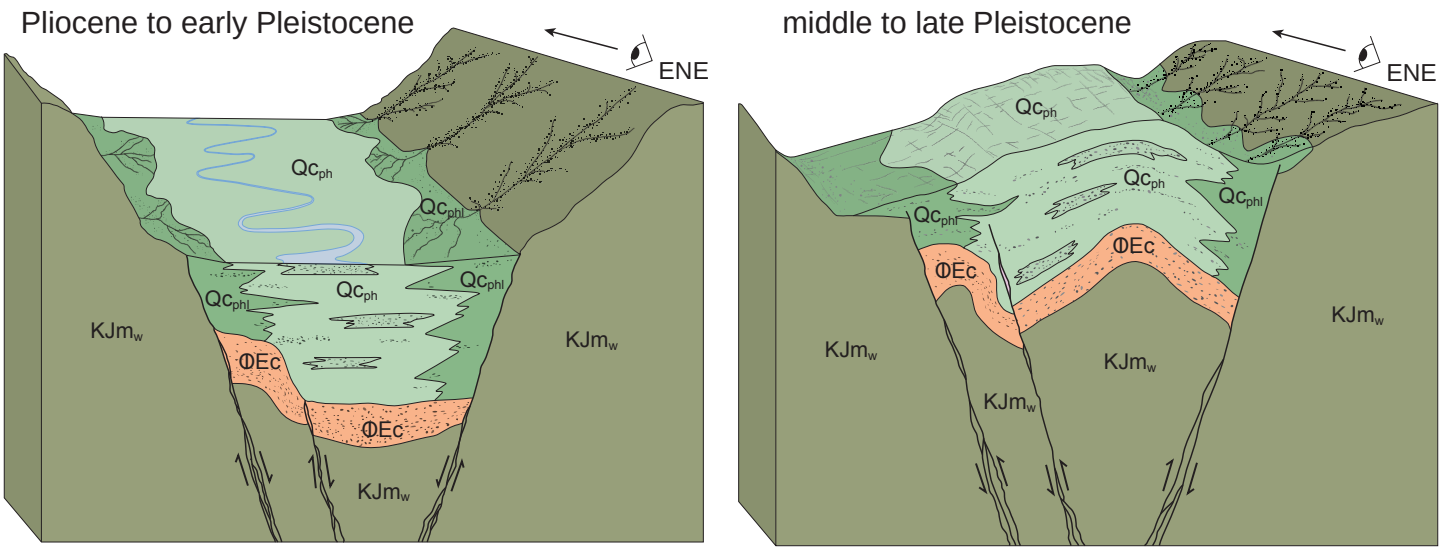

Figure 9. East–northeast-looking block diagrams showing the development of the Explorer Falls basin (EFB). Although the rocks of Bulson Creek (unit ΦEc) might have been deposited in the proto-EFB during the Eocene–Oligocene, here we show the Quaternary development of the basin. The diagram's location is east of the Everett basin and Cross Section B, where only the rocks of Bulson Creek are preserved between Cretaceous and Quaternary units. **A)** The EFB graben in the Pliocene to early Pleistocene contained marginal alluvial fans (unit Qc$_{phl}$)—with distinct locally-derived WMB detritus—that interfinger with axial Cascade Range provenance alluvium of the Pilchuck River (unit Qc$_{ph}$). The homogeneous composition of the marginal facies suggests prolonged erosion of the WMB uplands. **B)** Inversion of the EFB occurs due to rejuvenation of the basin-bounding Carpenter Creek and Three Lake Hill faults as reverse faults. Basin inversion leads to intrabasinal deformation, including folding, tilting, and local uplift. We do not show the cross-cutting strike-slip Woods Creek fault zone which has offset the bounding faults of the EFB.

PLIO-PLEISTOCENE TO HOLOCENE TECTONICS

Regional Faults

Geologic mapping of the Lake Roesiger quadrangle continues our efforts to better understand the southern Whidbey Island (SWIF), Cherry Creek (CCFZ), Woods Creek (WCFZ), and Monroe fault zones and the Everett and Explorer Falls basin (EFB). Sherrod and others (2008) mapped the SWIF southeastward from Whidbey Island to the Maltby quadrangle west of the Lake Roesiger area (Fig. 1). In a series of six geologic maps, Dragovich and others (2007, 2009a,b,c, 2010a,b, 2011a,b, 2012) mapped the Rattlesnake Mountain fault zone and correlated it with the SWIF. All of these studies indicate that the SWIF is a strike-slip fault zone with several active or potentially active segments. Dragovich and others (2010a,b) correlated the main strand of the Rattlesnake Mountain fault zone with the Cottage Lake lineament of the SWIF (Sherrod and others, 2008). East and southeast of the present map area, the CCFZ is a locally active left-lateral, northeast-striking strike-slip fault zone (Fig. 1) that is likely a conjugate of the SWIF (Dragovich and others, 2011, 2012, 2013, 2014a). The northwest-striking, right-lateral WCFZ is spatially associated with shallow earthquakes (Appendix B) and kinematically linked to the CCFZ east of the study area. This perhaps suggests that strain is being transferred from the CCFZ to the WCFZ.

Structurally Controlled Basins and Valleys

EXPLORER FALLS BASIN

Overview

The Explorer Falls basin (EFB) is a fault-bound graben that preserves Tertiary sedimentary rocks (unit ΦEc) and a thick succession of Pleistocene nonglacial basin strata (Dragovich and others, 2014a). The EFB was initially mapped in the northwestern part of Lake Chaplain quadrangle and our new work maps the basin westward through the Lake Roesiger quadrangle where it merges stratigraphically with the Everett basin (Fig. 1; Fig. M3). Both basins are defined by Tertiary and, locally, Quaternary stratigraphic sections that thicken due to tectonism. Mapping in both quadrangles indicates that the EFB is at least 8 km wide and 16 km long and is bound by the Carpenter Creek fault on the north and the Three Lakes Hill fault on the south. This study confirms the tentative results of Dragovich and others (2014a) and finds that: (1) deposits with a Cascade Range provenance (unit Qc$_{ph}$) are confined to the basin axis and form a thick sequence of Pleistocene alluvium, (2) alluvial deposits with a local provenance (unit Qc$_{phl}$) are found in a mappable band along the east–northeast-striking basin-bounding faults, (3) basin deposits are tilted or folded—and locally uplifted—to form an inverted basin and (4) Tertiary strata of unit ΦEc are preserved in the EFB and locally form the basement for Pleistocene deposits.

As shown in Figure 9 we envision a meandering or possibly braided Pilchuck River flowing westward from the Cascade Range during the Pleistocene. Deposits of this river system interfingered with alluvial fans shed across active basin margin faults. Deformation of the basin after deposition of the Pleistocene basin

fill locally tilted, uplifted, and warped these deposits. The strong structural control on valley location during the Pleistocene documented here adds to a growing list of structurally controlled river valleys in the area, including the Snoqualmie River (SWIF and Rattlesnake Mountain fault zone) and Skykomish River (Monroe fault and folds). We speculate that the bounding faults of the EFB may be part of an intersecting set of Tertiary normal faults (along with the Pilchuck River fault), but further study is warranted (Fig. 1).

Pleistocene Pilchuck River Alluvium and Age of the Basin

Unconsolidated deposits in the EFB were previously correlated with a pre-Hamm Creek interglacial interval but the amount of weathering and several new IRSL ages indicate an early to middle Pleistocene age (>370–540 ka; Appendix A). We use composition, sedimentology, geochemistry, stratigraphic architecture, age, and detrital zircon ages to show that the nonglacial alluvium preserved in the EFB is a Pleistocene deposit of the ancient Pilchuck River. We use the term Pilchuck River provenance (PP; Table 1) to refer to sediments derived from the Cascade Range that are similar to, but also distinctly different from, sediments of the modern and ancient Skykomish River (SP; Table 1). In general, PP deposits are older than most SP deposits, and range from early- to mid-Pleistocene to possibly Pliocene in age. One of the most important differences between PP and SP deposits is their differing populations of detrital zircon ages which reflect long-term differences in the geology of each river's drainage basin; this is discussed in greater detail below. We use the term local provenance (LP; Table 1) to refer to locally derived alluvium both in (unit Qc_{phl}) and directly south (locally derived facies of unit Qc_o) of the map area.

Deposits in the EFB are locally greater than 215–245 m thick. Although a basin thickness of ~425 m can be calculated using our subsurface data and the elevation of sediments atop Three Lakes Hill (Cross Section B), this composite thickness ignores any post-depositional uplift of Three Lakes Hill and probably results in an overestimate. In the northwestern corner of the Lake Chaplain quadrangle, these strata are tilted 5–15° to the west, and have anomalously high elevation compared to areas of modern deposition (Dragovich and others, 2014a). This suggests that the EFB was deformed after the middle Pleistocene. This later episode of deformation appears to have 'inverted' the former basin and may reflect a change in the kinematics of the bounding faults.

Our new detrital zircon ages (sample 47A) were sampled directly beneath an IRSL age of >550 ka (Dragovich and others, 2014a) and confirm field and petrographic observations that sand from Pleistocene alluvium of the Pilchuck River (unit Qc_{ph}) is mostly derived from WMB metasediments and less from granitic sources (Appendix C). The detrital zircon ages are similar those obtained from three bedrock WMB metasedimentary samples (Appendix C) and also show a strong correlation with the age and distribution of geologic units presently exposed in the upstream modern Pilchuck River basin. Most compelling in the geologic fit is the major Cretaceous peak at about 90 Ma and also minor Eocene peaks consistent with plutonic rocks in the Pilchuck River basin such as the Bald Mountain pluton (Tabor and others, 2002).

Olympia beds in the nearby Skykomish River valley (sample 13–37A; Appendix C) are ~30 ka in age (Dragovich and others, 2014a) and contain a major 33 to 34 Ma age peak consistent with erosion of the Index batholith (Tabor and others, 1993; Yeats and Engels, 1971). This Eocene age peak is conspicuously absent in sample 47A. Three hypotheses could explain the differences in detrital zircon ages between these two samples: (1) significant erosion of the Cascade Range could have exposed the Index batholith since the mid Pleistocene, (2) unit Qc_{ph} in the eastern part of the EFB may be older than currently thought—perhaps Pliocene in age—thus allowing additional time to unroof the Index batholith, or (3) the differences could simply reflect a persistent drainage divide between the Pilchuck and Sultan river basins since the Pleistocene that isolated detritus from the Index batholith. We favor this last hypothesis and suspect that the basin is entirely Pleistocene in age—consistent with new and published IRSL ages. The Index batholith is exposed in ~51% of the Sultan River basin above Spada Lake, but is not currently exposed in the modern Pilchuck River basin. This perhaps provides the strongest evidence for a persistent drainage divide between these two rivers since at least the Pleistocene. Although significant Pleistocene–Holocene unroofing of the western part of the Index batholith might be expected given that 0.7–3.0 km of exhumation has occurred in the central Cascade Range since ~2.0 Ma (Reiners and others, 2002; Reiners and Brandon, 2006; Hren and others, 2007), a persistent drainage divide can explain the lack of detritus from the Index batholith in Pilchuck River (PP) deposits.

Bounding Faults of the Basin

The geographic distribution of the basin margin alluvial fan deposits (unit Qc_{phl}) provides compelling evidence for the extent of this Pleistocene basin (Fig. 10); these distinct sediments—with ~70–95% WMB metasedimentary clasts (Fig. 3)—are mapped as broad bands along the Carpenter Creek fault on the north and the Three Lakes Hill fault on the south and interfinger basinward with unit Qc_{ph} in several places (for example, significant site 39A). The band along the Three Lakes Hill fault is mappable for almost 10 miles across the southern basin margin. The spatial association of basin margin facies with surface exposures of east-northeast striking faults and locally prominent gravity gradients (see Fig. M1 and M2) gives us additional confidence in the location of the basin's southern limit.

Although the active basin-bounding faults were likely transtensional in the early- to mid-Pleistocene, we now suspect that many segments of the Three Lakes Hill and Carpenter Creek faults have been rejuvenated as reverse faults, similar to the Monroe fault farther south. We show reverse fault segments along these basin-bounding faults where high topography now exists along former basin margin depocenters (for example, Three Lakes Hill), folded Quaternary sediments of the EFB suggest active north-south contraction, and (or) earthquake hypocenter and focal mechanism data suggest active reverse faulting (Appendix B). Nearly ~80% of the recent earthquakes located in the EFB have a focal mechanism solution with reverse components (Appendix B).

The Carpenter Creek fault parallels an east-northeast-trending geomorphic lineament directly north of the map area (Figs. M3 and B1) and aligns with the Carpenter Creek earthquake cluster

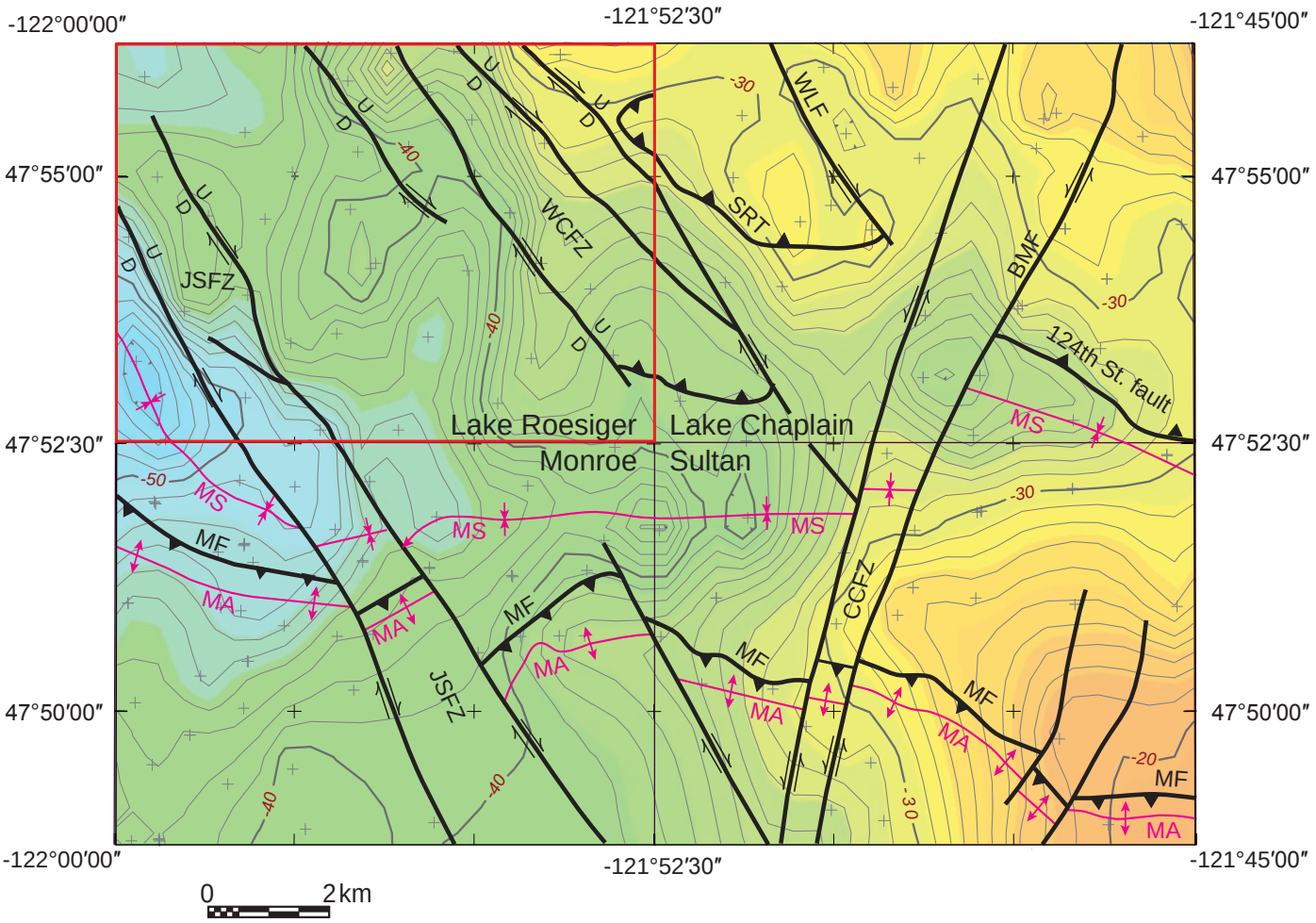

Figure 10. Isostatic gravity map of the northern halves of the Monroe and Sultan 7.5-minute quadrangles, and the southern halves of the Lake Roesiger (red outline) and Lake Chaplain quadrangles. Cooler colors indicate lower gravity values and warmer colors indicate higher values. Gravity contour interval is 2 mGal; small hachures indicate closed lows. Approximately 135 gravity measurements (gray crosses) constrain the contours. Superimposed fault and fold structures are simplified from Dragovich and others (2011a,b, 2013, 2014a, this study). To simplify this illustration, we show some reverse faults as thrusts (triangles on hangingwall). The structure, thickness, and distribution of the Olympia beds and Whidbey Formation in the Lake Roesiger quadrangle suggest that the Monroe syncline (MS) trends to the northwest across the southwestern corner of the quadrangle. We also suggest here that the Monroe fault (MF), Monroe anticline (MA), and Monroe syncline are all sub-parallel. See Dragovich and others (2011a) for more information about the Monroe syncline. BMF, Blue mountain fault; CCFZ, Cherry Creek fault zone; JSFZ, Johnsons Swamp fault zone; SRT, Sultan River thrust; WCFZ, Woods Creek fault zone; WLF, Woods Lake fault.

(Appendix B). This cluster forms a sub-parallel band of seismicity south of the Carpenter Creek fault, and contains reverse fault focal mechanisms (Quake 17 on the Map Sheet), consistent with rejuvenation as a reverse structure. Some reverse focal mechanisms are also associated with the Three Lakes Hill fault (for example, Quake 6 on the Map Sheet).

The intersection of the WCFZ with the Three Lakes Hill and Carpenter Creek faults produced several block faulted areas in the quadrangle. Three Lakes Hill is one such block and provides additional evidence for uplift and deformation of the EFB since the mid Pleistocene. The hill is bound by the Three Lakes Hill fault, strands of the WCFZ, and an intrabasinal reverse fault on the north. Unit Qc_{ph} on the hill is dated at >540 ka (age site 35A) and is topographically higher than 455 ±65 ka deposits of unit Qc_{phl} (age site 35B). The relationship of older sediments at higher elevations than younger sediments, combined with anomalous elevation of the hill and active seismicity on the bounding faults, all suggest that it is a major uplift or inverted block within the EFB. We further suggest that the age relationships indicate that unit Qc_{phl} was locally inset against an existing topographic high and that, at least locally, some basin inversion occurred in the mid-to-early Pleistocene.

SKYKOMISH RIVER VALLEY

Overview

Mapping of regional structures and Quaternary stratigraphy indicates that the lower Snoqualmie and Skykomish River valleys are structurally controlled by potentially active faults, folds, and fault-bounded basins. South and east of the current map area, Holocene to Pleistocene deposits with an SP provenance are observed at many stratigraphic levels in the Snoqualmie, Skykomish, and Tolt River valleys. These distinct sediments are commonly tilted or broadly folded and, combined with their vertical and lateral distribution, imply significant structural control of Pleistocene nonglacial river deposits by the SWIF, Carnation, and Monroe fault zones.

The Monroe fault is a north-verging reverse fault mapped directly south of the current study area and is primarily the contact between Eocene volcanic rocks and Jurassic–Cretaceous rocks of the WMB (Dragovich and others, 2011a,b, 2013). The east–west trending Monroe anticline and syncline—and the Skykomish River valley—parallel the Monroe fault (Dragovich and others, 2014a,b). The folds have progressively tightened Quaternary deposits, a process that has resulted in tighter folding of the older Whidbey Formation compared to the younger Olympia beds in the core of the fold. This process, coupled with age, stratigraphy, and structural information suggest that the Monroe fault, anticline, and syncline are potentially active structures.

Farther south, the south-verging Carnation fault bounds the "Monroe highlands" and may be linked at depth with the north-verging Monroe fault. Near the Carnation fault, SP-provenance Whidbey Formation is folded along the Tolt River anticline and uplifted to an elevation of about 900 ft. These deposits are also mapped in a synclinal basin south of the Carnation fault where they are up to 120 m thick (Dragovich and others, 2012), and near Fall City, where they are up to 240 m thick (Dragovich and others, 2007). In both of these locations, the thickness of SP-provenance deposits appears to result from Quaternary basin subsidence. Since deposition, these deposits have been uplifted and deformed, and record the Quaternary inversion of these and other sub-basins along the Snoqualmie and Tolt River valleys. The Snoqualmie River has been structurally trapped within transpressional or transtensional basins of the SWIF.

Skykomish River Alluvium

Analyses in the adjacent Monroe quadrangle show that Pleistocene to modern alluvial deposits of the Skykomish River are similar to their counterparts in the Snoqualmie River valley (Dragovich and others, 2011a,b). These sediments are predominately derived from Tertiary plutonic sources, such as the Index, Grotto, and Snoqualmie batholiths and we use the term SP (Table 1) to denote this Cascade Range provenance (Dragovich and others, 2011a,b, 2012, 2013, 2014a,b). In the southern part of the current map area, the Olympia beds and Whidbey Formation have an SP provenance and are preserved in the core and northern limb of the Monroe syncline. The stratigraphy and internal structure of these deposits is similar to the nonglacial stratigraphy in the Snoqualmie River valley to the southwest (Dragovich, 2007; Dragovich and others, 2007, 2009a,b,c, 2010a b, 2012). For example, SP sediments in nearby areas typically have contorted or chaotic bedding and (or) sand dikes and other liquefaction features similar to the 64 ka Olympia beds at age site 33E in the southwestern corner of the current map area.

Monroe Syncline

The Monroe syncline may have originally formed in the Eocene (see *Proto-Explorer Falls Basin*) but is now a potentially active fold cored by Olympia beds. The Monroe syncline and anticline were first mapped in the Monroe and Sultan quadrangles as north-verging flexural-slip folds accommodating north–south compression (Fig. 1; Dragovich and others, 2014b). A thick and deformed sedimentary basin exists within the Monroe syncline and likely formed as a result of flexural slip in the footwall of the Monroe fault. The core of the Monroe syncline north of the Skykomish River in the Sultan quadrangle contains at least 140 m of SP-provenance sediment where Dragovich and others (2013) obtained ages between 30 and 215 ka and >300 ka. The Monroe syncline is best observed in the gravity data from four quadrangles—including Lake Roesiger—which shows an elongate, east-trending gravity low (Fig. 10). The low values of this anomaly result from the thickness of Tertiary, Quaternary, and locally Holocene sediments in the basin. The lowest values coincide with the inferred location of the synclinal axis. The stratigraphy and sedimentary provenance of the sediments within the syncline suggest structural control of sedimentation in the Skykomish valley since at least the mid Pleistocene (>300 ka; Dragovich and others, 2014).

Whidbey Formation

The Whidbey Formation and underlying deposits of unit $Qc_{ph\text{-}south}$ both dip generally south towards the axis of the Monroe syncline in the southern part of the map area and farther south in the Monroe quadrangle (Fig. 1). This overall southerly tilt is consistent with outcrops of the unit at high elevation along the northern limb of the Monroe syncline in the area—it is mapped at ~360 ft elevation along the west fork of Woods Creek in the central-southwest part of the map area, descends to ~290 ft along Woods Creek in the southeastern corner of the map area, and is at ~20 ft elevation in the core of the Monroe syncline near Monroe. Although the top of Whidbey Formation has been scoured or eroded during deposition of younger units in some areas, this drop in elevation mirrors the gentle southerly tilt of strata in most locations. Our mapping in the Lake Roesiger quadrangle indicates that the northernmost extent of the Monroe syncline—and the mildly magnetically susceptible SP deposits—is near the latitude of Chain Lake, about ~1 mile south of Lake Cochran (see *Isostatic Gravity and Aeromagnetic Analyses*).

Olympia Beds

We map Olympia beds (unit Qc_o) in the southwestern corner of the Lake Roesiger quadrangle on the basis of their age (~64 ka), nonglacial SP composition, stratigraphic position, and structure (Cross Section A). Our mapping, combined with regional geology and gravity data (Fig. 10), indicate that the Olympia beds are preserved as an erosional remnant within the locally northwest-trending Monroe syncline where they locally overlie till, probably of Possession age, or the Whidbey Formation. Olympia beds occupy the central part of the syncline at four prominent locations: (1) east of the Blue Mountain fault, in the southwest part of the Lake Chaplain quadrangle, (2) west of the Sultan River fault, in the northwestern corner of the Sultan quadrangle, (3) near the city of Monroe, and (4) in the southwest corner of the Lake Roesiger quadrangle. The orientation of bedding in the Olympia beds—and other SP nonglacial deposits north of the Skykomish River mapped beneath them—indicate that these Pleistocene deposits are folded by the Monroe syncline. Dragovich and others (2011a,b) suggested that the elevation difference between outcrops of unit Qc_o is at least partially the result of folding and uplift across the Monroe fault and anticline, and our work here supports this interpretation. We attribute the

thinning of Olympia beds in the core of the Monroe syncline to Holocene and (or) late Pleistocene erosion.

Pleistocene to Holocene Fault Zones

DUBUQUE ROAD FAULT

The Dubuque Road fault is mapped in the northwestern part of the study area as a north-verging reverse fault within the EFB that projects into the adjacent quadrangle. Directly south of the subtle east–west trending geomorphic lineament of the fault (near significant site 23N), glacial till is tectonically sheared in several exposures along Dubuque road. The sheared till has penetrative sub-vertical to vertical fractures that are locally intruded by thin sand dikes (Fig. 2). These fractures also locally contain faint slickenlines and bound a semi-penetrative fabric defined by aligned pebbles. Although further work is warranted, we assign the till to the Vashon glacial interval on the basis of weak weathering of the matrix and clasts (0–0.5 mm weathering rinds on basalt clasts). This age assignment indicates that the Dubuque Road fault is active in the Holocene. Deformed sandstone of unit ΦEc was also observed near the edge of the quadrangle around significant site 37N.

Our interpretation of a reverse fault is made on the basis of field relationships in combination with abundant nearby subsurface well data and geophysical analyses (Fig. 4). Subsurface well logs show that units Qc_{ph}, Qc_{phl} and ΦEc all thicken directly north of the fault, and the overall stratigraphic geometry suggest a hangingwall anticline directly south of the fault (Fig. 4). Finally, it is noteworthy that unit Qc_{phl} is locally mapped north of the fault and may indicate uplift and exposure of WMB rocks during the Pleistocene, perhaps due to fault activity.

Figure 11. A deformed metagabbro (unit tz) west of the Sultan River thrust and within the Woods Creek fault zone (WCFZ) at site 44E. This photo looks northwest and shows the northwest-striking and sub-vertical fracture and cataclasite that is characteristic of the WCFZ. Shear has resulted in chloritization, with actinolized hornblende locally altered to chlorite and some pumpellyite. High brittle strain has transposed the gneissic metagabbro foliation sub-parallel to the steeply dipping brittle faults. A strong older sub-horizontal fracture cleavage is locally preserved in this large metagabbro outcrop and may be associated with the Sultan River thrust that we suspect resides at shallow depth in this area.

WOODS CREEK FAULT ZONE

The Woods Creek fault zone (WCFZ) is a four-mile-wide series of northwest-striking sub-parallel strike-slip and oblique-slip faults in the Lake Roesiger quadrangle. The Woods Lake fault is a strand of this fault zone that was originally mapped in the adjacent Lake Chaplain quadrangle based on geomorphic lineaments, geophysical anomalies, shallow seismicity, and was spatially correlated with a north–northwest trending tectonic zone (unit tz) observed at the surface and modeled in the subsurface (Dragovich and others, 2014a). To facilitate description, we informally name five additional strands of the WCFZ—Woods Creek fault nos. 1–5.

The WCFZ is a shallow crustal structure that post-dates the metamorphic fabric of the WMB and is Tertiary to Holocene in age. Individual fault strands cut or displace older Cretaceous features, such as the mélange belt cleavage fabric and well-bedded metasedimentary rocks with prominent Cretaceous-age foliation. In some fault-bound sub-domains of the WCFZ, the older foliation has been rotated into the northwest trend of the bounding faults as a result of high internal strain. Elsewhere, accumulated brittle strain is less and the foliation remains strongly oblique to the WCFZ.

Most kinematic indicators on fault strands of the WCFZ—such as en echelon veins and shallowly raking slickenlines on steep fracture and fault planes—suggest right-lateral or dextral-oblique offset. Adjacent to fault strands, bedding of the WMB has been locally transposed sub-parallel to the faults. This is particularly well exposed and widespread in the southeastern map area (near significant sites 44E and 26T) where evidence for brittle strike-slip deformation is abundant (Fig. 11). In this latter location, sub-vertical metachert beds form a resistant NNW-striking fin-shaped ridge that is surrounded by less-resistant and cataclastic metasandstone and meta-argillite.

Surface mapping, subsurface data, and geophysical analyses show that many strands of the WCFZ have an overall right-lateral-oblique sense of slip and that the fault zone as a whole accommodates west-side-down movement. This west-side-down slip is suggested by a westward decrease in the amplitude of magnetic anomalies (Fig. M1 and M2) that may indicate that the metagabbro within the Lake Chaplain nappe (Fig. 6) is down-dropped to the west across strands of the WCFZ. The once-large metagabbro

block within the WCFZ has also likely been offset right-laterally (magnetic anomalies GB2, GB3, and GB4 on Fig. M1) and reshaped into cigar- or watermelon-shaped pods with a northwest-trending long-axis (Cross Section A). Additional constraints come from surface mapping and subsurface data that show a significant increase in the thickness of sedimentary rocks (unit ΦEc) in the Everett basin west of the WCFZ (Cross Section A). Surface mapping also shows that strands of the WCFZ right-laterally offset the Pleistocene-age bounding faults of the EFB and locally exhume metagabbro along reverse faults within the WCFZ (Fig. 11; Fig. M1). Finally, west-side-down displacement was inferred along the similarly oriented Cherry Creek fault zone in the Lake Chaplain quadrangle based on the high elevation of the Blue Mountain klippe (likely correlative with the Lake Chaplain nappe), and easterly uplift or tilting of the EFB.

Seismicity along some fault strands of the WCFZ (Appendix B), and the general observation that the fault zone cuts and uplifts the mid to late Pleistocene basin fill and bounding faults of the Explorer Falls basin, suggests that at least some strands of the WCFZ may be active and may accommodate local inversion of the EFB, uplift of the Cascade Range, and promote deposition in the Everett basin. Mapping also suggests that the intersection of the WCFZ and the bounding faults of the EFB has resulted in local block faulting, uplift, and relatively shallow earthquake activity (Appendix B; Quake 16 on Map Sheet). Together, these data suggest that the CCFZ and WCFZ might be part of a family of structures that accommodate on-going uplift between the Cascade Range and basins in the Puget Lowland.

LAKE ROESIGER QUADRANGLE MAPPING—NEW INSIGHTS INTO ADJACENT QUADRANGLES

Mapping in the Lake Roesiger quadrangle has resulted in new insights into the mapping of the Lake Chaplain and Monroe quadrangles of Dragovich and others (2011a,b, 2014a,b). New mapping moves the intersection of the Woods Lake fault and the quadrangle boundary south to significant site 10M (Fig. M3) where Vashon advance outwash is faulted. The mapping of the Sultan River thrust and various strands of the WCFZ have refined their positions near quadrangle boundaries. Finally, we refine the previous mapping of the Monroe fault, anticline, and syncline in the northwest part of the Monroe quadrangle and southeast part of the Lake Roesiger quadrangle (Fig. 1). In this refinement, volcanic rocks of Mount Persis and the Blakeley Formation on Bald Hill east of the Monroe quadrangle become part of the Monroe anticline in the upper plate of the Monroe fault, consistent with earlier mapping by Dragovich and others (2002).

Dragovich and others (2014b) postulated that the Monroe fault merges with the SWIF and may partition some of the north–south compression. The new position of the Monroe syncline shown on Figure 1 is consistent with the inference of Dragovich and others (2014b) that the Monroe syncline is due to shortening or flexure adjacent to the Monroe fault. Its position also suggests that the Monroe fault extends farther NW than previously mapped by Dragovich and others (2011a) and this hypothesis is supported by gravity anomalies (Fig. 10). Further work in nearby quadrangles will continue to refine our interpretations of this neotectonically important area.

ACKNOWLEDGMENTS

This geologic map was funded in part by the U.S. Geological Survey (USGS) National Cooperative Geologic Mapping Program under award no. G14AC00212. We thank Patrick Schreiner (Everett Water Filtration Plant) for help in the field and providing historical information; Madeline Jones and Ryan Kroner (students at Colorado College) for help in the field; Scott Boroughs, Rick Conrey, and Charles Knaack (all from Washington State University) for geochemical analyses; Harrison Gray (USGS) for preparation of luminescence samples; and Jeff Jones (Snohomish County), and Sue Kahle and Theresa Olsen (USGS, Water Resources Division) for subsurface geologic information. We also thank our colleagues at the Washington Division of Geology and Earth Resources: Tim Walsh (for a review), Daniel Eungard (for well data), and Tara Salzer (for logistical support).

REFERENCES CITED

Anderson, M. L.; Blakely, R. J.; Brocher, T. M.; Pratt, T. L.; Wells, R. E.; Haugerud, R. A.; Bush, M., 2006, Structure of the Seattle uplift from seismic, gravity, magnetic, geologic, and geomorphic data [abstract]: Eos (American Geophysical Union Transactions), v. 87, no. 52, Supplement T41A-1554.

Associated Earth Sciences, Inc., 2001, Proposed borrow pit dewatering impact analysis—Trilogy at Redmond Ridge, King County, Washington: Associated Earth Sciences, Inc., 1 v.

Associated Earth Sciences, Inc., 2002, Final hydrogeologic and geotechnical assessment report—Pegasus Thoroughbred Training Center, King County, Washington: Associated Earth Sciences, Inc., 1 v.

Associated Earth Sciences, Inc., 2003, Proposed Snoqualmie Ridge II project—Environmental impact statement—Technical report on geology, soils, and groundwater: Associated Earth Sciences, Inc., [under contract to] Quadrant Corporation, 1 v.

Associated Earth Sciences, Inc., 2004, Environmental impact statement—Technical report on geology, soils and ground water, Redmond Ridge East UPD/FCC and Panhandle preliminary plat, King County, Washington: Associated Earth Sciences, Inc., 1 v.

Associated Earth Sciences, Inc., 2007, Summary of SRS-1 No. 1 infiltration pond, general geologic hazard, and geotechnical engineering recommendations, recreation complex, Redmond Ridge East, King County, Washington: Associated Earth Sciences, Inc., 1 v.

Barnett, E. A.; Barnett, E. A.; Kelsey, H. M.; Sherrod, B. L.; Blakely, R. J.; Hughes, J. F.; Schermer, E. R.; Haugerud, R. A.; Weaver, C. S.; Siedlecki, E., 2006, Active faulting at the northeast margin of the greater Puget Lowland—A paleoseismic and magnetic-anomaly study of the Kendall scarp, Whatcom County, northwest Washington [abstract]: Eos (American Geophysical Union Transactions), Abstract S31A-0183, v. 87, no. 52.

Bhatia, M. R.; Crook, K. A. W., 1986, Trace element characteristics of graywackes and tectonic setting discrimination of sedimentary basins: Contributions to Mineralogy and Petrology, v. 92, no. 2, p. 181-193.

Blakely, R. J.; Wells, R. E.; Weaver, C. S., 1999, Puget Sound aeromagnetic maps and data: U.S. Geological Survey Open-File Report 99-514, version 1.0. [http://pubs.usgs.gov/of/1999/of99-514/]

Booth, D. B., 1984, Glacier dynamics and the development of glacial landforms in the eastern Puget Lowland, Washington: University of Washington Doctor of Philosophy thesis, 217 p., 1 plate. [http://hdl.handle.net/1773/6696]

Booth, D. B., 1986, The formation of ice-marginal embankments into ice-dammed lakes in the eastern Puget Lowland, Washington, U.S.A., during the late Pleistocene: Boreas, v. 15, no. 3, p. 247-263.

Booth, D. B., 1990, Surficial geologic map of the Skykomish and Snoqualmie Rivers area, Snohomish and King Counties, Washington: U.S. Geological Survey Miscellaneous Investigations Series Map I-1745, 2 sheets, scale 1:50,000, with 22 p. text. [http://pubs.er.usgs.gov/publication/i1745]

Bowring, J. F.; McLean, N. M.; and Bowring, S. A., 2011, Engineering cyber infrastructure for U-Pb geochronology: Tripoli and U-Pb_Redux: Geochemistry, Geophysics, and Geosystems, v. 12. [doi: 10.1029/2010GC003479]

Broecker, W. S.; Kulp, J. L.; Tucek, C. S., 1956, Lamont natural radiocarbon measurements, III: Science, v. 124, no. 3213, p. 154-165.

Brown, E. H., 2012, Obducted nappe sequence in the San Juan Islands–Northwest Cascades thrust system, Washington and British Columbia: Canadian Journal of Earth Sciences v. 49, no. 7, p. 796-817.

Cann, J. R., 1970, Rb, Sr, Y, Zr, and Nb in some ocean floor basaltic rocks: Earth and Planetary Science Letters, v. 10, no. 1, p. 7-11.

Capps, Gerald; Simmons, J. D.; Videgar, F. D., 1973, Geology of southern Snohomish County for land-use planning: Western Washington State College Department of Geology, 1 v.

Colman, S. M.; Pierce, K. L., 1981, Weathering rinds on andesitic and basaltic stones as a Quaternary age indicator, western United States: U.S. Geological Survey Professional Paper 1210, 56 p. [http://pubs.er.usgs.gov/publication/pp1210]

Danner, W. R., 1957, A stratigraphic reconnaissance in the northwestern Cascade mountains and San Juan Islands of Washington State: University of Washington Doctor of Philosophy thesis, 3 v., 562 p., 7 plates.

Dickinson, W. R., 1970, Interpreting detrital modes of graywacke and arkose: Journal of Sedimentary Petrology, v. 40, no. 2, p. 695-707.

Dragovich, J. D., 2007, Sand point count and geochemical data in the Fall City and Carnation 7.5-minute quadrangles, King County, Washington: Washington Division of Geology and Earth Resources Open File Report 2007-3, 2 Microsoft Excel files and 6 p. text. [http://www.dnr.wa.gov/publications/ger_ofr2007-3_fallcity_supplement.zip]

Dragovich, J. D.; Logan, R. L.; Schasse, H. W.; Walsh, T. J.; Lingley, W. S., Jr.; Norman, D. K.; Gerstel, W. J.; Lapen, T. J.; Schuster, J. E.; Meyers, K. D., 2002, Geologic map of Washington—Northwest quadrant: Washington Division of Geology and Earth Resources Geologic Map GM-50, 3 sheets, scale 1:250,000, with 72 p. text. [http://www.dnr.wa.gov/publications/ger_gm50_geol_map_nw_wa_250k.pdf]

Dragovich, J. D.; Anderson, M. L.; Walsh, T. J.; Johnson, B. L.; Adams, T. L., 2007, Geologic map of the Fall City 7.5-minute quadrangle, King County, Washington: Washington Division of Geology and Earth Resources Geologic Map GM-67, 1 sheet, scale 1:24,000. [http://www.dnr.wa.gov/publications/ger_gm67_geol_map_fallcity_24k.zip]

Dragovich, J. D.; Littke, H. A.; Anderson, M. L.; Hartog, Renate; Wessel, G. R.; DuFrane, S. A.; Walsh, T. J.; MacDonald, J. H., Jr.; Mangano, J. F.; Cakir, Recep, 2009a,Geologic map of the Snoqualmie 7.5-minute quadrangle, King County, Washington: Washington Division of Geology and Earth Resources Geologic Map GM-75, 2 sheets, scale 1:24,000. [http://www.dnr.wa.gov/publications/ger_gm75_geol_map_snoqualmie_24k.zip]

Dragovich, J. D.; Littke, H. A.; MacDonald, J. H., Jr.; DuFrane, S. A.; Anderson, M. L.; Wessel, G. R.; Hartog, Renate, 2009b, Geochemistry, geochronology, and sand point count data for the Snoqualmie 7.5-minute quadrangle, King County, Washington: Washington Division of Geology and Earth Resources Open File Report 2009-4, 35 p. text, with 3 Microsoft Excel files. [http://www.dnr.wa.gov/publications/ger_ofr2009-4_snoqualmie_suppl.zip]

Dragovich, J. D.; Walsh, T. J.; Anderson, M. L.; Hartog, Renate; DuFrane, S. A.; Vervoot, Jeff; Williams, S. A.; Cakir, Recep; Stanton, K. D.; Wolff, F. E.; Norman, D. K.; Czajkowski, J. L., 2009c, Geologic map of the North Bend 7.5-minute quadrangle, King County, Washington, with a discussion of major faults, folds, and basins in the map area: Washington Division of Geology and Earth Resources Geologic Map GM-73, 1 sheet, scale 1:24,000. [http://www.dnr.wa.gov/publications/ger_gm73_geol_map_northbend_24k.zip]

Dragovich, J. D.; Anderson, M. L.; MacDonald, J. H., Jr.; Mahan, S. A; DuFrane, S. A.; Littke, H. A.; Wessel, G. R.; Saltonstall, J. H.; Koger, C. J.; Cakir, Recep, 2010a,Supplement to the geologic map of the Carnation 7.5-minute quadrangle, King County, Washington—Geochronologic, geochemical, point count, geophysical, earthquake, fault, and neotectonic data: Washington Division of Geology and Earth Resources Open File Report 2010-2, 42 p., 8 digital appendices. [http://www.dnr.wa.gov/publications/ger_ofr2010-2_carnation_supplement.zip]

Dragovich, J. D.; Littke, H. A.; Anderson, M. L.; Wessel, G. R.; Koger, C. J.; Saltonstall, J. H.; MacDonald, J. H., Jr.; Mahan, S. A.; DuFrane, S. A., 2010b, Geologic map of the Carnation 7.5-minute quadrangle, King County, Washington: Washington Division of Geology and Earth Resources Open File Report 2010-1, 1 sheet, scale 1:24,000, with 21 p. text. [http://www.dnr.wa.gov/publications/ger_ofr2010-1_geol_map_carnation_24k.zip]

Dragovich, J. D.; Anderson, M. L.; Mahan, S. A.; Koger, C. J.; Saltonstall, J. H.; MacDonald, J. H., Jr.; Wessel, G. R.; Stoker, B. A.; Bethel, J. P.; Labadie, J. E.; Cakir, Recep; Bowman, J. D.; DuFrane, S. A., 2011a,Geologic map of the Monroe 7.5-minute quadrangle, King and Snohomish Counties, Washington: Washington Division of Geology and Earth Resources Open File Report 2011-1, 1 sheet, scale 1:24,000, with 24 p. text. [http://www.dnr.wa.gov/publications/ger_ofr2011-1_geol_map_ monroe_24k.zip]

Dragovich, J. D.; Mahan, S. A.; Anderson, M. L.; MacDonald, J. H., Jr.; Wessel, G. R.; DuFrane, S. A.; Cakir, Recep; Bowman, J. D.; Littke, H. A., 2011b, Analytical data from the Monroe 7.5-minute quadrangle, King and Snohomish Counties, Washington—Supplement to Open File Report 2011-1: Washington Division of Geology and Earth Resources Open File Report 2011-2, 58 p., 2 plates, 2 Microsoft Excel files. [http://www.dnr.wa.gov/publications/ger_ofr2011-2_monroe_supplement.zip]

Dragovich, J. D.; Anderson, M. L.; Mahan, S. A.; MacDonald, J. H., Jr.; McCabe, C. P; Cakir, Recep; Stoker, B. A.; Villeneuve, N. M.; Smith, D. T.; Bethel, J. P., 2012, Geologic map of the Lake Joy 7.5- minute quadrangle, King County, Washington: Washington Division of Geology and Earth Resources Map Series 2012-01, 2 sheets, scale 1:24,000, with 79 p. text and 1 Excel file. [http://www.dnr.wa.gov/publications/ger_ms2012-01_geol_map_lake_joy_24k.zip]

Dragovich, J. D.; Littke, H. A.; Mahan, S. A.; Anderson, M. L.; MacDonald, J. H., Jr.; Cakir, Recep; Stoker, B. A.; Koger, C. J.; Bethel, J. P.; Dufrane, S. A.; Smith, D. T.; Villeneuve, N. M., 2013, Geologic map of the Sultan 7.5- minute quadrangle, King and Snohomish Counties, Washington: Washington Division of Geology and Earth Resources Map Series 2013-01, 1 sheet, scale 1:24,000, with 52 p. text. [http://www.dnr.wa.gov/publications/ger_ms2013-01_geol_map_sultan_24k.zip]

Dragovich, J. D.; Frattali, C. L.; H. A.; Anderson, M. L.; Mahan, S. A.; MacDonald, J. H., Jr.; Stoker, B. A.; Smith, D. T.; Koger, C. J.; Cakir, Recep; Dufrane, S. A.; Sauer, K. B., 2014a,Geologic map of the Lake Chaplain 7.5- minute quadrangle, Snohomish County, Washington: Washington Division of Geology and Earth Resources Map Series 2014-01, 1 sheet, scale 1:24,000, with 51 p. text. [http://www.dnr.wa.gov/publications/ger_ms2014-01_geol_map_lake_chaplain_24k.zip]

Dragovich, J. D.; Mahan, S. A.; Anderson, M.; Macdonald, J. H., Jr.; Frattali, C.; Littke, H. A.; Stoker, B. A.; Koger, C. J.; Smith, D. T.; Dufrane, S. A., 2014b, The Monroe fault, anticline, and synclinal basin—A potentially active fault and fold system in the Skykomish River Valley, Snohomish County, Washington: Geological Society of America Abstracts with Programs, v. 46, no. 6, p. 779.

Evans, J. E.; Ristow, R. J., Jr., 1994, Depositional history of the southeastern outcrop belt of the Chuckanut Formation—Implications for the Darrington–Devil's Mountain and Straight Creek fault zones, Washington (U.S.A.): Canadian Journal of Earth Sciences, v. 31, no. 12, p. 1727-1743.

Frizzell, V. A., Jr.; Tabor, R. W.; Zartman, R. E.; Blome, C. D., 1987, Late Mesozoic or early Tertiary mélanges in the western Cascades of Washington. *In* Schuster, J. E., editor, Selected papers on the geology of Washington: Washington Division of Geology and Earth Resources Bulletin 77, p. 129-148. [http://www.dnr.wa.gov/publications/ger_b77_papers_on _wa_geology_pt2of3.pdf]

Frost, B. R.; Barnes, C. G.; Collins, W. J.; Arculus, R. J.; Ellis, D. J.; Frost, C. D., 2001, A geochemical classification for granitic rocks: Journal of Petrology, v. 42, no. 11, p. 2033-2048.

Fuller, R. E., 1925, The geology of the northeastern part of Cedar Lake quadrangle with special reference to the de-roofed Snoqualmie batholith: University of Washington Master of Science thesis, 96 p., 4 plates.

Harland, W. B.; Cox, A. V.; Llewellyn, P. G.; Pickton, C. A. G.; Smith, A. G.; Walters, R., 1982, A geologic time scale: Cambridge University Press, 131 p.

Hren, M. T.; Hilley, G. E.; Chamberlain, C. P., 2007, The relationship between tectonic uplift and chemical weathering rates in the Washington Cascades—Field measurements and model predictions: American Journal of Science, v. 307, no. 9, p. 1041-1063.

Jaffey, A. H., Flynn, K. F., Glendenin, L. E., Bentley, W. C., Essling, A. M., 1971, Precision measurement of half-lives and specific activites of ^{235}U and ^{238}U: Physical Review C, v. 4, p. 1889-1906. [doi: 10.1103/physRevC.4.1889]

Jett, G. A., 1986, Sedimentary petrology of the Western mélange belt, north Cascade Range, Washington: University of Wyoming Master of Science thesis, 85 p.

Jett, G. A.; Heller, P. L., 1988, Tectonic significance of polymodal compositions in mélange sandstones, Western mélange belt, north Cascade Range, Washington: Journal of Sedimentary Petrology, v. 58, no. 1, p. 52-61.

Johnson, D. M.; Hooper, P. R.; Conrey, R. M., 1999, XRF analysis of rocks and minerals for major and trace elements on a single low dilution Li-tetraborate fused bead: Advances in X-ray Analysis, v. 41, p. 843-867.

Johnson, S. Y., 1982, Stratigraphy, sedimentology, and tectonic setting of the Eocene Chuckanut Formation, northwest Washington: University of Washington Doctor of Philosophy thesis, 221 p., 4 plates.

Kelsey, H. M.; Sherrod, B. L.; Blakely, R. J.; Haugerud, R. A., 2012, Holocene faulting in the Bellingham forearc basin—Upper-plate deformation at the northern end of the Cascadia subduction zone: Journal of Geophysical Research, v. 117, B03409, 26 p.

Knaack, C.; Cornelius, S.; Hooper, P., 1994, Trace element analysis of rocks and minerals by ICP/MS: Department of Geology Washington State University Open-file Report, December 1994, 18 p.

Knoll, K. M., 1967, Surficial geology of the Tolt River area, Washington: University of Washington Master of Science thesis, 91 p., 1 plate.

Krogh, T. E., 1973, Low-contamination method for hydrothermal decomposition of zircon and extraction of U and Pb for isotopic age determinations: Geochemica Cosmochimica Acta, v. 37, p. 485-494.

Le Maitre, R. W.; Streckeisen, A.; Zanettin, B.; Le Bas, M. J.; Bonin, B.; Bateman, P., editors, 2002, Igneous rocks—A classification and glossary of terms; 2nd ed.: Cambridge University Press, Cambridge, U.K., 256 p.

Lees, J. M., 1999, Geotouch—Software for three and four-dimensional GIS in the earth sciences: Computers & Geosciences, v. 26, no. 7, p. 751-761.

Lees, J. M., 2007, RFOC—Graphics for spherical distributions and earthquake focal mechanisms, graphics for statistics on a sphere, as applied to geological fault data, crystallography, earthquake focal mechanisms, radiation patterns, ternary plots and geographical/geological maps: Comprehensive R Archive Network (CRAN). [accessed May 31, 2011, at http://streaming.stat.iastate.edu/CRAN/web/packages/RFOC/index.html].

Lees, J. M., 2008, GEOmap—Topographic and geologic mapping: Comprehensive R Archive Network (CRAN) [accessed May 31, 2011, at http://streaming.stat.iastate.edu/CRAN/web/packages/GEOmap/index.html].

Lovseth, T. P., 1975, The Devils Mountain fault zone, northwestern Washington: University of Washington Master of Science thesis, 29 p.

MacDonald, J. H., Jr.; Miller, R. B.; Dragovich, J. D.; Metzger, E. P.; Miller, J. S.; Harper, G. D., 2009, Geology and geochemistry of the De Roux unit and possibly correlative tectonostratigraphic terranes within the Cascade mountains, Washington: Geological Society of America Abstracts with Programs, v. 41, no. 7, p. 518.

MacDonald, J. H., Jr.; Dragovich, J. D.; Frattali, C. L.; Anderson, M. L.; Stoker, B. A.; Littke, H. A.; Dufrane, S. A.; Sauer, K.; Smith, D. T.; Koger, C. J., 2014, Geochemistry and metaigneous rocks from the Western mélange belt, Lake Chaplain, Snoqualmie, and Sultan 7.5-minute quadrangles, western Cascades, Washington: Evidence for a predominantly volcanic arc setting: Geological Society of America, Abstracts with Programs, v. 46, no. 6, p. 363.

Mackin, J. H., 1941, Glacial geology of the Snoqualmie–Cedar area, Washington: Journal of Geology, v. 49, no. 5, p. 449-481.

Marcus, K. L., 1991, The rocks of Bulson Creek—Eocene through Oligocene sedimentation and tectonics in the Lake McMurray area, Washington: Washington Geology, v. 19, no. 4, p. 14-15.

Mattinson, J. M., 2005, Zircon U-Pb chemical abrasion ("CA-TIMS") method: Combined annealing and multi-step partial dissolution analysis for improved precision and accuracy of zircon ages: Chemical Geology, v. 220, p. 47-66. [doi: 10.1016/j.chemgeo.2005.03.011]

McDonough, W. F.; Sun, S. S., 1995, The composition of the Earth: Chemical Geology, v. 120, no. 3-4 p. 223-253.

McFarland, C. R., 1981, Oil and gas exploration in Washington, 1900–1981: Washington Division of Geology and Earth Resources Information Circular 67R, 119 p. [http://www.dnr.wa.gov / publications/ger_ic67r_oil_gas_exploration_wa_1900-81.pdf]

McLennan, S. M.; Taylor, S. R.; McCulloch M. T.; Maynard, J. B., 1990, Geochemical and Nd-Sr isotopic composition of deep-sea turbidites—Crustal evolution and plate tectonic associations: Geochimica et Cosmochimica Acta, v. 54, p. 2015–2050.

Miller, R. B., 1985, The ophiolitic Ingalls Complex, north-central Cascades Mountains, Washington: Geological Society of America Bulletin, v. 96, no. 1, p. 27-42.

Miller, R. B., 1989, The Mesozoic Rimrock Lake inlier, southern Washington Cascades—Implications for the basement to the Columbia Embayment: Geological Society of America Bulletin, v. 101, no. 10, p. 1289-1305.

Minard, J. P., 1981, Distribution and description of the geologic units in the Maltby quadrangle, Washington: U.S. Geological Survey Open-File Report 81-100, 4 p., 1 plate, scale 1:24,000. [http://ngmdb.usgs.gov/Prodesc/proddesc_11856.htm]

Minard, J. P., 1985, Geologic map of the Maltby quadrangle, Snohomish and King Counties, Washington: U.S. Geological Survey Miscellaneous Field Studies Map MF-1746, 1 sheet, scale 1:24,000. [http://pubs.er.usgs.gov/publication/mf1746]

Morrison, R. B., editor, 1991, Quaternary nonglacial geology—Conterminous U.S.: Geological Society of America DNAG Geology of North America, v. K-2, 672 p., 8 plates in accompanying case.

Pearce, J. A., 1982, Trace element characteristics of lavas from destructive plate boundaries. *In* Thorpe, R. S., editor, Andesites—Orogenic andesites and related rocks: John Wiley & Sons [Chichester, U.K.], p. 525-548.

Pearce, J. A., 1996, A user's guide to basalt discrimination diagrams. *In* Wyman, D. A., editor, Trace element geochemistry of volcanic rocks—Applications for massive sulphide exploration: Geological Association of Canada Short Course Notes, v. 12, p. 79-113.

Pearce, J. A., 2008, Geochemical fingerprinting of oceanic basalts with applications to ophiolite classification and the search for Archean oceanic crust: Lithos, v. 100, no. 1-4, p. 14-48.

Pearce, J. A., 2014, Immobile element fingerprinting of ophiolites: Elements, v. 10, no. 2, p. 101-108.

Pessl, Fred, Jr.; Dethier, D. P.; Booth, D. B.; Minard, J. P., 1989, Surficial geologic map of the Port Townsend 30- by 60-minute quadrangle, Puget Sound region, Washington: U.S. Geological Survey Miscellaneous Investigations Series Map I-1198-F, 1 sheet, scale 1:100,000, 13 p. text. [http://ngmdb.usgs.gov/prodesc/proddesc_9029.htm]

Pettijohn, F. J., 1957, Sedimentary rocks; 2nd ed.: Harper & Row, 718 p.

Porter, S. C.; Swanson, T. W., 1998, Radiocarbon age constraints on rates of advance and retreat of the Puget lobe of the Cordilleran ice sheet during the last glaciation: Quaternary Research, v. 50, no. 3, p. 205-213.

Prescott, J. R.; Hutton, J. T., 1994, Cosmic ray contributions to dose rates for luminescence and ESR dating—Large depths and long-term time variations: Radiation Measurements, v. 23, p. 497-500.

Reiners, P. W.; Ehlers, T. A.; Garver, J. I.; Mitchell, Sara Gran; Montgomery, D. R.; Vance, J. A.; Nicolescu, Stefan, 2002, Late Miocene exhumation and uplift of the Washington Cascade Range: Geology, v. 30, no. 9, p. 767-770.

Reiners, P. W.; Brandon, M. T., 2006, Using thermochronology to understand orogenic erosion: Annual Review of Earth and Planetary Sciences, v. 34, p. 419-466. [doi: 10.1146/annurev.earth.34.031405.125202]

Rigg, G. B., 1958, Peat resources of Washington: Washington Division of Mines and Geology Bulletin 44, 272 p. [http://www.dnr.wa.gov/publications/ger_b44_peat_reasources_wa_1.pdf; http://www.dnr.wa.gov/publications/ger_b44_peat_reasources_wa_2.pdf; http://www.dnr.wa.gov/publications/ger_b44_peat_reasources_wa_3.pdf]

Roser, B. P.; Korsch, R. J., 1988, Provenance signatures of sandstone-mudstone suites determined using discriminant function analysis of major-element data: Chemical Geology, v. 67, no. 1-2 p. 119-139.

Sauer, K.; Dragovich, J. D.; Macdonald, J. H., Jr.; Frattali, C.; Anderson, M.; Dufrane, S. A.; Gordon, S. M., 2014, Tectonic implications of detrital zircon geochronology and neodymium isotopes of the arkosic petrofacies of the Western mélange belt, Lake Chaplain quadrangle, western Cascades, Washington: Geological Society of America Abstracts with Programs, v. 46, no. 6, p. 363.

Sherrod, B. L.; Blakely, R. J.; Weaver, C. S.; Kelsey, H. M.; Barnett, Elizabeth; Liberty, Lee; Meagher, K. L.; Pape, Kristin, 2008, Finding concealed active faults—Extending the southern Whidbey Island fault across the Puget Lowland, Washington: Journal of Geophysical Research, v. 113. [B05313, doi:10.1029/2007JB005060, 2008]

Siddall, M.; Rohling, E. J.; Thompson, W. G.; Waelbroeck, C., 2008, Marine isotope stage 3 sea level fluctuations: Data synthesis and new outlook, Reviews of Geophysics, v. 46, RG4003. [doi:10.1029/2007RG000226.]

Siedlecki, E. M., 2008, The geometry and earthquake history of the Boulder Creek fault—A paleoseismic, seismic refraction and ground penetrating radar study, Whatcom County, Washington: Western Washington University Master of Science thesis, 81 p., with CD containing appendices.

Simonetti, Antonio; Heaman, L. M.; Hartlaub, R. P.; Creaser, R. A.; MacHattie, T. G.; Bohm, Christian, 2005, U-Pb zircon dating by laser ablation-MC-ICP-MS using a new multiple ion counting Faraday collector array: Journal of Analytical Atomic Spectrometry, v. 20, no. 8, p. 677-686.

Tabor, R. W., 1994, Late Mesozoic and possible early Tertiary accretion in western Washington State—The Helena–Haystack mélange and the Darrington–Devils Mountain fault zone: Geological Society of America Bulletin, v. 106, no. 2, p. 217-232.

Tabor, R. W.; Frizzell, V. A., Jr.; Booth, D. B.; Waitt, R. B.; Whetten, J. T.; Zartman, R. E., 1993, Geologic map of the Skykomish River 30- by 60-minute quadrangle, Washington: U.S. Geological Survey Miscellaneous Investigations Series Map I-1963, 1 sheet, scale 1:100,000, 42 p. text. [http://pubs.usgs.gov/imap/i1963/]

Tabor, R. W.; Frizzell, V. A., Jr.; Booth, D. B.; Waitt, R. B., 2000, Geologic map of the Snoqualmie Pass 30- by 60-minute quadrangle, Washington: U.S. Geological Survey Geologic Investigations Series Map I-2538, 1 sheet, scale 1:100,000, 57 p. text. [http://pubs.usgs.gov/imap/i2538]

Tabor, R. W.; Booth, D. B.; Vance, J. A.; Ford, A. B., 2002, Geologic map of the Sauk River 30- by 60-minute quadrangle, Washington: U.S. Geological Survey Geologic Investigations Series Map I-2592, 2 sheets, scale 1:100,000, with 67 p. text. [http://pubs.er.usgs.gov/usgspubs/i/i2592]

Thorson, R. M., 1989, Glacio-isostatic response of the Puget Sound area, Washington: Geological Society of America Bulletin, v. 101, no. 9, p. 1163-1174.

Troost, K. G.; Booth, D. B.; Wisher, A. P.; Shimel, S. A., 2005, The geologic map of Seattle—A progress report: U.S. Geological Survey Open-File Report 2005-1252, version 1.0, 1 sheet, scale 1:24,000. [http://pubs.usgs.gov/of/2005/1252/]

U.S. Geological Survey Geologic Names Committee, 2010, Divisions of geologic time—Major chronostratigraphic and geochronologic units: U.S. Geological Survey Fact Sheet 2010-3059, 2 p. [http://pubs.usgs.gov/fs/2010/3059/]

Vance, J. A.; Dungan, M. A.; Blanchard, D. P.; Rhodes, J. M., 1980, Tectonic setting and trace element geochemistry of Mesozoic ophiolitic rocks in western Washington: American Journal of Science, v. 280-A, p. 359-388.

Varnes, D. J., 1978a, repr. 1995, Landslide classification system. *In* Dragovich, J. D.; Brunengo, M. J., Landslide map and inventory, Tilton River–Mineral Creek area, Lewis County, Washington: Washington Division of Geology and Earth Resources Open File Report 95-1, 165 p., Plate 3. [http://www.dnr.wa.gov/publications/ger_ofr95-1_lewis_co_ landslides_plates.pdf; http://www.dnr.wa.gov/publications/ger_ofr95-1_lewis_co_landslides_text.pdf]

Varnes, D. J., 1978b, Slope movement types and processes. *In* Schuster, R. L.; Krizek, R. J., editors, Landslides—Analysis and control: National Academy of Sciences Transportation Research Board Special Report 176, p. 11-33, 1 plate.

Wells, R. E.; Blakely, R. J.; Weaver, C. S., 1998, Tectonics and earthquake potential of Cascadia—Effects of rotation and northward transport of forearc crustal blocks in Oregon and Washington [abstract]: Eos (American Geophysical Union Transactions), v. 79, no. 24, Supplement, p. W115.

Whetten, J. T.; Carroll, P. R.; Gower, H. D.; Brown, E. H.; Pessl, Fred, Jr., 1988, Bedrock geologic map of the Port Townsend quadrangle, Washington: U.S. Geological Survey Miscellaneous Investigations Series Map I-1988-G, scale 1:100,000. [http://ngmdb.usgs.gov/prodesc/proddesc_9030.htm]

Wolfe, J. A.; Forest, C. E.; Molnar, Peter, 1998, Paleobotanical evidence of Eocene and Oligocene paleoaltitudes in midlatitude western North America: Geological Society of America Bulletin, v. 110, no. 5, p. 664-678.

Yeats, R. S.; Engels, J. C., 1971, Potassium-argon ages of plutons in the Skykomish-Stillaguamish areas, North Cascades, Washington: U.S. Geological Survey Professional Paper 750-D, p. D34-D38. [http://pubs.er.usgs.gov/publication/pp750D]

Appendix A. Infrared Stimulated Luminescence Age Data

Infrared Stimulated Luminescence ages for sediment samples are presented in Table A1. See Dragovich and others (2011b) for a discussion of the infrared stimulated luminescence methodology. The petrographic and geochemical examination of sand from the age sites, combined with deposit stratigraphy, indicate a Cascade Range (ancient Skykomish River) provenance (SP; Table 1) for deposits of the Olympia nonglacial interval, Whidbey Formation, and southern outcrops of the pre-Hamm Creek interglacial interval (units Qc_o, Qc_{ws}, and $Qc_{ph\text{-}south}$). A Cascade Range (ancient Pilchuck River) provenance (PP; Table 1) is indicated for deposits of the pre-Hamm Creek interglacial interval (unit Qc_{ph}) in the Pleistocene Explorer Falls basin.

Table A1. Infrared stimulated luminescence ages (IRSL) from the Lake Roesiger 7.5-minute quadrangle, including elemental concentrations, cosmic and total dose rates, equivalent doses, and ages from fine-grained feldspar. Sample numbers are bold. See Map Sheet for sample locations. Gy, Gray (unit of absorbed radiation creating luminescence); WMB, Western mélange belt; SP, Skykomish River provenance (Table 1). See *Description of Map Units* for further information and Appendix D for sand geochemistry of the indicated age sites. Analyses performed by Shannon Mahan and staff, USGS.

IRSL Sample ID (geologic unit)		Water content (%)[a]	K (%)[b]	U (ppm)[b]	Th (ppm)[b]	Cosmic dose additions (Gy/ka)[c]	Equivalent dose (Gy)	Total dose rate (Gy/ka)	Age[d]
33A (Qc_{ph})		20 (43)	1.66 ±0.04	1.27 ±0.20	5.37 ±0.51	0.17 ±0.01	>1000	2.72 ±0.15	>370 ka
TRS	sec. 16, T29N R7E	Sand sample from North Lake Roesiger Road, directly northeast of the northern tip of Lake Roesiger. Road cut is ~2 m high and exposes very compact, stratified, and weathered, fine to coarse sand with few silt beds. Contains abundant flattened sticks, logs, and detrital wood. Petrographic analysis of the sample shows abundant angular to subangular monocrystalline quartz (~25%), plagioclase (~20%), mica (~15%), polycrystalline quartz (~15%), hornblende (~5%), and K-spar (~5%). Lithic grains (~15%) are dominated by metasedimentary units like metachert, phyllite, and rare granitic and volcanic grains. Composition indicates a WMB source with less granitic detritus. See site 6T in Appendix D for geochemical analysis of this sand sample.							
Lat/long. (degrees)	47.999824 -121.907247								
Elev. (ft)	~710								
Material	sand								
Provenance	PP								
33B (Qc_{ph})		20 (37)	1.42 ±0.04	1.01 ±0.18	3.32 ±0.29	0.13 ±0.01	>1000	2.20 ±0.11	>455 ka
TRS	sec. 21, T29N R7E	Sand sample from a ~4 m deep rill (small ephemeral creek cutbank) directly east of South Lake Roesiger Road near the central east shore of Lake Roesiger. Very compact, well sorted, thickly bedded coarse micaceous river channel sand with silt rip-up clasts and silty sand interbeds. Petrographic analysis reveals abundant monocrystalline quartz (~35%), plagioclase (~20%), hornblende (~10%), K-spar (~8%), significant biotite and white mica (15%), and few pyroxenes. Lithic grains (~12%) include meta-argillite, metachert, phyllite, and metasandstone mostly sourced from WMB with less granitic detritus. See site 33B in Appendix D for geochemical analysis of this sand sample.							
Lat/long. (degrees)	47.988475 -121.915171								
Elev. (ft)	~600								
Material	sand								
Provenance	PP								
33C (Qc_{ws})		25 (39)	0.88 ±0.04	1.33 ±0.20	3.31 ±0.34	0.16 ±0.01	144 ±10.8	1.87 ±0.12	77 ±6.5 ka
TRS	sec. 21, T28N R7E	Sand sample from an 8 m-tall private road cutbank west of the east fork of Woods Creek in the south central part of the map. The cutbank is 4.5 m high and exposes dense, thinly bedded, brown silt, and tannish grey silty fine sand. This outcrop displays very good bedding. Petrographic analysis of the sample shows abundant angular to subangular monocrystalline quartz (~35%), plagioclase (~25%), hornblende (~10%), K-spar (~5%), abundant mica (~20%), and few epidote and polycrystalline quartz grains. The composition of this sample indicates a strong granitic provenance.							
Lat/long. (degrees)	47.893403 -121.917285								
Elev. (ft)	~270								
Material	fine sand								
Provenance	SP								
33D ($Qc_{ph\ south}$)		10 (28)	1.17 ±0.04	1.50 ±0.21	3.39 ±0.43	0.16 ±0.01	>1000	2.34 ±0.15	>430 ka
TRS	sec. 28, T28N R7E	Sand sample from a 4.5 m-high cutbank along Woods Creek Road near the southern edge of the study area. Moderately dense, well stratified, laminated sand with thin to medium beds of tan silt. Petrographic analysis of the sample shows significant monocrystalline quartz (~25%), plagioclase (~25%), mica (~5%), K-spar (7%), polycrystalline quartz (~7%), and hornblende (~3%). Lithic grains (30%) include significant granitics as well as foliated metamorphic aggregates. This sample has a distinct granitic provenance, is located in the Monroe synclinal basin, and is thus early Pleistocene Skykomish River alluvium. See site 33D in Appendix D for geochemical analysis of this sand sample.							
Lat/long. (degrees)	47.878915 -121.917678								
Elev. (ft)	~40								
Material	coarse sand								
Provenance	SP								

IRSL Sample ID (geologic unit)		Water content (%)[a]	K (%)[b]	U (ppm)[b]	Th (ppm)[b]	Cosmic dose additions (Gy/ka)[c]	Equivalent dose (Gy)	Total dose rate (Gy/ka)	Age[d]
33E (Qc_o)		17 (23)	1.38 ±0.04	2.68 ±0.26	6.24 ±0.43	0.13 ±0.01	226 ±14.7	3.48 ±0.15	65 ±4.5 ka
TRS	sec. 25, T28N R6E	Sand sample from a 1.5 m-high road cut along 183rd Ave SE in the southwest corner of the map area that exposes dense, tan, mottled silt and fine to coarse sand. Bedding is convoluted but dips generally to the southwest. Petrographic analysis shows abundant monocrystalline quartz (~35%), plagioclase (~25%), hornblende (~12%), K-spar (~5%), mica (~15%), some lithic grains, and few polycrystalline quartz grains. These sands have a granitic provenance. Within uncertainty, this sample is in the Olympia nonglacial interval (~20–60 ka). The 65 ka age suggests proximity to the base of the Olympia beds near the axis of the Monroe syncline. A till on the steep slope below the road and to the east is interpreted to be Possession-age till directly under these Olympia beds. Sample is located within the Everett basin.							
Lat/long. (degrees)	47.881487 -121.985772								
Elev. (ft)	~355								
Material	fine silty-sand								
Provenance	SP								
33F (Qc_{ws})		22 (28)	0.73 ±0.04	1.11 ±0.16	2.66 ±0.28	0.11 ±0.01	132 ±6.64	1.62 ±0.10	81 ±4.7 ka
TRS	sec. 35, T28N R7E	Sand sample from Woods Creek at a 9.1 m-high cutbank in the northeast corner of the Monroe quadrangle that exposes dense, well sorted, thin to medium bedded micaceous sand with silt (Fig. M3). Petrographic analysis reveals monocrystalline quartz (~25%), plagioclase (~25%), hornblende (~7%), mica (~5%), K-spar (~8%), polycrystalline quartz (~15%), and rare epidote and pyroxene grains. Contains various rock fragments (~15%) including metamorphic and granitic lithic grains. These sands have a granitic provenance. See the Monroe quadrangle for previous mapping of the Whidbey Formation directly south of the Lake Roesiger quadrangle.							
Lat/long. (degrees)	47.872953 -121.883999								
Elev. (ft)	~210								
Material	sandy silt								
Provenance	SP								
35A (Qc_{phl})		7 (28)	0.74 ±0.05	1.77 ±0.26	2.65 ±0.31	0.06 ±0.01	>1000	1.86 ±0.12	>540 ka
TRS	sec. 33, T29N R7E	Sand sample from north end of Three Lakes Hill in a very steep slide scarp. Outcrop is about 1.5 m high and exposes dense micaceous pebbly sand with interbedded laminated silt. Petrographic analysis of the sample reveals angular to sub-angular grains of monocrystalline quartz (~20%), plagioclase (~20%), mica (~5%), K-spar (~5%), and hornblende (~5%) with brown weathering products (~20%). Contains significant polycrystalline quartz and metasedimentary rock fragments (~20%) including phyllite, metachert, metasandstone, foliate quartzose aggregates and some granitic lithic grains. Composition indicates distinct WMB source and less granitic detritus. This is consistent with the composition of pebbles in the outcrop (although vein quartz is more obvious in the pebble fraction). See site 35A in Appendix D for geochemical analysis of this sand sample.							
Lat/long. (degrees)	47.957294 -121.923242								
Elev. (ft)	~1058								
Material	sand								
Provenance	PP								
35B (Qc_{phl})		7 (33)	0.57 ±0.05	0.54 ±0.16	2.36 ±0.26	0.15 ±0.01	525 ±63	1.18 ±0.09	445 ±65 ka
TRS	sec. 4, T28N R7E	Sand sample from a partially overgrown sand and gravel pit directly off the main logging road along the southern part of Three Lakes Hill. The 1.5–4.57 m-high pit wall exposes mostly coarse sand with medium to thick beds of gravelly coarse sand. Gravel clasts include orange metatuff probably from unit ~~M~~vr, various WMB metasedimentary and metaigneous clasts, and a few undivided volcanic clasts and granite. Petrographic analysis of the sand reveals subangular to subrounded mostly WMB metasedimentary grains (~80%) including metachert, meta-argillite, metasandstone, phyllite, and foliate quartzose aggregate grains. Also contains some plagioclase (~5 %), polycrystalline quartz (~5%), hornblende (~3%), metagabbro (~5%), and a few detrital prehnite grains (~2%). Distinct lithic-rich local facies of the Explorer Falls basin. See site 35B in Appendix D for geochemical analysis.							
Lat/long. (degrees)	47.938491 -121.913245								
Elev. (ft)	~530								
Material	sand								
Provenance	LP								

[a] Field moisture, with number in parentheses indicating the complete sample saturation %. Ages calculated using approximately 60% of saturation values.

[b] Analyses obtained using high-resolution gamma spectrometry (HPGe detector).

[c] Cosmic doses and attenuation with depth were calculated using the methods of Prescott and Hutton (1994).

[d] Feldspar from 4–11 micron polymineral silt. Exponential fit used for multiple aliquot additive dose. Errors to one sigma. Fade tests indicate ~2 g/decade correction.

Appendix B. Seismicity in and Near the Lake Roesiger 7.5-minute Quadrangle

We present earthquake epicenters and focal mechanisms from in and around the Lake Roesiger and Lake Chaplain quadrangles from the Pacific Northwest Seismic Network (PNSN) to provide a sense of fault movement at depth. This broader area (Fig. B1) contains 616 epicenters and 37 focal mechanisms. Hypocenter depths less than 40 km are interpreted as crustal events. The focal mechanisms in Table B1 were prepared using the *RFOC* software package of Lees (1999, 2007, and 2008).

We tentatively correlate many shallow to moderately shallow earthquakes (0-20 km) in and near the Lake Roesiger area with activity on the Woods Creek fault zone (WCFZ) or fault strands of the Explorer Falls basin (EFB). Most focal mechanisms appear to record reverse fault solutions and are associated with the EFB. However, the WCFZ appears to have several strike-slip mechanisms; for example, FM_16 is a strike-slip event spatially associated with WCFZ strand no. 2 and FM_23 has a dextral oblique-normal solution near WCFZ strand no. 5.

In the EFB, both the Three Lakes Hill fault and the Carpenter Creek fault are spatially associated with relatively shallow earthquakes. We tentatively project the Carpenter Creek fault into the adjoining Granite Falls quadrangle along a lineament observed in lidar (Fig. M3). Furthermore, we suggest that this fault is associated with the seismic zone (informally named Carpenter Creek earthquake cluster) located just south of the lineament (Fig. B1). The correlation of this cluster with the Carpenter Creek fault is strengthened by the number of reverse-offset focal mechanisms in the cluster and geologic evidence that suggests the basin-bounding fault for the EFB strikes northeast and dips steeply south in this area.

Similarly, we suspect that parts of the Three Lakes Hill fault have been rejuvenated as reverse faults as shown by spatially associated earthquakes and focal mechanisms with reverse-sense solutions (for example, FM_6 and FM_14). Of the 11 shallow earthquakes (0–18 km depth) with focal mechanism solutions in the EFB, 10 have a reverse or reverse-oblique fault solution. Of these, half (45%) strike between N20°E to N100°E and are subparallel to the east–northeast trend of the EFB. We also speculate that some generally east–west striking reverse fault focal mechanisms might be related to rejuvenation of Cretaceous thrust faults that are common in the Western mélange belt (for example, FM_27 and FM_36). Finally, the concentration of shallow seismicity at the intersection of faults or fault zones (for example, the intersection of the WCFZ and the Three Lakes Hill fault) might be related to the low strength and broad thickness of the tectonic zones where these faults intersect.

Table B1. Earthquake focal mechanisms in the Lake Roesiger and surrounding area. This table provides the ID, strike, dip, and rake for both nodal planes of the focal mechanism. Reported focal mechanisms are labeled with the focal mechanism ID number on Figure B1. The earthquake identification number gives the date (yr/month) and time (day, hr, second) in sequential order without spaces; it is a unique identifier to link its original data reported on the PNSN website (http://www.pnsn.org).

Focal mechanism ID no.	Latitude Longitude	Strike (°) 1	Dip(°) 1	Rake (°) 1	Strike (°) 2	Dip (°) 2	Rake (°) 2	Preferred fault type	Focal mechanism illustration	Earthquake ID; depth (km); magnitude	Location (quadrangle)
FM_1	47.8790 -121.9930	50	25	150	168	78	68	reverse-oblique strike-slip		60432732; 17.76; 1.1	Lake Roesiger
FM_2	47.8480 -121.9050	120	40	50	348	61	118	oblique reverse		60434667; 23.07; 1.5	Monroe
FM_3	47.8770 -122.0140	180	40	140	303	66	57	reverse-oblique strike-slip		60434917, 21.59; 1.2	Snohomish
FM_4	48.0120 -121.8570	330	20	50	192	75	103	oblique reverse		60458026; 66.61; 1.6	Verlot
FM_5	47.9410 -122.0540	40	65	-80	197	27	-110	normal		60517947; 27.80; 1.6	Snohomish
FM_6	47.9540 -121.8840	0	80	70	244	22	152	oblique reverse		10858833; 17.84; 3.3	Lake Roesiger
FM_7	47.8540 -122.0190	5	90	-20	95	70	180	normal-oblique strike-slip		10840748; 24.70; 2.5	Maltby
FM_8	47.9130 -121.9030	70	70	110	203	28	47	oblique reverse		10846918; 5.98; 1.8	Lake Roesiger
FM_9	47.9080 -121.8230	15	60	50	254	48	138	oblique reverse		10088068; 4.40; 3.8	Lake Chaplain
FM_10	47.9090 -121.8240	90	90	-40	180	50	180	normal-oblique strike-slip		10088198; 3.15; 3.5	Lake Chaplain
FM_11	47.8750 -122.0340	60	15	140	189	80	78	reverse- oblique strike-slip		10179728; 17.37; 2.2	Maltby
FM_12	47.8610 -121.8690	165	45	110	318	48	71	oblique reverse		10214853; 18.54; 2.0	Sultan

Focal mechanism ID no.	Latitude Longitude	Strike (°) 1	Dip(°) 1	Rake (°) 1	Strike (°) 2	Dip (°) 2	Rake (°) 2	Preferred fault type	Focal mechanism illustration	Earthquake ID; depth (km); magnitude	Location (quadrangle)
FM_13	47.8390 -121.9930	25	35	110	181	57	77	oblique reverse		10226628; 24.06; 2.3	Monroe
FM_14	47.9520 -121.8940	50	45	100	216	46	80	reverse		10245558; 17.83; 2.6	Lake Roesiger
FM_16	47.9220 -121.9230	15	55	40	259	58	137	reverse- oblique strike-slip		10254553; 16.34; 3.4	Lake Roesiger
FM_17	47.9960 -121.9340	25	35	90	205	55	90	reverse		10280373; 11.50; 2.2	Lake Roesiger
FM_18	47.8790 -122.0360	80	55	90	260	35	90	reverse		10294663; 18.81; 2.5	Snohomish
FM_19	47.8620 -122.0300	100	50	130	227	54	52	oblique reverse		10304783; 14.04; 1.3	Maltby
FM_20	47.8810 -121.9620	195	80	150	291	61	12	reverse- oblique strike-slip		10337608; 17.01; 1.8	Lake Roesiger
FM_21	47.9060 -122.0200	155	50	90	335	40	90	reverse		10337923; 13.83; 1.8	Snohomish
FM_22	47.8670 -122.0040	5	40	100	172	51	82	reverse		10485948; 19.72; 2.5	Maltby
FM_23	47.9620 -121.9180	135	20	-160	26	83	-71	normal-oblique strike-slip		10518933; 11.22; 1.9	Lake Roesiger
FM_24	47.8500 -121.9410	65	55	-120	290	45	-55	oblique normal		10540763; 24.45; 1.9	Monroe
FM_25	47.9640 -121.9240	290	65	-130	173	46	-36	oblique normal		10536458; 11.10; 1.9	Lake Roesiger
FM_26	47.9310 -121.8380	105	25	80	296	65	95	reverse		10587458; 15.68; 2.4	Lake Chaplain
FM_27	47.9470 -121.7460	95	50	100	260	41	79	reverse		10587608; 11.58; 2.3	Wallace Lake
FM_28	48.0090 -121.8520	50	85	100	166	11	26	reverse		10621193; 17.11; 2.3	Verlot
FM_29	48.0080 -121.8550	175	40	110	330	53	74	oblique reverse		10646943; 13.06; 2.7	Verlot
FM_30	48.0220 -121.8330	0	65	120	126	38	43	oblique reverse		10647093; 13.57; 3.5	Verlot
FM_31	48.0150 -121.8340	130	50	50	3	54	128	oblique reverse		10662698; 17.00; 2.6	Verlot
FM_32	47.9000 -122.0600	105	55	140	221	58	43	reverse- oblique strike-slip		10684883; 26.00; 1.8	Snohomish
FM_33	47.8530 -122.0380	65	50	90	245	40	90	reverse		10698348; 26.02; 2.5	Maltby
FM_34	47.9390 -122.0150	55	60	80	254	31	106	reverse		10785083; 8.45; 2.2	Snohomish
FM_35	47.9010 -121.9750	50	45	100	216	46	80	reverse		10793748; 22.71; 2.5	Lake Roesiger
FM_36	47.9330 -121.8560	55	40	90	235	50	90	reverse		10813778; 19.90; 2.4	Lake Chaplain
FM_37	47.96480 -121.86680	25	80	80	250	14	135	reverse		60865551; 16.20; 1.8	Lake Chaplain
FM_38	47.93070 -121.91820	25	10	-150	265	85	-81	normal-oblique strike slip		60731746; 13.3; 1.7	Lake Roesiger

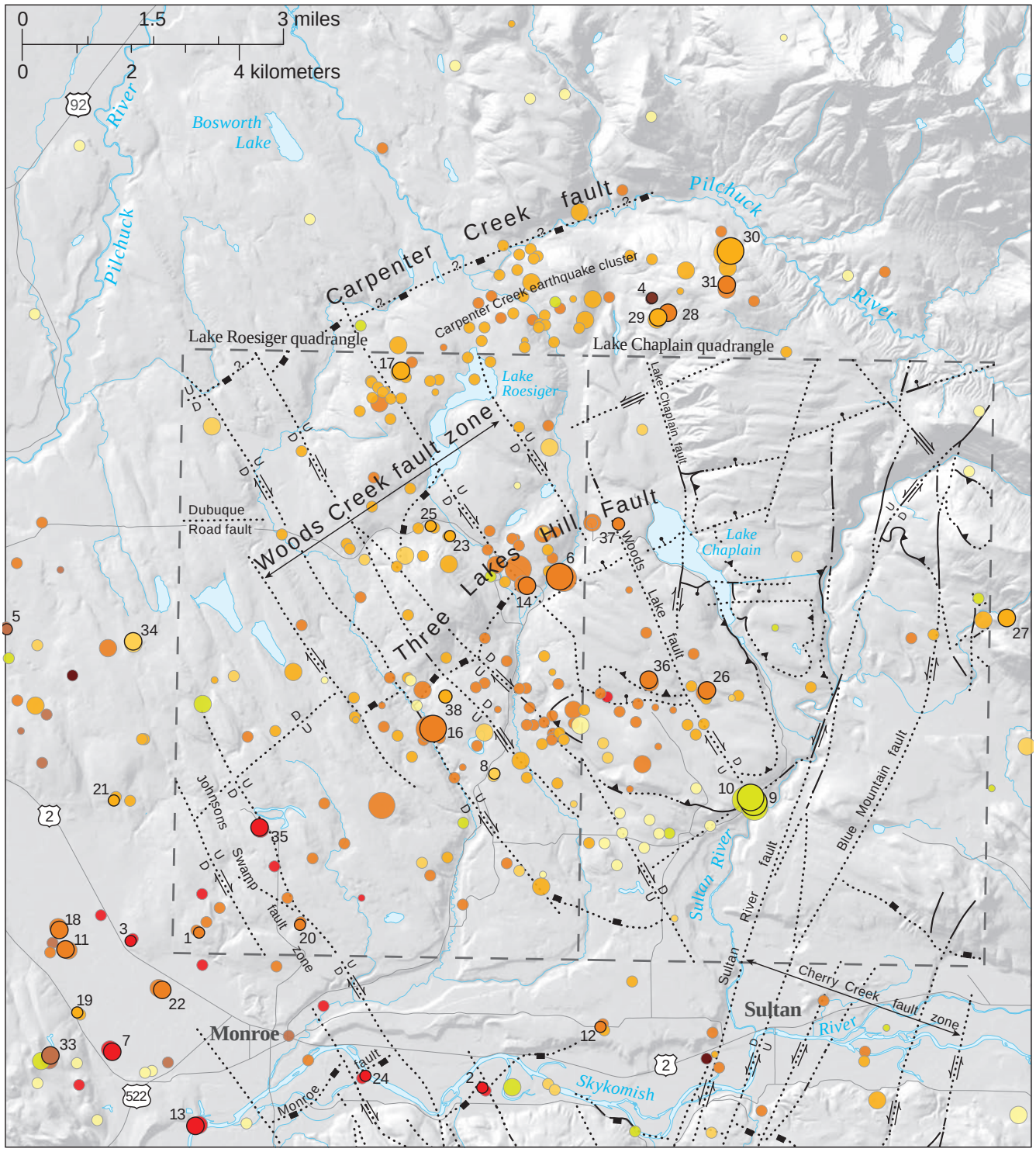

Depth (km)
- 0 – 2.5
- 2.6 – 5
- 5.1 – 10
- 10.1 – 15
- 15.1 – 20
- 20.1 – 25
- 25.1 – 30
- 30.1 – 34.2

Magnitude
- 0 – 1
- 1.1 – 2
- 2.1 – 3
- 3.1 – 5

Focal Mechanisms
- 38 (number corresponds to Table B1)

Figure B1. Earthquake epicenters in and around the Lake Roesiger and Lake Chaplain 7.5-minute quadrangles (dashed boxes). See Table B1 for focal mechanism data corresponding to numbered hypocenters shown with bold outlines. Faults are simplified from our current mapping (see Map Sheet for explanation of fault symbology) and Dragovich and others (2011a, 2013). See Figure M3 for a more detailed lidar view of the Carpenter Creek fault.

Appendix C. U-Pb Zircon Geochronology

Sample 47A—Pre-Hamm Creek nonglacial sand

We obtained detrital zircon U-Pb ages from a 3 m-high outcrop in a rill-like ephemeral creek 210 m east of the Lake Roesiger quadrangle (Fig.M3) at 760 ft elevation. The results are shown in Figure C1 and Table C1. The outcrop contains tilted, compact, and well stratified micaceous medium to coarse sand with some interbedded pebbly sand and silt beds. Basalt clasts have 5–7 mm weathering rinds and the sand is distinctly weathered. Sample contains monocrystalline quartz (~25%), plagioclase (~20%) polycrystalline quartz (~10%), biotite and white mica (~15%), some K-spar (~5%), and hornblende (~5%). Metasedimentary lithic grains (~15%) are prominent and vary from meta-argillite and metasandstone to foliate phyllite and similar foliate quartz aggregates such as metachert. Other lithic grain types (~5%) include blue amphibole, few granitics, chlorite, and epidote. Geochemical affinities for this sample support inputs from local WMB rocks and Cenozoic plutons to the east (see *Geochemistry*). An IRSL age of >550 ka was obtained by Dragovich and others (2014a) at this site (their sample 13-37D) and the detrital zircon sample was taken 10–20 cm below sample 13-37D.

We separated zircons using standard crushing, gravimetric, and magnetic techniques. A random selection of zircons were mounted in a standard 1-inch epoxy grain mount and polished to expose the grain centers. Backscatter electron and cathodoluminescence images were taken to aid in identifying suitable areas for analysis, avoiding areas such as cracks, inherited cores, inclusions, and metamic zones.

Analyses were conducted at the Canadian Centre for Isotopic Microanalysis (CCIM) plasma mass spectrometry lab using procedures modified from Simonetti and others (2005). The analytical setup consists of a New Wave UP-213 laser ablation system and DSN-100 desolvating nebulizer "Y connected" to a Nu I plasma multi-collector inductively coupled plasma mass spectrometer (MC-ICPMS). We operated the laser at 40 µm beam diameter, 4 Hz repetition rate at a fluence of ~3 J/cm^2. Data were collected statically in 30 one second integrations. Prior to and during each analytical session, we analyzed zircon reference materials GJ1 and LH9415 repeatedly to correct for U-Pb fractionation and instrument bias/drift. During all analyses a 0.5 ppb Tl solution was aspirated using the DSN-100. The simultaneous measurement of Tl allows estimation of Pb isotope mass bias (β) by applying an exponential mass fractionation law, assuming $\beta Tl \approx \beta Pb$, and a natural $^{205}Tl/^{203}Tl$ of 2.3871. For further details see Simonetti and others (2005).

All data were reduced offline using an Excel-based program. The uncertainties reported here are a quadratic combination of the standard error of a single measurement and the standard deviation of the zircon reference means. Overall standard reproducibility is approximately 3% (2σ) for $^{206}Pb/^{238}U$ and ~1% for $^{207}Pb/^{206}Pb$. For young zircons only $^{206}Pb/^{238}U$ ages are reported due to the low abundance of ^{207}Pb. No common Pb correction was performed due to the relative insensitivity of $^{206}Pb/^{238}U$ measurements to small amounts of common Pb and the uncertainties associated with subtracting the ^{204}Hg background.

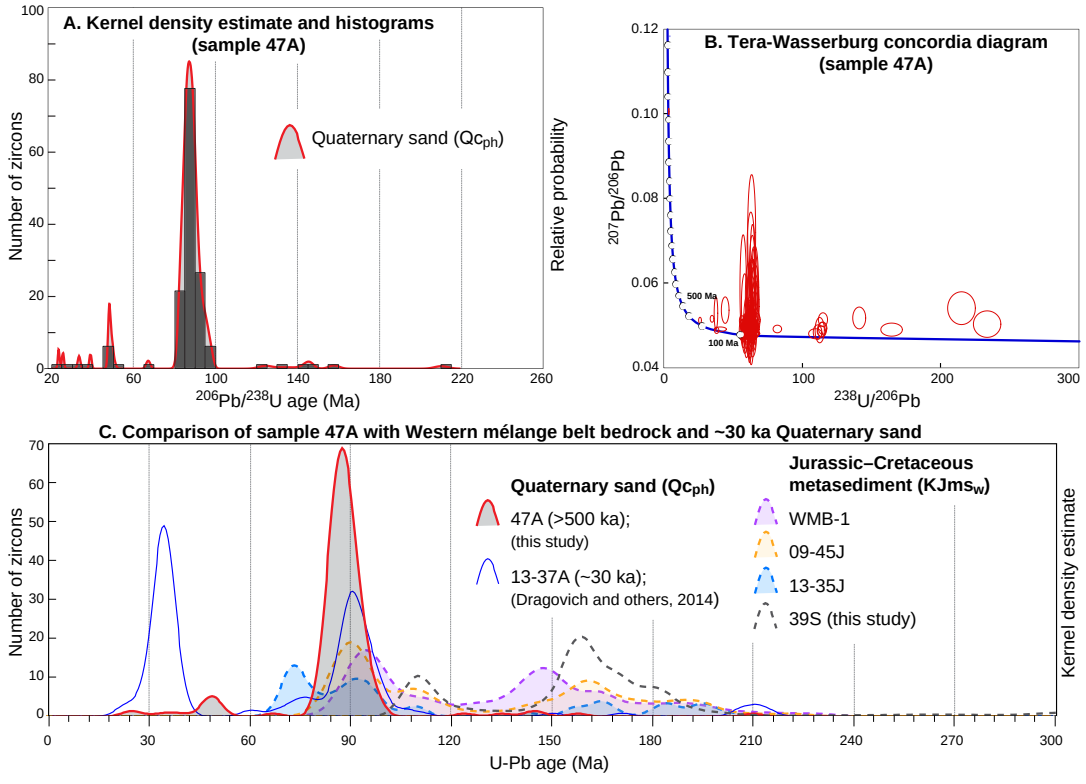

Figure C1. A) Probability density plot with histogram for sample 47A shows the age distribution for the younger age peak (80-100 Ma). **B)** Tera-Wasserburg concordia diagram of all sampled zircons (n=146); white dots along the concordia curve represent ages determined by the relationship between $^{207}Pb/^{206}Pb$ and $^{238}U/^{206}Pb$ ratios. Data point error ellipses are 2σ. **C)** Detrital zircon age comparison between three previously published WMB metasandstone age spectra (Dragovich and others, 2014a; Dragovich and others, 2009a,b; Brown, 2012), and two Quaternary sand age spectra: unit Qc$_o$ sample 13-37A (Dragovich and others, 2014a), and unit Qc$_{ph}$ sample 47A (this study). We suggest that the general lack of an Index batholith peak at ~33–34 Ma in early Pleistocene to Pliocene sample 47A as compared with the latest Pleistocene sample 13-37A is partly related to uplift of the Cascade Range or a persistent drainage divide between the Pilchuck and Sultan River basins.

Table C1. Sample 47A U-Pb detrital zircon data from unit Qc_{ph} in the Lake Roesiger 7.5-minute quadrangle. We obtained U-Pb age information for 146 zircons from a well-sorted sand deposit. Out of 147 analyzed grains, one analysis (not shown) was rejected because of insufficient count rates, a high common Pb component, ablation of subsurface inclusions, or the grain not being zircon. Some zircon grains have core to rim analyses represented by the letters (for example, zircon 106 has five analyses from 106A to 106E). cps, counts per second; * ^{204}Pb values are for reference only.

Zircon grain	^{206}Pb (cps)	^{204}Pb (cps)*	^{238}U/^{206}Pb ±2σ	^{207}Pb/^{206}Pb ±2σ	^{206}Pb/^{238}U age (Ma) ±2σ
1	12341	0	73.83 ±2.15	0.0510 ±0.0020	87 ±3
2	19256	0	127.47 ±4.68	0.0480 ±0.0010	50 ±2
3	36734	0	72.61 ±2.11	0.0500 ±0.0010	88 ±3
4	21663	0	69.17 ±2.72	0.0500 ±0.0010	93 ±4
5	16748	0	68.20 ±2.28	0.0490 ±0.0010	94 ±3
6	18330	0	71.33 ±3.03	0.0500 ±0.0010	90 ±4
7	58146	0	71.24 ±2.50	0.0500 ±0.0010	90 ±3
8	41978	35	67.10 ±1.92	0.0500 ±0.0010	95 ±3
9	11146	30	77.27 ±2.74	0.0510 ±0.0020	83 ±3
10	29978	23	72.69 ±2.45	0.0490 ±0.0010	88 ±3
11	25476	23	67.96 ±2.92	0.0500 ±0.0010	94 ±4
12	16459	49	73.27 ±1.68	0.0500 ±0.0010	87 ±2
13	135878	28	77.59 ±2.01	0.0480 ±0.0004	83 ±2
14	7867	45	71.49 ±2.47	0.0510 ±0.0020	90 ±3
15	7957	58	71.15 ±2.52	0.0510 ±0.0020	90 ±3
16	24919	53	70.76 ±1.71	0.0490 ±0.0010	90 ±2
17	9208	39	73.29 ±1.81	0.0490 ±0.0010	87 ±2
18	15196	30	73.57 ±2.11	0.0500 ±0.0010	87 ±2
19	42143	34	71.48 ±1.68	0.0490 ±0.0010	90 ±2
20	15369	31	71.83 ±2.24	0.0490 ±0.0010	89 ±3
21	140078	46	47.36 ±4.12	0.0490 ±0.0004	135 ±12
22	16925	49	71.32 ±2.16	0.0490 ±0.0010	90 ±3
23	24080	12	72.07 ±2.25	0.0500 ±0.0010	89 ±3
24	19906	12	95.37 ±2.94	0.0490 ±0.0010	67 ±2
25	11010	2	70.38 ±2.14	0.0500 ±0.0010	91 ±3
26	9913	8	73.54 ±2.26	0.0470 ±0.0010	87 ±3
27	18525	14	76.63 ±2.59	0.0500 ±0.0010	84 ±3
28	37791	12	75.52 ±3.66	0.0480 ±0.0010	85 ±4
29	13021	20	72.97 ±3.48	0.0490 ±0.0010	88 ±4
30	18145	25	75.80 ±2.05	0.0490 ±0.0010	84 ±2
31	39147	10	74.93 ±3.23	0.0500 ±0.0010	85 ±4
32	29254	5	75.70 ±2.79	0.0490 ±0.0010	85 ±3
33	18531	5	74.22 ±1.99	0.0520 ±0.0020	86 ±2
34	14590	13	73.04 ±2.55	0.0510 ±0.0030	88 ±3
35	17894	17	75.64 ±2.19	0.0500 ±0.0010	85 ±2
36	6374	24	272.19 ±9.45	0.0500 ±0.0030	24 ±1
37	33292	22	70.91 ±2.09	0.0490 ±0.0010	90 ±3
38	38300	15	73.24 ±3.03	0.0480 ±0.0004	87 ±4
39	25202	7	74.24 ±2.91	0.0480 ±0.0010	86 ±3
40	35053	19	70.78 ±2.70	0.0500 ±0.0010	90 ±3
41	16327	39	67.50 ±2.30	0.0490 ±0.0010	95 ±3
42	12607	38	72.94 ±3.10	0.0500 ±0.0010	88 ±4
43	29225	35	72.30 ±1.99	0.0490 ±0.0010	89 ±2
44	12618	26	71.44 ±2.23	0.0480 ±0.0010	90 ±3
45	47476	34	72.48 ±2.02	0.0480 ±0.0004	88 ±2
46	6338	23	43.63 ±1.23	0.0530 ±0.0030	146 ±4
47	8537	21	74.36 ±2.46	0.0510 ±0.0010	86 ±3
48	35922	23	74.65 ±1.79	0.0500 ±0.0010	86 ±2
49	45580	14	75.34 ±2.75	0.0490 ±0.0010	85 ±3
50	11610	14	74.76 ±1.87	0.0490 ±0.0010	86 ±2
51	28161	24	73.75 ±2.07	0.0490 ±0.0004	87 ±2
52	30245	27	76.23 ±2.31	0.0490 ±0.0010	84 ±3
53	9690	4	70.72 ±2.96	0.0480 ±0.0020	91 ±4
54	15553	0	73.98 ±1.93	0.0460 ±0.0010	87 ±2
55	152022	2	74.57 ±2.45	0.0480 ±0.0004	86 ±3
56	22764	16	71.70 ±2.91	0.0500 ±0.0030	89 ±4
57	21528	4	74.27 ±2.72	0.0480 ±0.0010	86 ±3
58	11071	11	72.23 ±1.99	0.0490 ±0.0010	89 ±2
59	17577	7	44.19 ±1.52	0.0490 ±0.0010	144 ±5
60	17587	7	74.77 ±2.79	0.0480 ±0.0010	86 ±3
61	32204	6	69.20 ±2.87	0.0500 ±0.0010	92 ±4
62	6981	31	73.86 ±2.26	0.0610 ±0.0040	87 ±3
63	34692	30	69.49 ±2.23	0.0500 ±0.0010	92 ±3
64	9766	30	72.78 ±2.05	0.0550 ±0.0010	88 ±2
65	31407	35	40.35 ±1.29	0.0520 ±0.0010	158 ±5
66	37480	11	76.45 ±2.18	0.0500 ±0.0010	84 ±2
67	6779	23	73.75 ±1.68	0.0540 ±0.0020	87 ±2
68	6010	28	72.44 ±2.22	0.0550 ±0.0010	88 ±3
69	14252	35	77.67 ±2.63	0.0510 ±0.0010	82 ±3
70	22277	27	73.67 ±2.19	0.0500 ±0.0010	87 ±3
71	60925	18	74.21 ±2.09	0.0480 ±0.0010	86 ±2
72	70339	33	68.26 ±1.76	0.0480 ±0.0002	94 ±2
73	9016	24	74.85 ±1.78	0.0530 ±0.0010	86 ±2
74	7663	29	74.99 ±2.64	0.0510 ±0.0010	85 ±3
75	5463	40	74.41 ±1.98	0.0540 ±0.0020	86 ±2
76	19697	29	75.03 ±2.86	0.0500 ±0.0010	85 ±3
77	10223	25	73.72 ±2.43	0.0530 ±0.0010	87 ±3
78	19237	22	76.07 ±1.71	0.0500 ±0.0010	84 ±2
79	27513	26	73.11 ±1.64	0.0490 ±0.0010	88 ±2
80	31949	26	73.02 ±2.15	0.0500 ±0.0010	88 ±3
81	32543	44	30.19 ±0.96	0.0510 ±0.0010	210 ±7
82	17792	33	70.54 ±1.73	0.0490 ±0.0010	91 ±2
83	5014	32	164.38 ±4.46	0.0520 ±0.0020	39 ±1
84	13525	62	74.97 ±2.93	0.0500 ±0.0010	85 ±3
85	19871	23	76.80 ±2.13	0.0500 ±0.0010	83 ±2
86	42514	27	70.53 ±2.08	0.0500 ±0.0004	91 ±3
87	40458	18	51.42 ±2.65	0.0540 ±0.0030	124 ±6
88	7406	23	191.68 ±7.43	0.0490 ±0.0010	34 ±1
89	8933	76	250.59 ±9.54	0.0540 ±0.0030	26 ±1
91	14764	50	65.32 ±1.57	0.0510 ±0.0010	98 ±2
92	7937	52	71.84 ±1.70	0.0540 ±0.0020	89 ±2
93	13619	58	72.32 ±1.72	0.0510 ±0.0010	89 ±2
94	14631	73	71.16 ±3.81	0.0500 ±0.0010	90 ±5
95	16128	60	66.51 ±2.06	0.0500 ±0.0010	96 ±3

Zircon grain	^{206}Pb (cps)	^{204}Pb (cps)*	^{238}U/^{206}Pb ±2σ	^{207}Pb/^{206}Pb ±2σ	^{206}Pb/^{238}U age (Ma) ±2σ
96	31459	60	69.95 ±2.45	0.0510 ±0.0020	92 ±3
97	51413	43	76.60 ±3.22	0.0480 ±0.0004	84 ±3
98A	5020	35	67.81 ±2.23	0.0550 ±0.0060	94 ±3
98B	6151	50	71.31 ±2.00	0.0500 ±0.0030	90 ±2
98C	5266	49	72.38 ±1.83	0.0520 ±0.0030	88 ±2
98D	2698	53	66.58 ±2.23	0.0590 ±0.0100	96 ±3
99A	17154	44	70.38 ±2.18	0.0510 ±0.0030	91 ±3
99B	5762	33	74.83 ±1.76	0.0560 ±0.0080	86 ±2
100A	2108	58	72.02 ±1.86	0.0530 ±0.0100	89 ±2
100B	6102	46	72.17 ±1.77	0.0470 ±0.0040	89 ±2
101A	5454	64	71.03 ±2.11	0.0470 ±0.0030	90 ±3
101B	10297	53	72.79 ±2.16	0.0470 ±0.0030	88 ±3
102A	3648	42	69.38 ±2.06	0.0500 ±0.0060	92 ±3
102B	2267	35	69.79 ±1.91	0.0510 ±0.0100	92 ±2
103A	5319	20	74.73 ±2.03	0.0470 ±0.0020	86 ±2
103B	5169	22	73.30 ±1.70	0.0470 ±0.0050	87 ±2
104A	9243	31	131.09 ±3.18	0.0490 ±0.0020	49 ±1
104B	16523	20	129.26 ±2.96	0.0490 ±0.0010	50 ±1
104C	23985	8	132.50 ±2.87	0.0490 ±0.0010	48 ±1
104D	19918	7	132.96 ±3.04	0.0490 ±0.0010	48 ±1
104E	15147	5	133.82 ±3.14	0.0520 ±0.0010	48 ±1
104F	14873	7	133.54 ±2.91	0.0500 ±0.0010	48 ±1
105A	5288	14	74.46 ±2.75	0.0480 ±0.0040	86 ±3
105B	8531	22	74.15 ±2.13	0.0490 ±0.0020	86 ±2
106A	5834	26	69.25 ±2.13	0.0490 ±0.0030	92 ±3
106B	4898	37	69.20 ±1.75	0.0480 ±0.0030	92 ±2
106C	4135	21	67.93 ±1.80	0.0480 ±0.0040	94 ±2
106D	5167	48	66.68 ±1.55	0.0480 ±0.0030	96 ±2
106E	8184	30	65.52 ±1.82	0.0490 ±0.0020	98 ±3
107A	3093	30	74.58 ±2.33	0.0600 ±0.0040	86 ±3
107B	6476	30	72.74 ±1.95	0.0520 ±0.0030	88 ±2
108A	4889	38	76.65 ±2.52	0.0590 ±0.0040	84 ±3
108B	3940	31	73.00 ±2.53	0.0690 ±0.0070	88 ±3
109A	6423	26	76.43 ±1.85	0.0550 ±0.0020	84 ±2
109B	6019	27	70.79 ±1.93	0.0570 ±0.0060	90 ±2
110	2420	22	73.88 ±2.67	0.0590 ±0.0050	87 ±3
111A	3717	25	76.63 ±2.77	0.0550 ±0.0050	84 ±3
111B	4001	19	76.57 ±2.00	0.0550 ±0.0050	84 ±2
111C	2530	37	73.71 ±2.74	0.0720 ±0.0110	87 ±3
111D	1919	27	74.26 ±1.99	0.0630 ±0.0070	86 ±2
111E	5639	50	71.61 ±1.73	0.0570 ±0.0040	89 ±2
112A	3713	25	75.62 ±2.37	0.0610 ±0.0070	85 ±3
112B	15505	25	72.50 ±1.78	0.0510 ±0.0020	88 ±2
113A	97422	5	70.89 ±2.44	0.0490 ±0.0010	90 ±3
113B	99037	6	71.89 ±1.82	0.0500 ±0.0010	89 ±2
113C	78746	2	70.84 ±2.14	0.0490 ±0.0010	90 ±3
114A	3949	7	74.50 ±1.72	0.0650 ±0.0080	86 ±2
114B	6441	17	75.01 ±1.77	0.0570 ±0.0050	85 ±2
115	30539	12	77.92 ±1.72	0.0490 ±0.0010	82 ±2
116	2983	8	76.56 ±2.31	0.0600 ±0.0070	84 ±3
117	30241	5	72.04 ±2.13	0.0510 ±0.0010	89 ±3
118	3881	5	76.83 ±2.45	0.0560 ±0.0050	83 ±3
119	17496	1	71.29 ±2.73	0.0510 ±0.0020	90 ±3

Sample 31S—Rhyolite of Hughes Lake

The Hughes Lake Rhyolite was sampled at 500 ft elevation approximately 1.5 km southeast of Hughes Lake (age site 31S on the Map Sheet) from a ~1 m-high logging road cut-slope. The surrounding outcrop and hill is the only location where these rocks were observed. See sample 11S in Appendix D for geochemical analyses and detailed location information. Outcrop and petrographic descriptions for unit Mvr are given under *Tertiary Volcanic, Intrusive, and Sedimentary Rocks.* We propose that the rhyolite is an eroded dome that intruded the Western mélange belt near the intersection of the Woods Creek fault zone and the Three Lakes Hill fault. We assume that the rhyolite is preserved in the subsurface within the Explorer Falls basin.

Zircons were separated using standard crushing and density separation techniques. Selected grains were then prepared for CA-ID-TIMS using a procedure modified from Mattinson (2005). Zircons were annealed at 900°C for 60 hours and then partially digested in concentrated HF in a Parr vessel held at 215°C for 12 hours. The partially digested grains were then sequentially rinsed in ultrapure H_2O and 6.2N HCl before being individually loaded in Teflon microcapsules. The capsules were then spiked with the EARTHTIME ^{205}Pb-^{233}U-^{235}U isotopic tracer and the grains were then completely dissolved in concentrated HF held at 215°C for 48 hours. The resulting solutions were dried down, dissolved in 6.2N HCl held at 180°C for ~12 hours, dried down once again, converted to 3N HCl, and U and Pb were separated on anion exchange columns following the procedure of Krogh (1973). Following U and Pb separation, the solutions were dried down, redissolved in silica gel, and loaded onto outgassed, zone-refined Re filaments for analysis on the VG Sector 54 thermal ionization mass spectrometer at MIT. All isotopic ratios are corrected for mass dependent fractionation, contamination with Pb during laboratory work (Pbc), and for initial exclusion of Th during zircon crystallization. Data reduction was done using the *U-Pb_Redux* software package (Bowring and others, 2011) and used the decay constants for ^{238}U and ^{235}U presented in Jaffey and others (1971). The ^{206}Pb/^{238}U chronometer provides the most precise date for rocks of this age and we report a weighted mean ^{206}Pb/^{238}U date for sample 31S (Fig. C2 and Table C2). Uncertainty is reported in the format ±X/Y/Z, where X is the analytical uncertainty, Y is the analytical uncertainty plus the uncertainty in the isotopic composition of the tracer, and Z is the uncertainty in X and Y plus the uncertainty in the ^{238}U decay constant.

Seven zircons were dated from sample 31S using chemical-abrasion isotope-dilution thermal ionization mass spectrometry

(CA-ID-TIMS) U-Pb geochronology and the results are reported in Figure C2 and Table C2. Six of the seven grains have Th-corrected, $^{206}Pb/^{238}U$ dates that give a weighted mean date of 23.300 ±0.017/0.020/0.032 Ma with a mean square weighted deviation (MSWD) of 1.7 that indicates that age dispersion within these six grains can be explained by analytical uncertainty alone. A single zircon gave a Th-corrected $^{206}Pb/^{238}U$ date of 14.291 ±0.042 Ma. We think that this grain was sourced from unit Qgl_v sediment that contaminated the surface of the sample and do not attribute any significance to its date. This contamination is consistent with the poorly exposed nature of the rhyolite outcropping and our inability to completely remove the dried sandy silt from the samples with a simple washing. However, it is important to note that if this grain did come from sample 31S, then the sample must be <14.291 ±0.042/0.042/0.0451 Ma in age. The 23.300 ±0.032 Ma age is similar to the 18.25 ±0.43 Ma to 22.76 ±0.33 Ma age of the volcanic rocks of Snoqualmie Falls (Dragovich and others, 2009a,b), which are probably the extrusive equivalents of the Miocene Snoqualmie batholith.

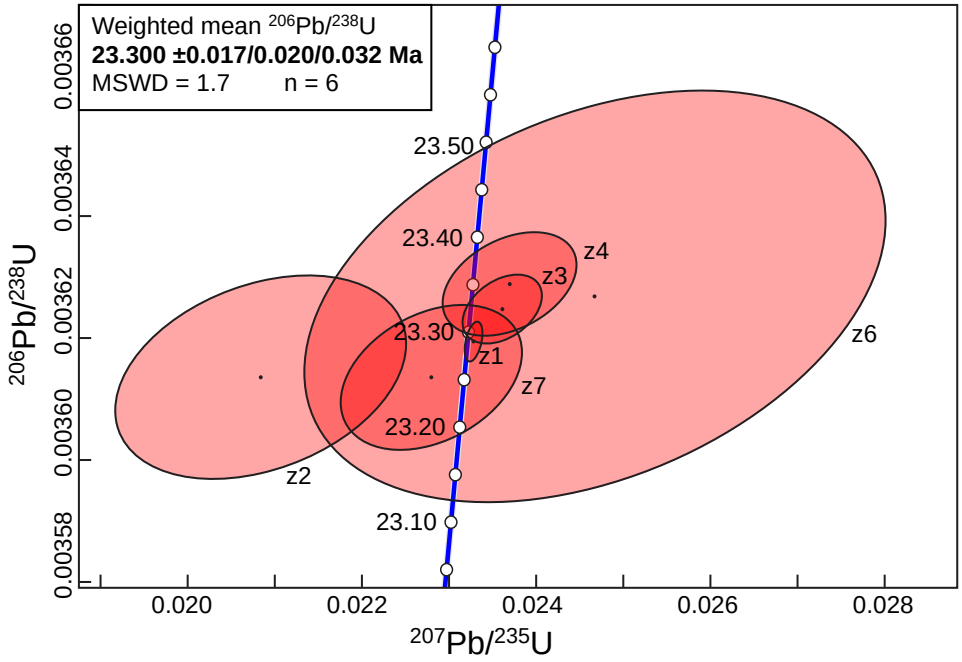

Figure C2. Concordia diagram of six of the seven sampled zircon grains from sample 31S. A single zircon (sample z5) was excluded from the plot and weighted mean because it was significantly younger (14.291 ±0.042 Ma) than the remaining samples. We think that this grain was sourced from Quaternary sediments that contaminated the surface of the sample and do not attribute any significance to its date. However, it is important to note that if this grain is from the original volcanic sample, it constrains the rock's age to <14.291 Ma.

Table C2. Sample 31S U-Pb CA-IDTIMS single zircon data (unit Mvr) in the Lake Roesiger 7.5-minute quadrangle.

Zircon grain	Dates (Ma) ±2σ			Discordance (%)[c]	Correction Coefficient	Composition			Isotopic Ratios ±2σ				
	$^{206}Pb/^{238}U$[a]	$^{207}Pb/^{235}U$[b]	$^{207}Pb/^{206}Pb$[b]			Th/U[d]	Pbc (pg)[e]	Pb/Pbc[f]	$^{206}Pb/^{204}Pb$[g]	$^{208}Pb/^{206}Pb$[h]	$^{206}Pb/^{238}U$[a,h]	$^{207}Pb/^{235}U$[h]	$^{207}Pb/^{206}Pb$[a,h]
z1	23.290 ±0.021	23.36 ±0.10	40.1 ±9.8	42.14	0.430	0.34	0.35	62	3826	0.109	0.003619 ±0.090	0.02327 ±0.44	0.046649 ±0.41
z2	23.25 ±0.110	20.9 ±1.70	-230 ±200	110.06	0.333	0.91	0.45	3	189	0.291	0.003614 ±0.46	0.0208 ±8.0	0.041820 ±7.9
z3	23.324 ±0.036	23.68 ±0.45	69 ±45	66.09	0.405	0.72	0.31	11	640	0.232	0.003625 ±0.16	0.02360 ±1.9	0.047239 ±1.9
z4	23.351 ±0.054	23.77 ±0.76	76 ±75	69.28	0.374	0.38	0.46	6	396	0.121	0.003629 ±0.23	0.02368 ±3.2	0.047354 ±3.2
z5	14.291 ±0.042	15.85 ±0.52	267 ±74	94.68	0.361	1.39	0.95	7	344	0.446	0.002219 ±0.29	0.01573 ±3.3	0.051418 ±3.2
z6	23.34 ±0.220	24.7 ±3.30	172 ±310	86.45	0.372	0.60	0.33	1	103	0.192	0.003627 ±0.93	0.0247 ±14	0.049341 ±13
z7	23.252 ±0.076	22.9 ±1.00	-7 ±110	414.91	0.349	0.55	0.33	5	286	0.176	0.003614 ±0.33	0.0228 ±4.6	0.045753 ±4.5

[a] Corrected for initial Th/U disequilibrium using radiogenic ^{208}Pb and Th/U[magma] = 2.80000.

[b] Isotopic dates calculated using the decay constants λ_{238} = 1.55125E-10 and λ_{235} = 9.8485E-10 (Jaffey and others, 1971).

[c] % discordance = 100 - (100 * ($^{206}Pb/^{238}U$ date) / ($^{207}Pb/^{206}Pb$ date))

[d] Th contents calculated from radiogenic ^{208}Pb and the $^{207}Pb/^{206}Pb$ date of the sample, assuming concordance between U-Th and Pb systems.

[e] Total mass of common Pb.

[f] Ratio of radiogenic Pb (including ^{208}Pb) to common Pb.

[g] Measured ratio corrected for fractionation and spike contribution only.

[h] Measured ratios corrected for fractionation, tracer and blank.

Sample 39S—Meta-argillite

Sample is from a 1–3 m-high outcrop on private property at 485 ft elevation, directly east of Lake Cochran, along Woods Creek Road. This sample was also analyzed for whole-rock geochemistry and has a mafic volcanic arc affinity (see Geochemistry section for more information). This sample occurs within the Woods Creek fault zone and is locally strongly fractured. Metagabbro is faulted against these metasedimentary rocks on the west side of the property. The outcrop exposes meta-argillite, locally with thin sub-vertical beds of fine-grained lithofeldspathic metasandstone that strike northwest and parallel the Woods Creek fault zone. A moderately strong cleavage is sub-parallel to the discontinuous bedding. Meta-argillite and metasandstone beds contain subangular to subrounded grains of monocrystalline quartz (~30%), plagioclase (~25%), polycrystalline quartz (~15%), lithic fragments dominated by felsic to intermediate microlitic volcanic grains (~20%), and some detrital mica. Metamorphic minerals include epidote, chlorite, and pumpellyite. These volcanic lithic metasandstone interbeds are probably similar to the lithic petrofacies of Jett and Heller (1988) and the volcanic provenance metasedimentary rocks described by Dragovich and others (2014a) directly east of the map area. For further information, see detailed description of unit KJms$_w$ and *Mesozoic Tectonics and the Western Mélange Belt—Selected Notes.*

Detrital zircons were obtained through standard crushing and heavy liquid mineral separation procedures. In order to avoid picking bias, the entire zircon separate was poured onto sticky tape and subsequently mounted on a 1-inch round epoxy puck. Grains were imaged to identify internal zoning using the cathodoluminescence detector on the JEOL JSM-7100FT field emission scanning electron microscope at the University of Nevada, Reno. These images were used to guide the analyses, which focused on the core of each grain. Zircons were analyzed for U-Pb geochronology in the laser ablation inductively coupled plasma mass spectrometer (LA-ICP-MS) laboratory at the University of California–Santa Barbara using a Nu Instruments Plasma HR multi-collector ICP-MS and the 193 nm Photon Machines excimer laser. A spot size of 15 µm was used with laser energies consistent with an ablation pit depth of ~6 µm (60 shots/analysis). In order to avoid bias based on size or morphology, analyses were performed in a systematic pattern across the mount. Results are reported in Figure C3 and Table C3.

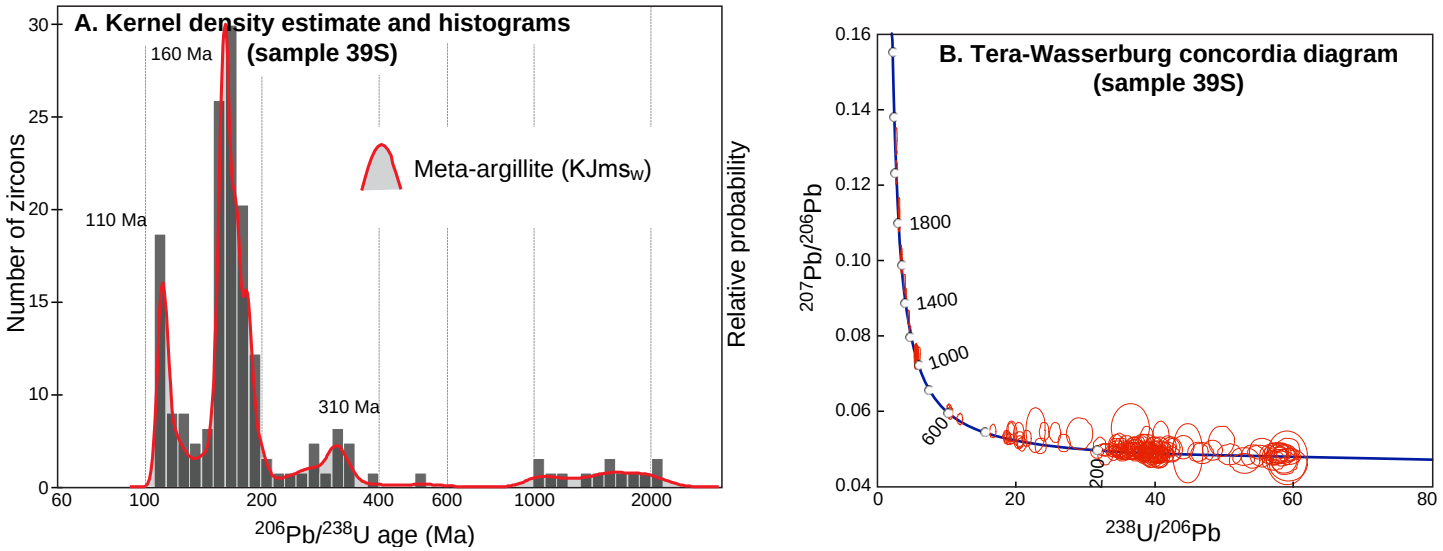

Figure C3. Age distribution and concordia plot for sample 39S. **A)** Histogram and kernel density estimate plot (Vermeesch, 2012) to show the age distribution of detrital zircons. Major age peaks, defined by populations of 3 or more overlapping dates, are labeled. X-axis scale is logarithmic. **B)** Tera-Wasserburg concordia plot with all analyses shown. Data point ellipses include 2σ uncertainty.

Table C3. Sample 39S U-Pb detrital zircon data from unit KJms$_w$ in the Lake Roesiger 7.5-minute quadrangle. We obtained U-Pb age information for 151 zircons from an interbedded section of meta-argillite and metasandstone. cps, counts per second; * ^{204}Pb values are for reference only.

Zircon grain	^{206}Pb (cps)	^{204}Pb (cps)*	^{238}U/^{206}Pb ±2σ	^{207}Pb/^{206}Pb ±2σ	^{206}Pb/^{238}U age (Ma) ±2σ
1	4860	1	40.06 ±0.91	0.0500 ±0.0020	159 ±4
2	70800	4	4.09 ±0.10	0.0910 ±0.0020	1437 ±40
3	8412	2	39.25 ±1.00	0.0500 ±0.0020	162 ±4
4	23880	8	39.84 ±0.95	0.0480 ±0.0010	160 ±4
5	22020	-42	34.86 ±0.80	0.0490 ±0.0010	182 ±4
6	3648	-30	42.43 ±1.30	0.0500 ±0.0030	150 ±5
7	21366	-6	36.95 ±0.94	0.0500 ±0.0010	172 ±4
8	30006	-2	37.88 ±0.86	0.0500 ±0.0010	168 ±4
9	28704	48	40.14 ±0.99	0.0490 ±0.0010	159 ±4
10	10722	5	32.94 ±0.85	0.0500 ±0.0010	193 ±5

Zircon grain	^{206}Pb (cps)	^{204}Pb (cps)*	^{238}U/^{206}Pb ±2σ	^{207}Pb/^{206}Pb ±2σ	^{206}Pb/^{238}U age (Ma) ±2σ
11	66480	7	4.55 ±0.11	0.0850 ±0.0020	1318 ±31
12	6246	10	36.97 ±0.97	0.0510 ±0.0020	172 ±5
13	11310	-7	21.55 ±0.54	0.0530 ±0.0020	292 ±7
14	27450	13	34.20 ±0.84	0.0500 ±0.0010	186 ±5
15	11430	16	57.50 ±1.42	0.0500 ±0.0020	111 ±3
16	16920	0	52.85 ±1.30	0.0480 ±0.0010	121 ±3
18	1420	30	29.15 ±1.56	0.0550 ±0.0030	216 ±11
19	4170	6	50.81 ±1.45	0.0490 ±0.0020	126 ±4
20	5010	8	57.14 ±1.35	0.0470 ±0.0020	112 ±3
21	4638	5	38.18 ±0.94	0.0510 ±0.0020	166 ±4
22	6834	48	36.17 ±0.89	0.0500 ±0.0020	176 ±4
23	33960	8	38.94 ±0.97	0.0510 ±0.0010	163 ±4
24	7830	7	37.62 ±0.92	0.0510 ±0.0020	169 ±4
25	7272	30	40.57 ±1.04	0.0470 ±0.0020	157 ±4
26	20616	13	20.55 ±0.44	0.0520 ±0.0010	306 ±7
27	13830	48	57.60 ±1.38	0.0490 ±0.0010	111 ±3
28	62400	7	19.11 ±0.44	0.0530 ±0.0010	329 ±8
29	5052	7	40.92 ±1.02	0.0480 ±0.0020	156 ±4
30	11514	9	38.88 ±0.99	0.0490 ±0.0020	164 ±4
31	6102	-5	40.83 ±0.98	0.0480 ±0.0020	156 ±4
32	1078	30	59.07 ±2.43	0.0480 ±0.0060	108 ±5
33	4542	12	25.64 ±0.68	0.0550 ±0.0020	246 ±6
34	16026	30	31.69 ±0.77	0.0500 ±0.0010	200 ±5
35	14970	13	34.86 ±0.82	0.0500 ±0.0010	182 ±4
36	33648	9	39.09 ±0.94	0.0490 ±0.0010	163 ±4
37	22320	5	35.36 ±0.90	0.0490 ±0.0010	180 ±5
38	4938	-36	39.84 ±1.08	0.0510 ±0.0020	159 ±4
39	14640	54	35.11 ±0.89	0.0500 ±0.0010	181 ±5
40	1572	36	22.83 ±1.14	0.0550 ±0.0050	275 ±14
41	6372	8	38.79 ±0.98	0.0500 ±0.0020	164 ±4
42	17088	11	38.71 ±0.93	0.0530 ±0.0020	164 ±4
43	8076	-48	57.77 ±1.33	0.0490 ±0.0020	111 ±3
44	4794	8	58.24 ±1.57	0.0490 ±0.0030	110 ±3
45	12630	7	40.80 ±1.09	0.0490 ±0.0020	156 ±4
46	10182	23	38.24 ±0.92	0.0490 ±0.0020	167 ±4
47	4134	0	38.82 ±0.91	0.0520 ±0.0030	163 ±4
48	5388	12	32.87 ±0.89	0.0490 ±0.0020	193 ±5
49	8214	-3	40.82 ±0.94	0.0490 ±0.0020	156 ±4
50	12834	9	37.3 ±0.97	0.0490 ±0.0010	171 ±4
51	3184	6	55.43 ±1.44	0.0640 ±0.0030	113 ±3
52	41520	10	4.78 ±0.11	0.0810 ±0.0020	1215 ±28
53	37860	9	37.91 ±0.94	0.0490 ±0.0010	168 ±4
54	149100	2	11.92 ±0.34	0.0580 ±0.0010	519 ±14
55	3179	-13	40.80 ±1.13	0.0500 ±0.0030	156 ±4
56	25680	-36	41.86 ±0.99	0.0500 ±0.0020	152 ±4
57	36186	8	3.93 ±0.10	0.0940 ±0.0020	1510 ±43
58	3984	24	39.34 ±1.02	0.0480 ±0.0020	162 ±4
59	22920	1	37.88 ±0.93	0.0490 ±0.0010	168 ±4
60	15120	60	40.93 ±0.96	0.0490 ±0.0010	156 ±4
61	10362	4	34.9 ±0.83	0.0520 ±0.0020	181 ±4
62	1181	7	47.87 ±1.85	0.1150 ±0.0090	122 ±5
63	6912	8	42.54 ±0.97	0.0510 ±0.0020	149 ±3
64	4008	4	55.46 ±1.48	0.0500 ±0.0030	115 ±3
65	12324	24	34.12 ±0.78	0.0490 ±0.0020	186 ±4
66	256440	42	5.58 ±0.13	0.0760 ±0.0020	1104 ±25
67	248940	7	37.72 ±0.85	0.0500 ±0.0010	169 ±4
68	6360	-30	34.38 ±0.76	0.0510 ±0.0020	185 ±4
69	8118	-8	55.07 ±1.43	0.0500 ±0.0010	116 ±3
70	7206	5	59.24 ±1.47	0.0480 ±0.0020	108 ±3
71	971	48	38.17 ±2.04	0.1350 ±0.0100	149 ±8
72	75660	6	5.83 ±0.14	0.0740 ±0.0020	1032 ±24
73	10572	1	40.44 ±1.14	0.0480 ±0.0020	158 ±4
74	12174	0	39.14 ±1.01	0.0510 ±0.0010	162 ±4
75	13638	-18	39.92 ±0.91	0.0490 ±0.0020	160 ±4
76	14256	-1	41.55 ±1.00	0.0490 ±0.0010	153 ±4
77	24996	-48	40.14 ±0.94	0.0500 ±0.0010	159 ±4
78	3450	5	44.11 ±1.27	0.0510 ±0.0030	144 ±4
79	7404	8	26.93 ±0.73	0.0520 ±0.0020	235 ±6
80	3180	54	38.26 ±1.21	0.0510 ±0.0030	166 ±5
81	1645	-30	39.12 ±1.43	0.0630 ±0.0060	160 ±6
82	11544	14	41.02 ±1.13	0.0500 ±0.0020	155 ±4
83	22386	0	37.79 ±0.98	0.0510 ±0.0010	168 ±4
84	6984	42	34.54 ±0.98	0.0510 ±0.0020	184 ±5
85	20280	-54	40.7 ±0.95	0.0510 ±0.0010	156 ±4
86	6258	6	38.39 ±0.98	0.0500 ±0.0020	166 ±4
87	8640	9	40.55 ±0.99	0.0490 ±0.0020	157 ±4
88	4098	-7	57.08 ±1.57	0.0490 ±0.0020	112 ±3
89	105120	13	3.13 ±0.08	0.1140 ±0.0020	1864 ±38
90	2622	17	58.58 ±1.58	0.0480 ±0.0030	109 ±3
91	6330	-42	37.31 ±1.00	0.0510 ±0.0020	170 ±5
92	11598	1	19.30 ±0.44	0.0550 ±0.0020	325 ±7
93	6702	0	39.68 ±1.17	0.0480 ±0.0020	161 ±5
94	271200	12	5.98 ±0.17	0.0760 ±0.0020	992 ±27
95	16434	-1	40.82 ±0.97	0.0490 ±0.0010	156 ±4
96	49860	9	3.48 ±0.1.00	0.0990 ±0.0020	1605 ±40
97	3426	1	49.63 ±1.52	0.0520 ±0.0030	128 ±4
98	5070	-6	37.09 ±1.00	0.0510 ±0.0020	171 ±5
99	13440	-13	40.60 ±1.00	0.0500 ±0.0020	157 ±4
100	39840	13	2.75 ±0.07	0.1230 ±0.0030	2007 ±38
101	6156	-48	35.59 ±0.92	0.0500 ±0.0020	178 ±5
102	1603	19	59.28 ±2.24	0.0460 ±0.0040	108 ±4
103	5994	54	35.92 ±0.97	0.0510 ±0.0030	177 ±5
104	20538	54	36.90 ±0.94	0.0500 ±0.0010	172 ±4
105	5064	42	39.06 ±1.12	0.0490 ±0.0030	163 ±5
106	15120	42	39.40 ±1.02	0.0500 ±0.0020	161 ±4
107	17562	-12	37.04 ±0.88	0.0500 ±0.0010	172 ±4
108	13320	36	32.08 ±0.72	0.0520 ±0.0020	198 ±4
109	5760	0	39.64 ±1.06	0.0490 ±0.0020	161 ±4
110	6462	6	24.05 ±0.57	0.0550 ±0.0020	261 ±6
111	38706	9	3.12 ±0.10	0.1110 ±0.0030	1811 ±41
112	3264	-6	54.14 ±1.43	0.0490 ±0.0030	118 ±3
113	11142	1	40.39 ±0.97	0.0490 ±0.0020	158 ±4

Zircon grain	^{206}Pb (cps)	^{204}Pb (cps)*	^{238}U/^{206}Pb ±2σ	^{207}Pb/^{206}Pb ±2σ	^{206}Pb/^{238}U age (Ma) ±2σ
114	56580	48	41.61 ±0.97	0.0490 ±0.0010	153 ±4
115	18600	7	32.54 ±0.87	0.0500 ±0.0010	195 ±5
116	6102	-7	35.15 ±0.87	0.0510 ±0.0020	181 ±4
117	10578	18	36.50 ±1.05	0.0500 ±0.0020	174 ±5
118	263160	11	3.47 ±0.09	0.1020 ±0.0020	1657 ±38
119	10884	42	35.41 ±0.84	0.0500 ±0.0020	180 ±4
120	5148	9	57.34 ±1.51	0.0490 ±0.0020	111 ±3
121	10068	-5	23.55 ±0.70	0.0510 ±0.0020	268 ±8
122	9966	12	20.47 ±0.58	0.0530 ±0.0020	307 ±9
123	3990	-4	19.38 ±0.62	0.0550 ±0.0020	324 ±10
124	3750	12	20.41 ±0.65	0.0540 ±0.0030	308 ±10
125	4494	7	57.97 ±1.39	0.0490 ±0.0020	110 ±3
126	2567	13	58.75 ±1.64	0.0480 ±0.0030	109 ±3
127	19890	-8	39.97 ±0.96	0.0520 ±0.0020	159 ±4
128	3204	0	40.88 ±0.98	0.0540 ±0.0030	155 ±4
129	1242	36	44.76 ±1.78	0.0490 ±0.0060	142 ±6
130	452	-12	55.25 ±4.12	0.0590 ±0.0080	114 ±9
131	1800	-4	52.97 ±1.80	0.0470 ±0.0030	121 ±4
132	22140	0	16.69 ±0.38	0.0550 ±0.0010	375 ±8

Zircon grain	^{206}Pb (cps)	^{204}Pb (cps)*	^{238}U/^{206}Pb ±2σ	^{207}Pb/^{206}Pb ±2σ	^{206}Pb/^{238}U age (Ma) ±2σ
133	1346	-6	57.77 ±1.82	0.0440 ±0.0040	111 ±4
134	13170	11	20.86 ±0.55	0.0520 ±0.0020	302 ±8
135	11616	8	42.34 ±1.05	0.0490 ±0.0020	150 ±4
136	21060	-42	34.00 ±0.88	0.0500 ±0.0010	187 ±5
137	3801	6	59.17 ±1.43	0.0500 ±0.0030	108 ±3
138	11274	11	34.95 ±0.90	0.0500 ±0.0010	182 ±5
139	23364	8	39.57 ±1.04	0.0500 ±0.0010	161 ±4
140	6678	18	36.87 ±0.89	0.0500 ±0.0020	172 ±4
141	6648	-48	46.23 ±1.20	0.0500 ±0.0020	138 ±4
142	19020	8	2.72 ±0.12	0.1320 ±0.0030	2121 ±40
143	4908	8	41.86 ±1.04	0.0510 ±0.0020	152 ±4
144	13446	-5	58.38 ±1.51	0.0480 ±0.0010	109 ±3
145	6408	12	34.45 ±0.91	0.0520 ±0.0020	184 ±5
146	970	12	36.50 ±2.25	0.0560 ±0.0050	173 ±11
147	16920	1	58.48 ±1.60	0.0490 ±0.0010	109 ±3
148	11040	11	39.29 ±1.03	0.0490 ±0.0020	162 ±4
149	17640	11	36.47 ±0.88	0.0500 ±0.0010	174 ±4
150	5070	36	46.84 ±1.35	0.0490 ±0.0020	136 ±4
151	4986	12	48.33 ±1.19	0.0500 ±0.0020	132 ±3

Appendix D. Geochemical Data

Whole-rock major- and trace-element analyses were performed on glacial and nonglacial sand and rock using x-ray fluorescence (XRF) and inductively coupled plasma source mass spectrometry (ICP-MS) at the GeoAnalytical Laboratory of Washington State University (WSU). Grinding of samples was completed at WSU using a tungsten carbide mill for XRF analyses and iron equipment for ICP-MS analyses. Estimates of accuracy and precision, as well as discussion of analytical methods for both XRF and ICP-MS at WSU, are given by Johnson and others (1999) and Knaack and others (1994), respectively. We prepared the Quaternary sand with 2 mm (mesh no. 10) and 0.075 mm (mesh no. 200) sieves at the DNR laboratory in Olympia, Washington prior to grinding at WSU, so that only the sand-size fraction was chemically analyzed. Although most samples were well-sorted sand, sieving provides a better comparison between sand samples, eliminating or reducing erroneous results that may ensue from inclusion of fines and pebbles in the sand samples. As part of their quality check, WSU re-analyzed sample 5Q using both XRF and ICP-MS methods. We present an average for both analyses in the tables below.

Table D1. Unnormalized x-ray fluorescence data from the Lake Roesiger 7.5-minute quadrangle. Dark gray shading, IRSL age sample; light gray shading, U-Pb zircon sample; *, all iron reported as Fe^{2+} (FeO); **, average of two analyses; ***, chemical index of alteration (CIA). CIA = {(Al_2O_3/101.96)/[(Al_2O_3/101.96) + (CaO/56.08) + (Na_2O/61.98) + (K_2O/94.20)]}*100.

Sample Unit	Latitude Longitude	SiO_2 (wt %)	TiO_2 (wt %)	Al_2O_3 (wt %)	FeO* (wt %)	MnO (wt %)	MgO (wt %)	CaO (wt %)	Na_2O (wt %)	K_2O (wt %)	P_2O_5 (wt %)	LOI (wt %)	Total (wt %)	Ni ppm	Cr ppm	V ppm	Cu ppm	Ga ppm	Zn ppm	CIA***
2A KJigb$_W$	47.942362 -121.897678	58.21	0.67	16.77	8.21	0.19	3.11	7.27	3.11	0.53	0.10	1.69	99.87	0.29	0.98	225	117	15	72	47.00
5Q** KJms$_W$	47.921928 -121.931204	68.51	0.45	14.12	3.52	0.06	1.47	3.35	3.47	2.04	0.10	2.66	99.77	12.64	35.18	82	11	16	56	50.21
6T Qc$_{ph}$	47.999821 -121.907264	71.70	0.49	13.73	3.66	0.03	1.49	1.74	2.26	0.95	0.03	2.66	98.75	28.61	52.17	69	38	16	70	63.45
9AB Qc$_{ph}$	47.988939 -121.914186	75.59	0.38	11.76	2.67	0.04	1.14	1.72	1.84	0.97	0.03	2.97	99.12	22.83	45.96	65	16	13	50	62.01
16D KJms$_W$	47.920334 -121.900228	65.00	0.78	14.89	6.85	0.10	2.19	1.26	3.31	1.66	0.15	3.84	100.03	39.98	73.01	143	44	15	105	60.97
17D KJms$_W$	47.906884 -121.825862	68.71	0.69	12.94	5.63	0.11	3.05	1.61	3.50	0.67	0.13	2.90	99.93	59.49	195.02	148	30	13	70	57.91
19D Qc$_{ph}$	47.956159 -121.931941	67.07	0.63	15.33	4.42	0.04	1.82	1.92	1.97	0.97	0.04	5.19	99.39	27.44	76.64	125	28	19	99	66.31
26J Qc$_{phl}$	47.94839 -121.888474	64.04	0.58	12.12	6.97	0.13	6.19	1.80	1.91	0.94	0.12	5.05	99.87	368.77	648.96	134	60	11	89	61.95
302C KJms$_W$	47.915869 -121.882983	66.12	0.54	15.80	4.19	0.08	1.83	1.82	4.72	1.58	0.14	2.67	99.49	18.33	49.69	90	11	18	61	55.27
31S Mvr	47.953052 -121.88857	75.71	0.12	13.02	0.77	0.04	0.15	0.25	3.56	3.91	0.03	1.90	99.47	4.61	5.19	5	3	12	23	55.24
31V Qc$_{phl}$	47.957463 -121.878995	63.11	0.69	13.48	6.91	0.14	5.39	1.51	2.17	1.26	0.16	5.15	99.98	281.85	402.88	147	69	14	97	63.67
33B Qc$_{ph}$	47.988473 -121.915157	69.98	0.52	13.76	3.80	0.04	1.54	1.91	2.07	1.06	0.05	4.07	98.80	23.42	60.47	93	27	16	72	63.16
33D Qc$_{ph}$	47.878913 -121.917687	70.49	0.35	14.54	2.96	0.05	1.39	2.85	3.36	1.34	0.08	2.35	99.76	36.65	61.35	69	21	14	41	54.47
33G Qa	47.873027 -121.884002	74.50	0.41	9.67	4.08	0.09	3.03	1.28	2.09	0.82	0.09	3.33	99.41	116.03	246.57	84	20	10	58	59.24
35A Qc$_{ph}$	47.957271 -121.92326	68.65	0.71	12.81	4.47	0.08	1.74	1.90	1.98	1.05	0.06	5.66	99.12	48.56	126.46	103	28	14	70	62.02

Sample Unit	Latitude Longitude	SiO_2 (wt %)	TiO_2 (wt %)	Al_2O_3 (wt %)	FeO* (wt %)	MnO (wt %)	MgO (wt %)	CaO (wt %)	Na_2O (wt %)	K_2O (wt %)	P_2O_5 (wt %)	LOI (wt %)	Total (wt %)	Ni ppm	Cr ppm	V ppm	Cu ppm	Ga ppm	Zn ppm	CIA***
35B Qc_{phl}	47.938484 -121.913251	62.22	0.65	12.48	6.78	0.12	7.02	1.73	2.10	1.08	0.16	5.07	99.42	311.25	462.95	144	52	13	89	61.60
36N $KJms_w$	47.999792 -121.884889	57.95	0.84	17.18	7.51	0.06	3.66	0.85	1.75	2.66	0.20	6.47	99.14	89.87	186.00	201	74	19	118	70.17
37V Qc_{phl}	47.977237 -121.988382	61.99	0.72	14.08	7.22	0.10	4.85	1.44	2.06	1.48	0.16	5.07	99.16	284.20	538.22	175	60	15	108	64.93
39R $KJigb_w$ Amph	47.947682 -121.892196	56.26	1.23	15.18	11.30	0.11	3.79	8.04	2.81	0.15	0.10	1.22	100.19	5.19	0.20	319	4	16	13	43.92
39S $KJms_w$	47.920835 -121.900837	62.07	0.75	15.17	5.77	0.14	2.57	4.40	3.40	0.89	0.18	4.32	99.65	45.77	83.69	151	56	17	108	51.05
40D Qga_v	47.878043 -121.983177	70.94	0.52	12.31	3.79	0.08	2.29	2.46	2.75	1.05	0.11	2.99	99.28	78.89	193.94	86	25	12	48	54.87
47A Qc_{ph}	47.983933 -121.873416	71.35	0.61	12.25	3.80	0.05	1.32	1.92	1.79	0.82	0.05	4.33	98.28	24.21	107.11	94	29	14	64	62.57

Table D2. Unnormalized inductively coupled plasma mass spectrometry data from the Lake Roesiger 7.5-minute quadrangle. All data is reported in parts per million (ppm). Dark gray shading, IRSL age sample; light gray shading, U-Pb zircon sample; **, average of two analyses.

Sample Unit	Latitude Longitude	La	Ce	Pr	Nd	Sm	Eu	Gd	Tb	Dy	Ho	Er	Tm	Yb	Lu	Ba	Th	Nb	Y	Hf	Ta	U	Pb	Rb	Cs	Sr	Sc	Zr
2A $KJigb_w$	47.942362 -121.897678	4.62	10.25	1.61	8.03	2.43	0.93	2.94	0.53	3.44	0.76	2.18	0.33	2.12	0.34	250	1.04	0.93	19.55	0.94	0.20	0.27	1.87	9.25	0.28	363	29.13	21
5Q** $KJms_w$	47.921928 -121.931204	28.67	52.23	5.91	21.38	4.03	1.13	3.27	0.49	2.81	0.55	1.47	0.22	1.37	0.21	757	7.84	9.06	14.71	3.26	0.85	2.22	11.08	56.66	1.53	203	8.99	121
6T Qc_{ph}	47.999821 -121.907264	7.50	13.52	1.82	7.48	1.60	0.70	1.51	0.23	1.42	0.28	0.79	0.12	0.72	0.12	464	1.52	3.75	7.75	1.91	0.45	0.62	6.46	27.90	1.61	302	7.88	70
9AB Qc_{ph}	47.988939 -121.914186	7.39	15.22	1.90	7.63	1.75	0.68	1.69	0.29	1.71	0.36	0.95	0.15	0.90	0.15	374	1.87	3.22	9.16	1.93	0.45	0.67	6.15	26.69	1.13	246	8.80	70
16D $KJms_w$	47.920334 -121.900228	15.17	31.42	3.82	14.88	3.34	0.88	3.03	0.52	3.22	0.68	1.93	0.29	1.87	0.30	522	4.69	6.82	17.00	3.82	0.61	1.85	10.28	49.34	2.59	171	15.05	142
17D $KJms_w$	47.906884 -121.825862	12.74	25.62	3.47	14.47	3.65	1.07	3.75	0.64	4.05	0.83	2.35	0.34	2.12	0.33	221	2.56	4.38	22.05	3.03	0.47	1.05	6.08	20.41	1.26	171	18.13	112
19D Qc_{ph}	47.956159 -121.931941	9.94	19.69	2.88	12.46	3.11	1.26	3.19	0.53	3.25	0.67	1.82	0.27	1.67	0.26	428	1.79	4.36	17.41	2.20	0.46	0.72	8.60	31.59	2.11	285	13.39	81
26J Qc_{phl}	47.94839 -121.888474	9.75	20.66	2.72	11.46	2.90	0.94	3.06	0.51	3.25	0.66	1.80	0.27	1.63	0.24	359	2.12	3.96	16.68	2.01	0.43	0.87	7.40	27.39	1.70	106	19.51	74
302C $KJms_w$	47.915869 -121.882983	26.51	49.99	5.68	21.25	4.11	1.11	3.35	0.51	2.87	0.57	1.53	0.23	1.46	0.24	372	8.74	10.04	14.80	3.91	0.81	2.42	10.81	52.57	1.19	356	10.39	146
31S Mvr	47.953052 -121.88857	18.37	34.32	3.97	13.52	2.63	0.41	2.12	0.40	2.77	0.64	1.97	0.34	2.49	0.43	1009	10.98	7.25	18.33	2.70	0.85	4.82	10.75	96.31	3.43	90	2.84	71
31V Qc_{phl}	47.957463 -121.878995	11.69	24.45	3.32	14.12	3.66	1.04	3.74	0.63	3.92	0.79	2.17	0.32	1.99	0.30	440	2.83	5.04	19.93	2.52	0.37	1.07	8.56	36.90	2.43	117	20.90	90
33B Qc_{ph}	47.988473 -121.915157	8.81	16.19	2.48	10.35	2.37	0.89	2.21	0.36	2.07	0.42	1.13	0.16	1.01	0.15	431	1.78	4.12	10.93	2.17	0.32	0.71	7.15	31.35	1.78	279	11.10	77

Sample Unit	**Latitude Longitude**	**La**	**Ce**	**Pr**	**Nd**	**Sm**	**Eu**	**Gd**	**Tb**	**Dy**	**Ho**	**Er**	**Tm**	**Yb**	**Lu**	**Ba**	**Th**	**Nb**	**Y**	**Hf**	**Ta**	**U**	**Pb**	**Rb**	**Cs**	**Sr**	**Sc**	**Zr**
33D Qc_{ph}	47.878913 -121.917687	10.11	19.26	2.56	10.07	2.34	0.83	2.30	0.39	2.40	0.51	1.36	0.20	1.30	0.22	492	2.70	3.10	12.81	2.23	0.27	0.96	7.36	36.39	1.58	331	9.37	82
33G Qa	47.873027 -121.884002	6.47	13.22	1.73	7.09	1.73	0.56	1.80	0.31	1.94	0.41	1.14	0.17	1.12	0.18	329	1.56	3.00	10.35	1.71	0.25	0.65	4.20	21.93	0.88	129	10.20	63
35A Qc_{ph}	47.957271 -121.92326	10.35	23.34	2.76	11.00	2.70	0.82	2.58	0.43	2.63	0.52	1.41	0.21	1.37	0.22	365	2.52	5.40	13.40	3.00	0.41	1.01	6.86	30.17	1.61	209	13.64	116
35B Qc_{phl}	47.938484 -121.913251	9.94	21.09	2.83	11.91	3.08	0.96	3.19	0.55	3.43	0.70	1.94	0.29	1.81	0.28	391	2.33	4.39	18.22	2.21	0.34	0.97	7.11	30.65	2.37	119	20.46	82
36N $KJms_{w}$	47.999792 -121.884889	19.26	37.45	4.50	16.93	3.71	0.98	3.37	0.60	3.80	0.79	2.31	0.35	2.29	0.38	773	7.10	9.38	19.58	3.65	0.68	2.28	12.03	94.91	4.85	131	22.78	133
37V Qc_{phl}	47.977237 -121.988382	13.36	26.50	3.76	15.73	3.90	1.14	3.99	0.68	4.27	0.86	2.33	0.33	2.15	0.32	497	3.33	5.65	21.91	2.72	0.43	1.30	8.61	44.41	2.59	116	21.40	98
39R $KJigb_{w}$ Amph	47.947682 -121.892196	3.20	8.88	1.48	7.93	2.93	1.20	4.02	0.76	5.17	1.12	3.10	0.46	2.94	0.47	80	0.28	1.05	28.33	1.81	0.11	0.12	0.28	1.98	0.21	234	36.52	61
39S $KJms_{w}$	47.920835 -121.900837	17.56	36.02	4.56	18.13	4.26	1.28	4.04	0.67	4.02	0.83	2.28	0.34	2.20	0.36	204	5.02	7.19	21.09	3.52	0.52	1.87	10.25	28.04	1.80	216	17.76	126
40D Qga_{v}	47.878043 -121.983177	9.97	21.22	2.58	10.29	2.33	0.76	2.36	0.40	2.52	0.52	1.44	0.21	1.35	0.21	432	2.29	3.91	13.01	2.53	0.33	0.80	5.70	25.11	0.93	270	11.26	96
47A Qc_{ph}	47.983933 -121.873416	11.12	22.15	3.06	12.75	2.84	0.98	2.81	0.48	2.96	0.61	1.62	0.24	1.50	0.23	351	2.29	4.51	15.47	2.35	0.35	0.68	6.59	25.52	1.46	243	13.21	85